Multiphase Flows and Transport Phenomena SIG

2nd SIG Meeting, University College London

UK Fluids Network, 8th December 2017

Book of Posters

UK FLUIDS NETWORK

Table of Contents

P11	Dr Lachlan Mason	Imperial	Multiphase three-dimensional direct numerical simulation of a rotating impeller with code Blue
P12	Xinyue Jiang	UCL	Combining microfluidic devices with coarse capillaries to reduce the size of microbubbles
P13	Evita Roumpea	UCL	Plug flow studies of non-Newtonian liquids in micro-channels

LITA in a Transitional Surface Flow

Zachary Falgout, Mark Linne

School of Engineering, University of Edinburgh, Robert Stevenson Road, EH9 3FB, UK

THE UNIVERSITY of EDINBURGH

Background

In recent years, there have been observations of dense-fluid mixing, resembling the behavior of supercritical flows, well beneath the mixture critical point in spray/jet flows relevant to compression ignition combustion engines, where it has been assumed that evaporation is the primary mode of mass transfer between the liquid fuel and ambient gas. Despite the fact that the difference in these two scenarios is really in the nature of microscopic transport at extreme density gradients, many of the studies which raised this issue have been macroscopic imaging studies, using back-lit white-light shadow imaging or similar techniques[1–3]. An example is shown in Figure 1.

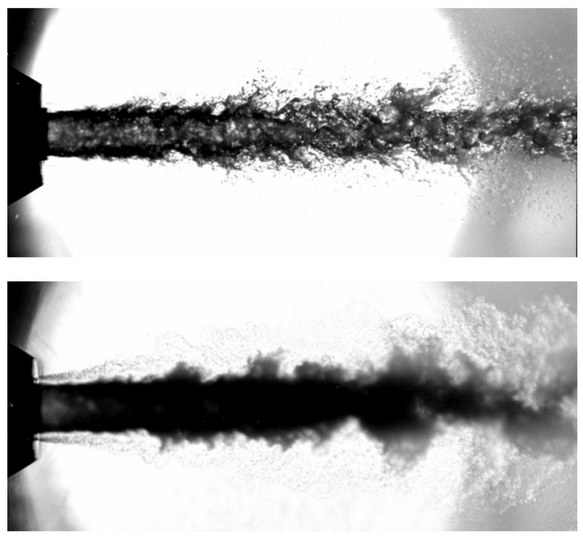

Figure 1: Two co-axial N_2/He mixing jets at 10 bar(*upper)* and 60 bar(*lower)* ambient pressure[3]

Our ***goal*** in this study is to directly measure microscopic thermodynamic and/or transport properties to clarify the nature of transport in these flows, and thereby to determine if this transition is, in fact, occurring and, if so, where as a function of thermodynamic state and time. Recent theoretical studies have suggested that the transition has a time-dependence that may control its effect on other important dynamics in spray mixing, like atomization[4–6].

Thermodynamic/transport signatures of supercritical flows are a singular decrease in sound speed near the critical point, as well as greatly enhanced thermal and mass diffusivity as compared to a saturated fluid-fluid interface. Currently, it is unknown if these trends are also observed in a time-dependent phase transition *beneath* the mixture critical point, which has been indicated to be possible by recent theoretical work [4–6].

Laser-Induced Thermal Acoustics (LITA)

LITA is a four-wave mixing technique that can be used to directly extract sound speed and other transport coefficients from flows. Two coherent laser beams centered on a resonance of the sample medium("pump" beams) cross to create an excited-state population grating, which quickly quenches to create a temperature/density grating. Since $\frac{\partial n}{\partial \rho} > 0$, this also generates an index grating that can be probed by a third laser beam at a non-resonant wavelength.

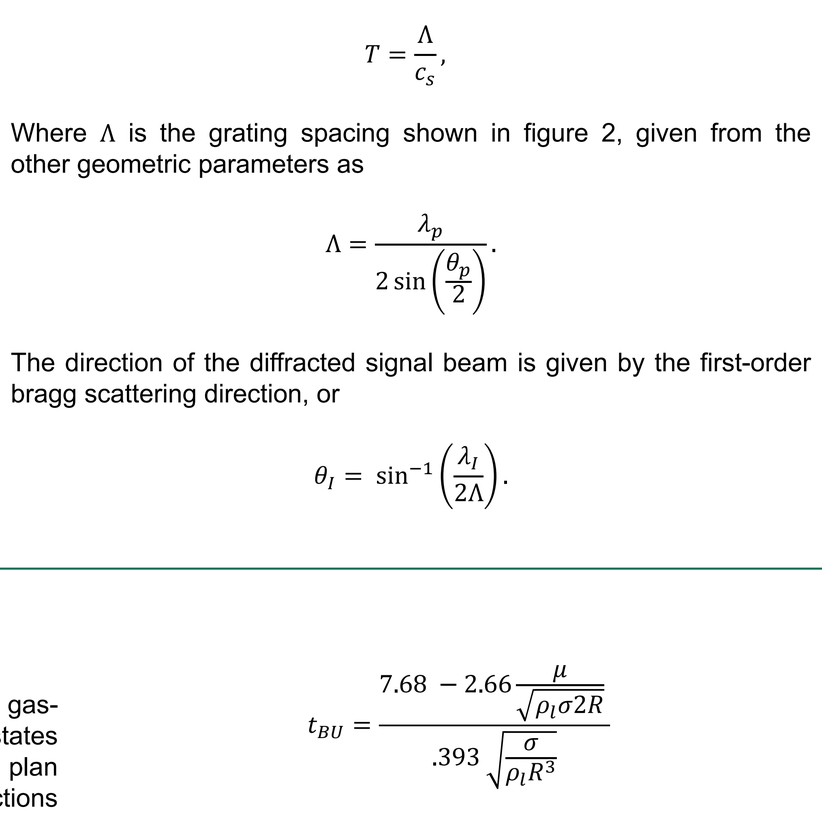

Figure 2: Illustration of the arrangement of a LITA experiment and important geometric parameters.

After the pump pulse, two counter-propagating density waves are established which create a standing wave. The period of the standing waves' amplitude oscillations, T, is directly related to the adiabatic sound speed:

$$T = \frac{\Lambda}{c_s},$$

Where Λ is the grating spacing shown in figure 2, given from the other geometric parameters as

$$\Lambda = \frac{\lambda_p}{2\sin\left(\frac{\theta_p}{2}\right)}.$$

The direction of the diffracted signal beam is given by the first-order bragg scattering direction, or

$$\theta_I = \sin^{-1}\left(\frac{\lambda_I}{2\Lambda}\right).$$

The diffracted probe beam intensity, I_s, at angle θ_I, modeled using 1-dimensional hydrodyanamics [7] for a single-phase fluid, depends on the adiabatic sound speed as well as a number of transport properties:

$$I_s \propto [\exp -\frac{t}{\tau_{th}} + \exp -\frac{t}{\tau_{ac}} \times \cos(2\pi \frac{c_s}{\Lambda} t + \Phi)] * L(t) * Z(t),$$

where τ_{th} and τ_{ac} are thermal and acoustic relaxation times, dependent upon viscosity, thermal diffusivity, and mass diffusivity, $L(t)$ is the pump intensity, and $Z(t)$ defines the rate of thermalization of the pump energy via quenching. A typical LITA signal is shown below to illustrate the sinusoidal signal over-layed on the exponentially decaying envelope.

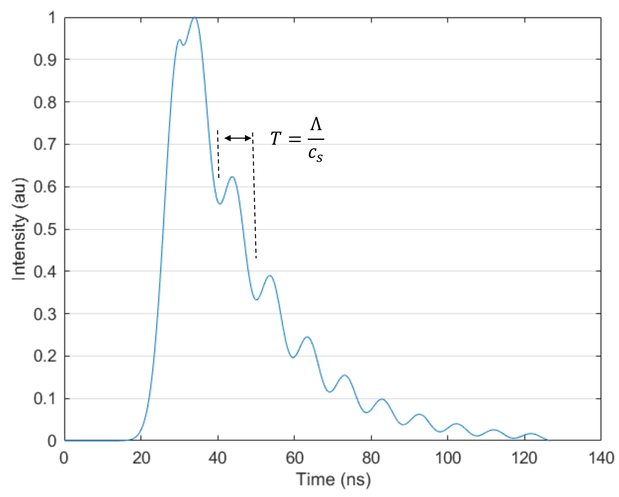

Figure 3: Representative LIGS signal

In the case of a binary mixture, a concentration grating also forms, and an additional mass diffusion relaxation mode occurs. This mode may be isolated from the thermal relaxation mode if the mass diffusivity is far lower than the thermal diffusivity. This allows the independent determination of the mass diffusion coefficient and thermal diffusivity, as well as the thermal diffusion ratio, k_T, which is also known as the Bearman-Kirkwood diffusion factor [8-9]. In this case, the exponential intensity decay can be expressed as the sum of to exponentials:

$$I_s \propto \exp(-D_T q^2)\left[T_0\left(\frac{\partial \epsilon}{\partial T}\right)_{P,C} + \frac{k_T D}{D_T - D}\left(\frac{\partial \epsilon}{\partial C}\right)_{\rho,T}\right]$$
$$+ \exp(-D q^2)\left[-\frac{k_T D}{D_T - D}\left(\frac{\partial \epsilon}{\partial C}\right)_{\rho,T} + \frac{k_T^2 D^2 T_o}{T_0 C_p (D_T - D)^2}\left(\frac{\partial \epsilon}{\partial T}\right)_{P,C}\right].$$

Experimental Design

The flow in this experiment is a laminar jet, intended to provide a gas-liquid interface exposed to extreme ambient thermodynamic states without the obfuscating effects of turbulence or atomization. The plan is to make LITA measurements at the surface of the jet. Two sections of the vessel are shown in Figure 2, which show the physical layout of the flow and the optical diagnostic. Ideally, the transition to dense fluid flow should occur before the jet breaks into large droplets. The most accurate estimation for transition time is currently that provided by Qiao et al [4]:

$$t_{trans} = t_L A(T_r) \ln(B(T_r) P_r),$$

where A and B are both cubic polynomials of the reduced temperature defined as the ratio between the ambient state, T_{amb} and p_{amb}, and the critical point of the fuel. This, so far, is only known for heptane, hexadecane, and dodecane. The breakup time of a jet in the Rayleigh regime at constant temperature is given by [10]:

$$t_{BU} = \frac{7.68 - 2.66\frac{\mu}{\sqrt{\rho_l \sigma 2R}}}{.393\sqrt{\frac{\sigma}{\rho_l R^3}}}$$

The determination of the ratio between these two times, or rather if $t_{trans} < t_{BU}$, then requires the lifetime of the liquid jet under purely evaporating conditions at a lower pressure. For a macroscopic jet, this calculation is rather involved, since it requires that the effect of thermodynamic state on transport coefficients be included. With only the analytical expressions shown here, it would seem that $\frac{t_{BU}}{t_{trans}} \to 0$ with increasing ambient temperature, given that surface tension decreases with increasing ambient temperature and pressure. The trend with jet diameter is less clear, given the unknown dependence of t_L.

Another concern is the effect of large gradients within the grating volume, since the desired probe region is likely to have large gradients in both density and temperature.

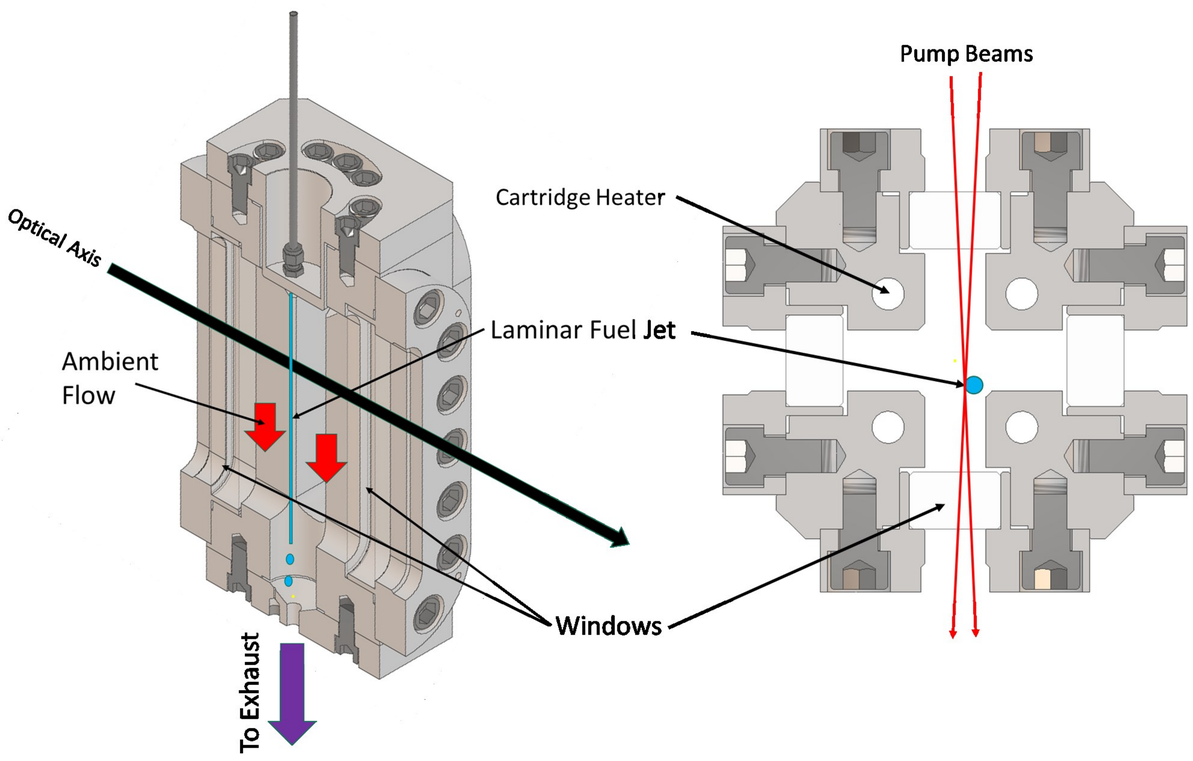

Figure 4: Experimental vessel with flow and diagnostic arrangement shown in two sections.

Future Plans

The experimental vessel is currently in the fabrication phase, and experiments will begin before the end of the year. In addition to LITA, Raman scattering and FRET experiments are planned. In the more distant future, light scattering techniques may also be used for their ability to extract additional parameters near the critical point, such as density fluctuations and the molecular correlation length.

References

1. Dahms, R., Manin, J., Pickett, L. & Oefelein, J. Understanding high-pressure gas–liquid interface phenomena in Diesel engines. *Proc. Combust. Inst.* (2012).
2. Crua, C., Manin, J. & Pickett, L. M. On the transcritical mixing of fuels at diesel engine conditions. *Fuel* **208,** 535–548 (2017).
3. Mayer, W. *et al.* Atomization and breakup of cryogenic propellants under high pressure subcritical and supercritical conditions. *J. Prop. Pow.* **14,** 835–842 (1998).
4. Mo, G. & Qiao, L. A molecular dynamics investigation of n alkanes vaporizing into nitrogen: transition from subcritical to supercritical. *Combust. Flame* **176,** 60–71 (2017).
5. Dahms, R. N. & Oefelein, J. C. On the transition between two-phase and single-phase interface dynamics in multicomponent fluids at supercritical pressures. *Phys. Fluids* **25,** 92103 (2013).
6. Dahms, R. N. Understanding the breakdown of classic two-phase theory and spray atomization at engine-relevant conditions. *Phys. Fluids* **28,** 42108 (2016).
7. Williams, S., Rahn, L. A., Paul, P. H., Forsman, J. W. & Zare, R. N. Laser-induced thermal grating effects in flames. *Opt. Lett.* **19,** 1681–1683 (1994).
8. Miller, R., Harstad, K. G. & Bellan, J. B. Direct numerical simulations of supercritical fluid mixing layers applied to heptane–nitrogen. *J. Fluid Mech.* **436,** 1–39 (2001).
9. K. Thyagarayan, P. Lallemand, Determination of the thermal diffusion ratio in a binary mixture by forced Rayleigh scattering, *Opt. Comm.,* **26,** 54-57, 1978
10. Dumouchel, C. On the experimental investigation on primary atomization of liquid streams. *Exp. Fluids* **45,** 371–422 (2008).

Acknowledgements:

This work is funded by the Air Force Office of Scientific Research(AFOSR) under grant FA9550-17-1-0129 and the Engineering and Physical Sciences Research Council(EPSRC) under grant EP/P011438/1

Coalescence of Initially Static Free Droplets

Thomas C. Sykes[1], Mark C. T. Wilson[2], David Harbottle[3], Zinedine Khatir[2], Harvey M. Thompson[2]

[1] EPSRC Centre for Doctoral Training in Fluid Dynamics, University of Leeds

[2] School of Mechanical Engineering, University of Leeds [3] School of Chemical and Process Engineering, University of Leeds

1. Introduction

An important aspect of droplet coalescence is the fate of the internal fluids and the associated extent of fluid mixing within the final droplet. Mixing is of great importance in applications such as microfluidic devices, spray driers and reactive inkjet printing (RIJ). In RIJ, two different reactive inks are deposited, which react to form the desired unjettable product.

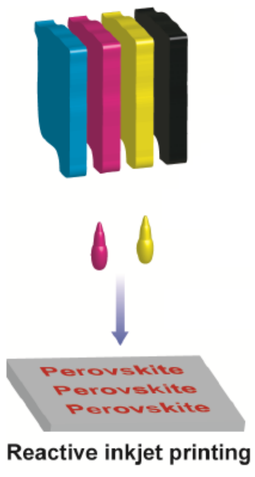

Reactive inkjet printing

Jiang, Z. et al., HAL Archive (2016)

Initially, free droplets consisting of the same fluid have been considered, which start from rest and are just touching, suspended in an immiscible fluid phase.

2. Effect of Ohnesorge Number

For a given droplet size ratio, the controlling dimensionless number is the Ohnesorge number,

$$\mathrm{Oh} = \frac{\mu_d}{\sqrt{\rho_d \sigma d_s}},$$

where μ_d is the droplet dynamic viscosity, ρ_d the droplet density, d_s the diameter of the smaller droplet and σ is the interfacial tension.

For nominally large Oh (=0.203), the smaller droplet lodges into the side of the larger droplet, with little mixing evident [1]:

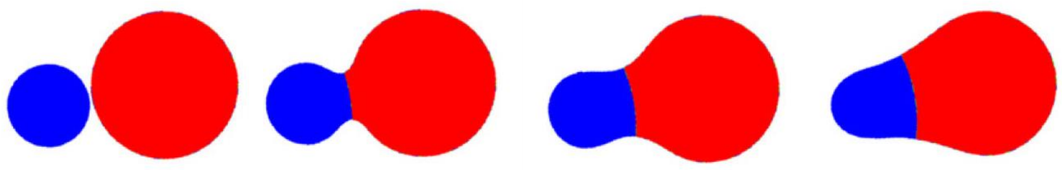

0 ms 10 ms 20 ms 30 ms

For smaller Oh (=0.012), the smaller droplet forms a jet which penetrates into the larger droplet, significantly enhancing mixing [1]:

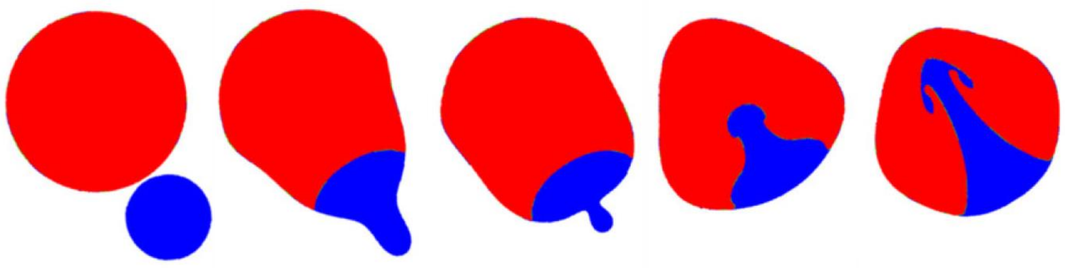

0 ms 12 ms 16 ms 28 ms 52 ms

3. Modelling Approach

A volume of fluid (VOF) approach is taken to solve the two-phase problem, modelling the system as a single fluid with non-constant properties. An indicator function is used to identify the droplet location in the surrounding phase. Conservation of mass and Navier-Stokes equations are constructed and discretised with the finite volume method.

This is implemented in **OpenFOAM**, an open-source C++ toolbox for numerical fluid simulation. A library solver (interFoam) is modified to solve a scalar transport equation for a passive scalar using a flux-corrected transport numerical scheme. The passive scalar is initialised as one in the smaller droplet and zero elsewhere, allowing the fluid from the smaller drop to be tracked into the larger droplet on coalescence.

4. Reducing Spurious Velocities

Spurious velocities often arise at interfaces in implicit interface capturing methods, mainly due to inaccurate interfacial curvature calculation, required for the interfacial tension implementation.

They are reduced by limiting the time step and smoothing the VOF indicator function in the curvature calculation with a Laplacian smoother, applied m times, as proposed by Hoang et al. [2]. This was implemented in OpenFOAM.

To assess the effect of smoothing, the relaxation of a 2D, stationary, circular droplet from a square initial shape was simulated and compared to Hoang's time series of maximum velocities (Hoang's result top). Smoothing is shown to reduce the spurious currents after the equilibrium shape is reached.

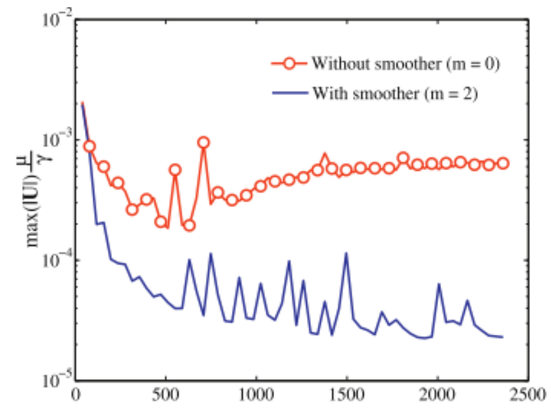

5. Preliminary Results

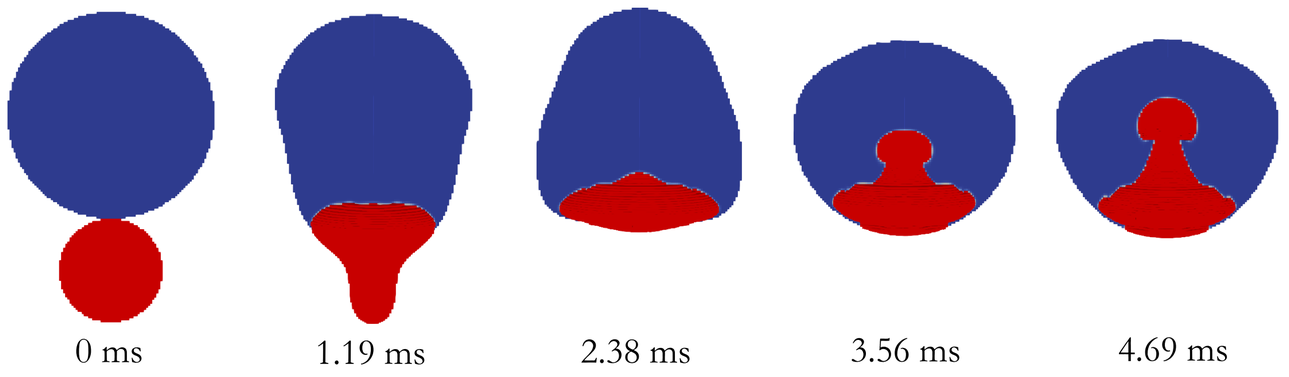

0 ms 1.19 ms 2.38 ms 3.56 ms 4.69 ms

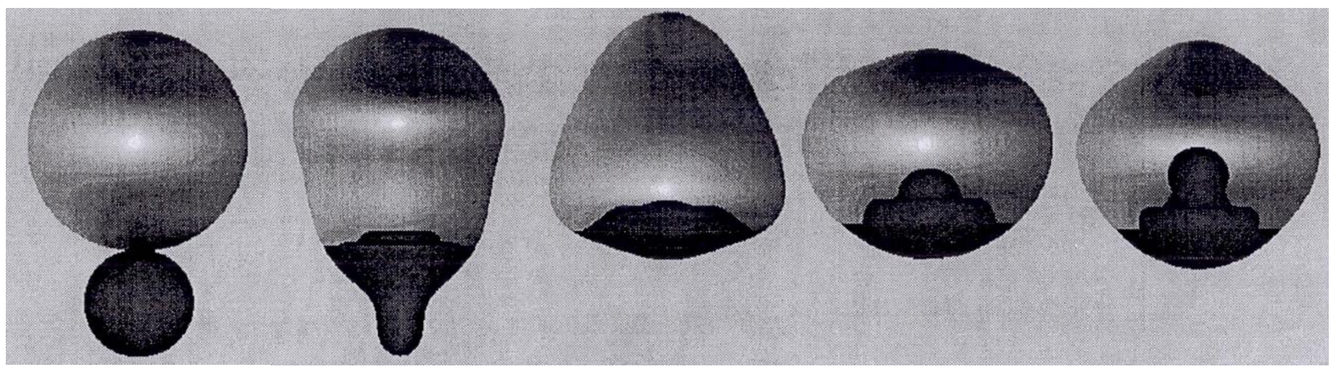

Free droplet coalescence with Oh=0.0024 is simulated and compared to the results of Nobari and Tryggvason [3] (bottom row, 3D surface rotated). The results are qualitatively similar for small times but the OpenFOAM simulation progresses faster in time. This may be due to smoothing (sec. 4) and is under investigation.

The total (combined) drop length shows the energy dissipating oscillations of the final drop.

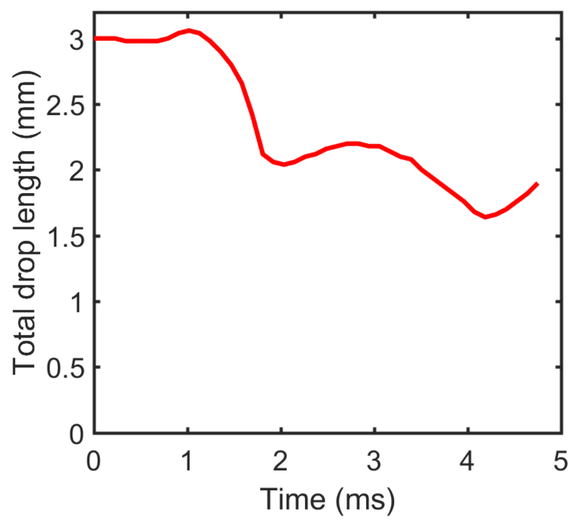

6. Conclusions & Future Work

- Smoothing in the curvature calculation reduces spurious velocities effectively.
- OpenFOAM appears to be a good tool for studying internal flows in coalescence.
- Further numerical tests and refinement are planned to improve the modelling.

Acknowledgements

This work was supported by the Engineering and Physical Sciences Research Council (EPSRC) Centre for Doctoral Training in Fluid Dynamics at the University of Leeds under Grant No. EP/L01615X/1.

References

[1] Sun, K. et al. (2015) Phys. Rev. E, **91**(2), doi: 10.1103/PhysRevE.91.023009
[2] Hoang, D. A. et al. (2013) Comp. Fluid., **86**, doi: 10.1016/j.compfluid.2013.06.024
[3] Nobari, M.R. and Tryggvason, G. (1994) NASA Technical Memorandum 106752.

www.fluid-dynamics.leeds.ac.uk mm13tcs@leeds.ac.uk @FluidsTom

Counter-Current Thermocapillary Migration of Bubbles in Self-Rewetting Liquids

Robson K. Nazareth[1], Pedro J. Saenz[2], Omar K. Matar[3], Khellil Sefiane[1], Prashant Valluri[1]

[1]Institute for Materials and Processes, The University of Edinburgh, Edinburgh EH9 3JL, UK

[2]Department of Mathematics, Massachusetts Institute of Technology, Cambridge, Massachusetts 02139, USA

[3]Department of Chemical Engineering, Imperial College London, London, SW7 2AZ, UK

Introduction

The fluid flow driven by variable surface tension along an interface in multiphase systems has been a mechanism of great importance to many industrial applications. Non-uniformities in surface tension create shear stresses at the interface that may induce fluid motion on the surround fluid by viscous forces. This phenomena known as Marangoni effect can be induced by temperature and concentration gradients. In the present work we concentrate on the thermally driven Marangoni effect, also know as the thermocapillary effect. The thermocapillary effect is particularly important for the motion of bubbles and drops, because it can be exploited to propel bubbles and drops in the opposite direction to the surface tension gradient. Since the pioneering work of Young et al. [1], studying rising bubbles on vertical temperature gradient, many publications have addressed to this topic [2]. However, this is still an incompletely understood phenomenon specially for liquids with a non-linear dependence of surface tension on temperature. In this work we study the counter-current thermocapillary migration of bubbles in self-rewetting liquids by means of numerical simulations. Our goal is to investigate the effects of viscosity and thermocapillarity on the bubble motion and compare our results with the theoretical work presented by Shanahan & Sefiane (2014) [3].

Problem formulation

Conservation equations

Mass:

$$\nabla . \boldsymbol{u} = 0$$

Momemtum:

$$\rho\left(\frac{\partial \boldsymbol{u}}{\partial t} + \boldsymbol{u}.\nabla\boldsymbol{u}\right) = -\nabla p + \frac{1}{Re}\nabla.\left(\mu(\nabla\boldsymbol{u} + \nabla\boldsymbol{u}^T)\right) + \frac{1}{ReCa}(\sigma\kappa\hat{\boldsymbol{n}} + \nabla_s\sigma)\delta_s$$

Energy:

$$\rho c_p\left(\frac{\partial T}{\partial t} + \boldsymbol{u}.\nabla T\right) = \frac{1}{Pe}\nabla.(\mathrm{k}\nabla T)$$

Interface:

$$\frac{\partial c}{\partial t} + \nabla.(c\boldsymbol{u}) = 0$$

Surface tension:

$$\sigma = \sigma_r + \Gamma(T-1)^2$$

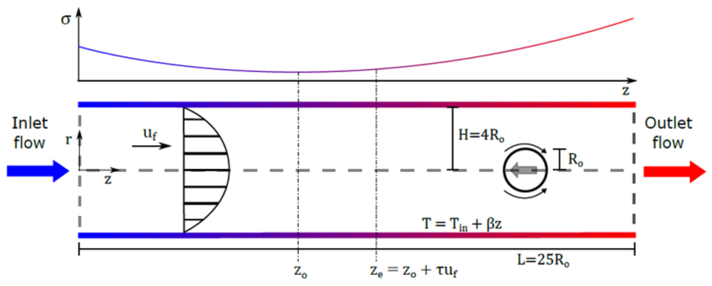

Fig. 1: Schematic of the mathematical model and, on top, the surface tension coefficient related to the temperature along the channel wall.

Scaling

- Length: $\tilde{R}_o$
- Velocity: $\tilde{U}_o = \tilde{u}_f$
- Temperature: $\Delta\tilde{T} = \tilde{T}_o - \tilde{T}_1$

Base set of parameters

$\rho_r = 1/1000$	$Pe = 0.1$
$\mu_r = 1/100$	$B = 0.1$
$c_{p_r} = 1/4$	$R = 1$
$k_r = 1/30$	$H = 4$
$\Gamma = 0.1745$	$L = 25$

Group numbers

$$Re = \frac{\tilde{\rho}_l\tilde{U}_o\tilde{R}_o}{\tilde{\mu}_l},\ Ca = \frac{\tilde{\mu}_l\tilde{U}_o}{\tilde{\gamma}_o(\Delta\tilde{T})^2},\ Pe = \frac{\tilde{U}_o\tilde{R}_o}{\tilde{\alpha}_l}$$

Counter-current thermocapillary migration

Fig. 2 illustrates a typical case of counter-current thermocapillary migration of a bubble inside a channel with self-rewetting fluid and positive temperature gradient. Unlikely in more classic fluids, the bubble is propelled against the flow towards the cold side until it comes to a halt at an equilibrium position located to the right of the surface-tension minimum.

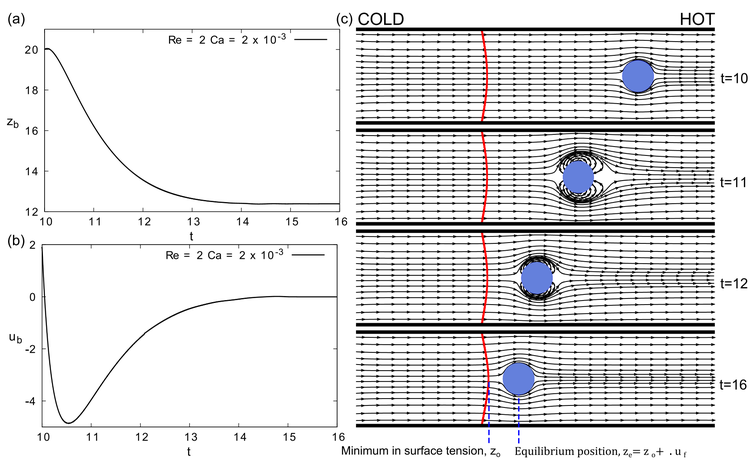

Fig. 2: Time evolution of (a) the center of mass z_b and (b) velocity u_b of the bubble; (c) panels showing the bubble motion with the streamlines (black lines), the bubbles (blue) and the isothermal line for T=1 corresponding to the minimum in surface tension (red line).

Parametric study

The role of Reynolds (Re) and capillary (Ca) numbers on the bubble dynamic is illustrated in Fig. 3:

- Increasing Ca the bubble equilibrium position (z_e) shifts downstream due to a decrease in the thermocapillary force in relation to the viscous forces.
- At moderate values Ca = O(10^{-3}) and high Re, the bubble starts to be subjected to damped oscillations due to the increase of inertia.
- Decreasing Ca, z_e shifts upstream and the bubble starts to present steady oscillations around the equilibrium position.

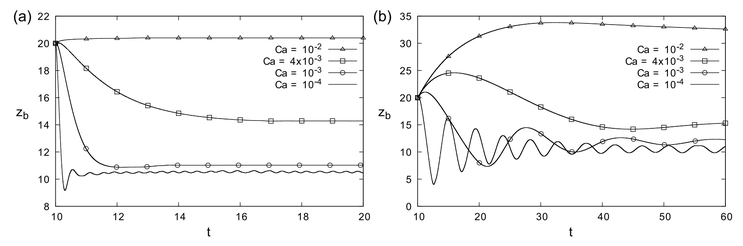

Fig. 3: Time evolution of the bubble center of mass, z_b, for different capillary numbers wit (a) Re = 1 and (b) Re = 100.

Based on the dynamics of the bubble observed in Fig. 3 we build a map on the parameter space of Re and Ca, that is illustrated in Fig. 4. In this map we identify four different possible behaviours of bubble motion:

i) "**Counter-current motion**" where the bubble migrates against the flow and asymptotically approaches a stable equilibrium position;

ii) "**Damped oscillations**" where the bubble migrates against the flow and oscillate before it comes to a halt at a stable equilibrium position;

iii) "**Sustained oscillations**" where the bubble presents steady oscillations around its equilibrium position;

iv) "**Co-current motion**" where the channel flow is much stronger than thermocapillarity and the bubble is dragged away downstream until it comes to a halt a an stable equilibrium position.

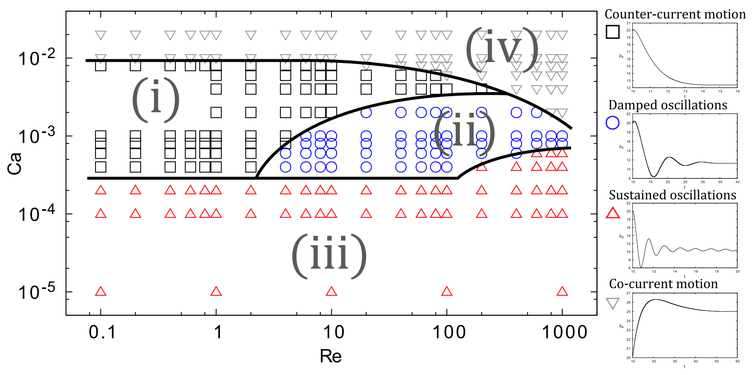

Fig. 4: Map with the four bubble behaviours in the parameter space of Re and Ca.

Bubble equilibrium position

We compare our results against the theoretical equilibrium position prescribed by,

$$z_e = z_o + \frac{3Ca}{4\Gamma B^2}u_f$$

Fig. 5 shows that the numerical results follows the same trend as the theory and that z_e grows linearly with Ca as predicted by the theory. There is a good agreement for low Ca, while for Ca > 10^{-3} the numerical results start to deviate from theory. This deviation increase for Re = 100 and it is because the theory does not account for bubble deformation the starts to be relevant for high Ca and Re.

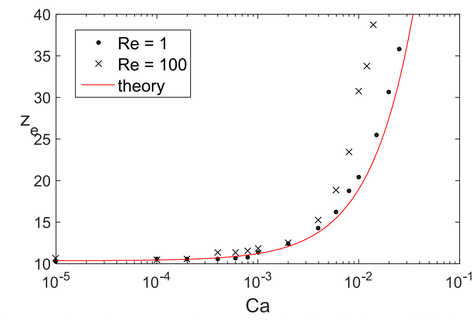

Fig. 5: Comparison between the numerical bubble equilibrium position for Re = 1 and Re = 100, and the theoretical prediction.

The effect of bubble deformation on z_e is illustrated in Fig. 6. In this figure we analyse the change of the bubble aspect ratio, A_r, as we increase Re for Ca = 0.01. Increasing Re the bubble become more oblate and z_e is shifted downstream. For Ca = 0.01 the equilibrium position predicted by eq. 1 is $z_e = 19.1$.

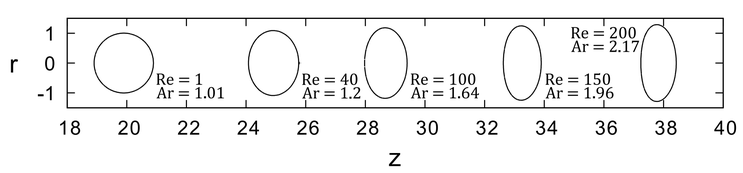

Fig. 6: Bubble shape at the equilibrium position for different values of Re and Ca = 0.01.

Transition regions

Transition from counter-current motion to damped oscillations

- Increasing Re increases the inertia that delay the response to the thermocapillary forces allowing the bubble to oscillate before it comes to a halt at a stable equilibrium position.

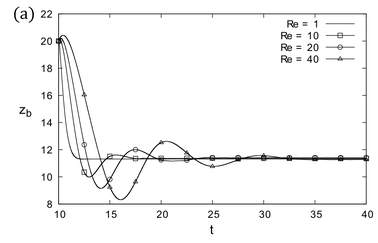

Fig. 7: Time evolution of the bubble center of mass, z_b, showing the transition from region (i) to region (ii) increasing Re for Ca = 0.001

Transition to co-current motion

- Increasing Ca it decreases the strength of the thermocapillary forces shifting z_e downstream until a point where the thermocapillary forces are not strong enough to overcome the viscous forces to move the bubble against the flow.

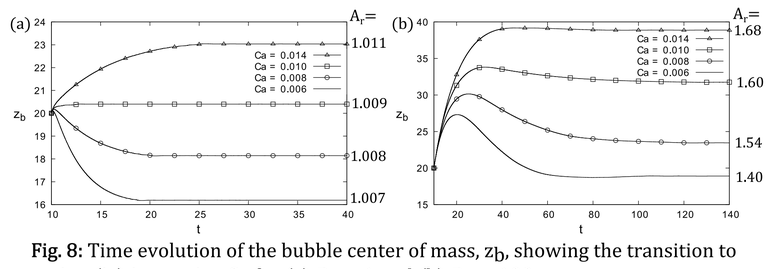

Fig. 8: Time evolution of the bubble center of mass, z_b, showing the transition to region (iv) increasing Ca for (a) Re = 1 and (b) Re = 100.

Transition to sustained oscillations

- Decreasing Ca it increases the strength of the thermocapillary forces shifting z_e upstream in direction to the surface tension minimum. After the bubble reaches the location of the surface tension minimum at Ca = 4x10^{-4}, increasing more the thermocapillary forces by decreasing Ca leads to the sustained oscillations.

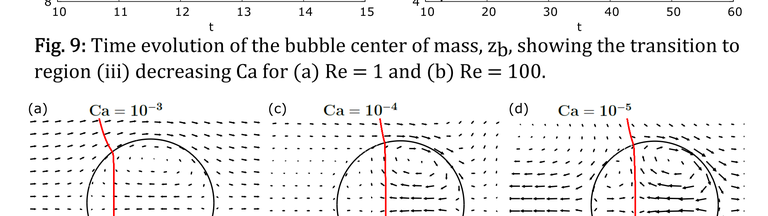

Fig. 9: Time evolution of the bubble center of mass, z_b, showing the transition to region (iii) decreasing Ca for (a) Re = 1 and (b) Re = 100.

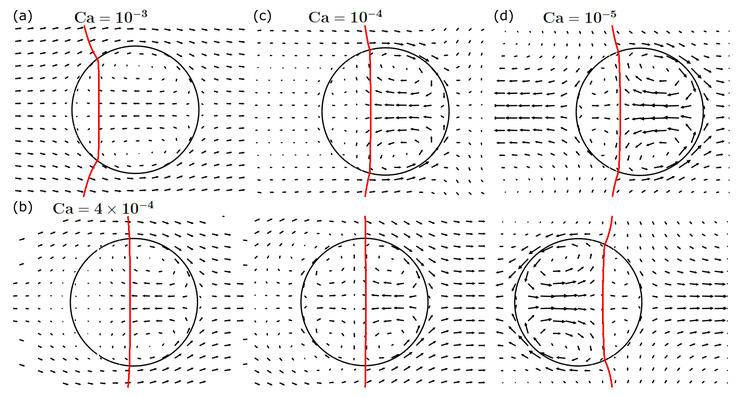

Fig 10: The vector field and the isothermal line corresponding to the surface tension minimum showing the transition to sustained oscillations for Re = 1. (a) and (b) show a stable equilibrium position and (c) and (d) show the oscillations around the equilibrium position.

Sustained oscillations

In Fig. 11 we compare the frequency of the oscillations against the theoretical prediction given by,

$$w = \sqrt{\frac{8\Gamma B^2}{ReCa} - \frac{9}{Re^2}}$$

- The frequency of the oscillations is inversely proportional to Re.
- The amplitude of the oscillations grows linearly with Re.

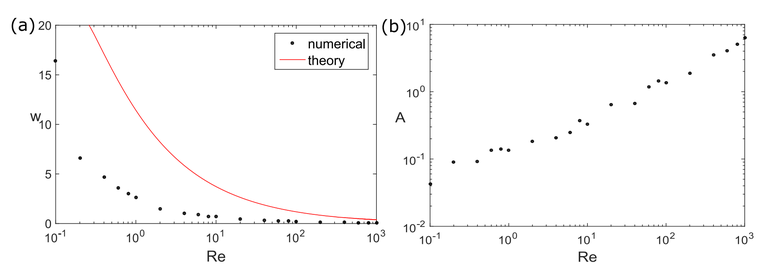

Fig. 11: (a) Frequency and (b) amplitude of the oscillations in function of Re for Ca = 10^{-4}.

References

[1] Young, N. O., Goldstein, J. S. & Block, M. J., *Journal of Fluid Mechanics* **6**, 350-356 (1959).

[2] Subramanian, R. S., Balasubramaniam, R. & Wozniak, G. Physics of Fluids in Microgravity. 149-177 (2002)

[3] Shanahan, M. E. R. & Sefiane, K., Scientific Reports 4, 4727 (2014)

Acknowledgments: The work was supported by the Science without Borders program from CAPES agency of Brazilian Ministry of Education and the European Commission´s Thermapower Project (294905).

Discussion

- We performed a parametric study on the thermocapillary migration of bubbles in self-rewetting liquids in the parameter space of Re and Ca and build a map showing the regions of four distinct dynamics.
- We have shown that the equilibrium position has a linear dependence with Ca as predicted by theory.
- We show how the bubble deformation affects z_e and how z_e deviates from theory as the bubble becomes more oblate.
- We show that the frequency of the sustained oscillation is inversely proportional to Re and that the amplitude of the oscillations grows linearly with Re.

Multiphase Large Eddie Simulation of a Pulsed Sieve-Plate Extraction Column

Daniel Theobald, Bruce Hanson, Michael Fairweather and Peter Heggs
School of Chemical and Process Engineering, University of Leeds, Leeds, LS2 9JT, UK

1. What is a PSPEC?

Pulsed Sieve-Plate Extraction Columns (PSPECs) are used primarily within the nuclear industry for reprocessing Spent Nuclear Fuel (SNF). SNF rich in unstable plutonium is dissolved in nitric acid and the usable plutonium and uranium in recovered via a solvent extraction process. PSPECs apply geometric constrains on the process to avoid criticality events arising from large volumes plutonium liquors.

- PSPECs are designed to provide interfacial mixing of two immiscible fluids, during counter-current flow, in order to facilitate mass transfer between phases by maximising effective mass transfer area via droplet formation.
- In order to achieve efficient levels of mass transfer, droplet size is minimised through the application of shear forces.
- A pulsed light phase is introduced at the bottom of the column and a heavy phase is fed at the upper end of the column. Gravitational effects from a density differential between the two fluids causes settling within the decanters at the top and bottom of the column for the light and heavy phases respectively, as well as providing the driving force for counter current flow.
- Pulsation of the light phase feed causes cyclic mixing of the fluid across the stationary perforated sieve-plates resulting in shear forces leading to droplet formation.

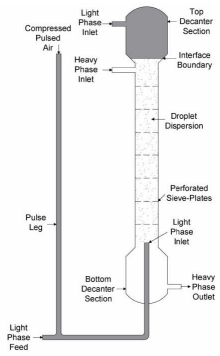

Fig. 1. *Generic Industrial PSPEC Design Used in SNF Reprocessing*

2. Why Study Them?

- PSPECs play an integral role in the reprocessing of spent nuclear fuel.
- Future nuclear fuels will contain higher levels of radioactively unsafe species to remove and at higher burn-up levels.
- This calls for greater flexibility and reliability from reprocessing equipment a the backend of the fuel cycle.
- More robust separation flow sheets will also rely on the optimisation of PSPECs.

3. What Has Been Done?

- Older research on these column has predominantly involved lab-based experimentation producing crude over-simplified correlations.
- This work fails to fundamentally describe the hydrodynamic behaviour of this equipment and results in inaccurate design tools and methodologies.
- Only a handful of CFD investigations have been conducted on PSPECs, mostly opting for inaccurate RANS methods.
    - This method of CFD modelling does not capture the inherently transient and multiscale characteristics of the PSPEC.
    - It also does not provide the level of detail required to understand the flow characteristics of these columns on a fundamental level.

4. Summary of Research

Presented here is research resulting from a framework of single-phase to multiphase modelling trials. These are intended to accurately simulate the internal flow phenomena arising in pulsed sieve-plate extraction columns representative of those found in industry. Three-dimensional unsteady flow calculations using large eddy simulation (LES) coupled with dynamic sub-grid scale modelling have been used to capture the transient effects of sinusoidal flow conditions using the open source CFD code OpenFOAM. Multiphase interface interactions are modelled using the volume of fluid method with appropriate heavy and light phase fluidic properties capturing surface tension, density and viscous effects.

5. Geometry and Mesh

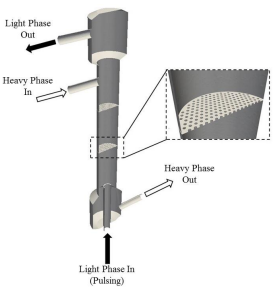

Fig. 2. *Y-Symmetry Plane Isometric View of the PSPEC Geometry used in CFD Simulations.*

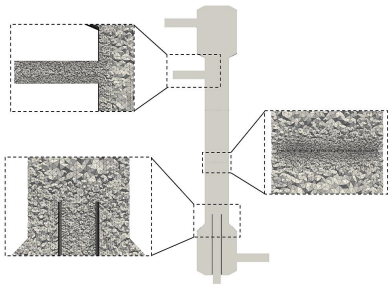

Fig. 3. *Unstructured Tetrahedral Mesh of 5.5 M Nodes Used in CFD Simulation.*

6. Results

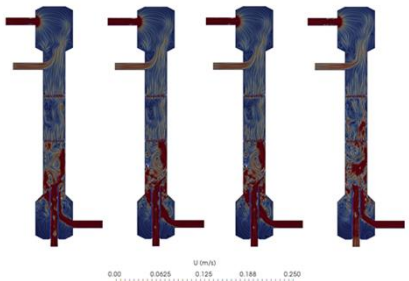

Fig. 4. *Velocity Field Profiles Within the Multiphase PSPEC, Visualised with a Surface LIC Filter at times 0 s, 0.25 s, 0.5 s, and 0.75s from Left to Right Respectively.*

Fig. 5. *Iso-surface of α Showing the Isolated Dispersed Phase Fluid.*

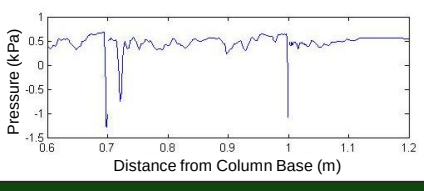

Fig. 6. *Pressure Plot across two Plates in the Y-Symmetry Plane for the multiphase Case at t = 0.25 s.*

7. Future Work

- Fix current issues presented by the modelling procedure thus far.
- Future work comparing multiphase RANS vs. LES CFD models for industrial column simulations will be published first quarter of 2018.
- Move towards three / four plate model using more advanced multiphase modelling methods: Eulerian-Eulerian, Population balance, Eulerian-Eulerian with mass transfer.

Acknowledgements

I would like to thank the UK's EPSRC and the GENIORS research consortium for taking interest in this project and funding this research. Additionally, I would like to thank the University of Leeds Advanced research computing (ARC) team for providing and maintaining the high performance computing facilities that were utilised throughout this project.

The University of Nottingham

UNITED KINGDOM · CHINA · MALAYSIA

Viscous Gas-Liquid Flows in vertical Pipes

Abubakr Ibrahim, Buddhika Hewakandamby, Barry J. Azzopardi

Introduction

High viscosity hydrocarbons have gained more attention owing to the increasing energy demand around the world and depletion of lighter reserves. When gas and liquid are introduced into a pipe, both phases arrange themselves in very random structures, as a result of interaction of very complex dynamic forces that are heavily dependent on the physical properties of the fluids being handled.

Little is known about two-phase flow characteristics in large diameter vertical pipes. Even less is known about the effect of viscosity on these characteristics. Limited number of investigations have been carried out to try to understand this effect. Regrettably, most of these investigations are either carried out using water solutions where surface tension changes dramatically with the change of viscosity (i.e. concentration of the solute). Or that the experiments are conducted in smaller diameter pipes, where the characteristics are remarkably different than larger diameters (D>100mm). Therefore most of published parametric studies are not conclusive and hence the confusion amongst the scientific community about the actual effect of viscosity on two phase vertical flows.

Aim and Objectives

- Aim is to study characteristics of viscous flows in vertical pipes
  - Effect of change of turbulence levels on evolution of phases
  - Effect of liquid viscosity increase on two-phase flow characteristics

Methodology

- The study is conducted in a 127mm pipe of 10.12m long. The rig is equipped with a positive displacement pump for the liquid (up to Uls 0.86m/s) and the gas is injected off the main lab compressors (up to Ugs 2.17m/s). A two planes ECT is fitted at 15D from the injection point. Another twin planes ECT is installed at 63D from the injection point followed by a WMS at 65D from injection. Figure 1 shows a drawing of the rig. A 5cP silicone oil is used in this experimental campaign.

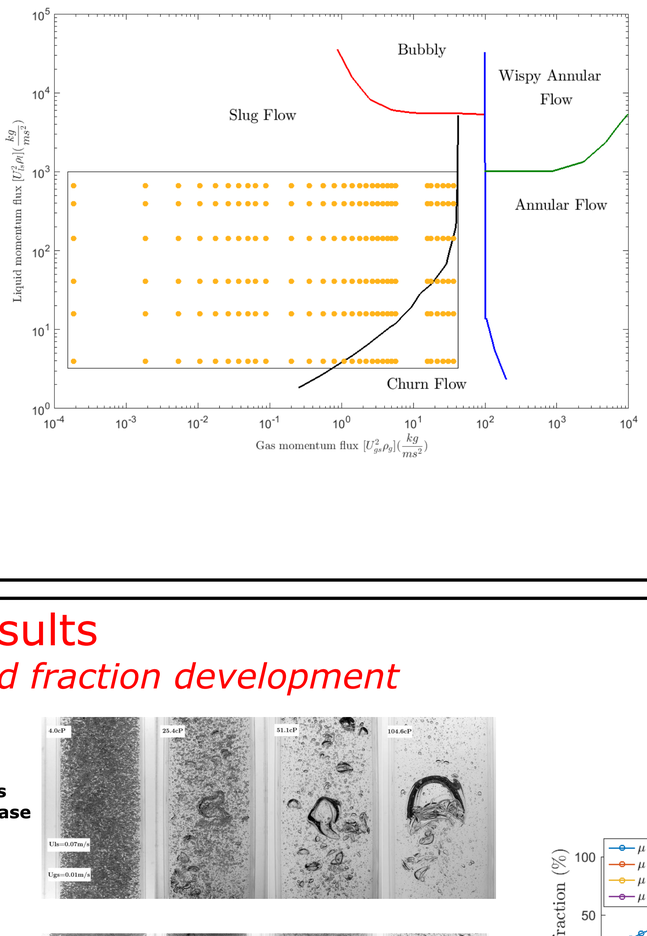

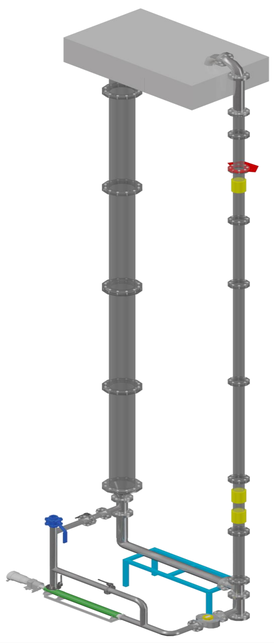

Results

Void fraction development

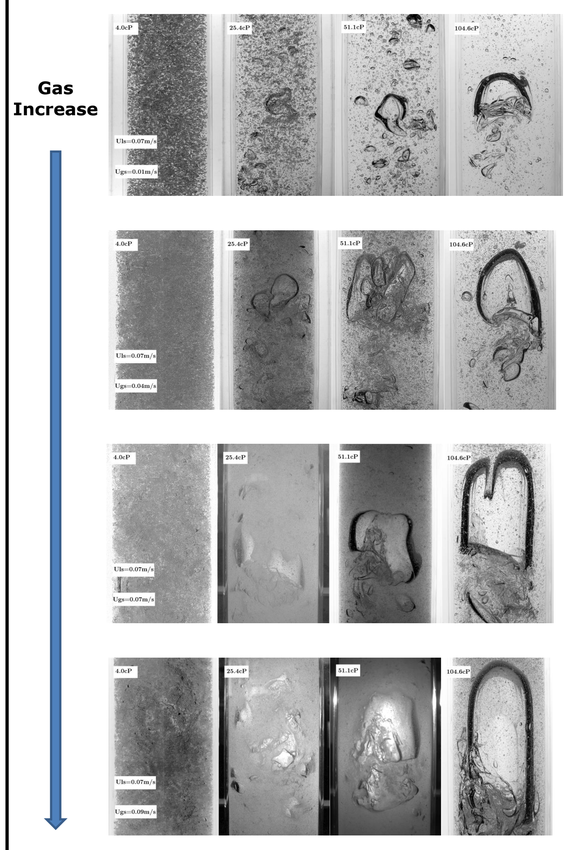

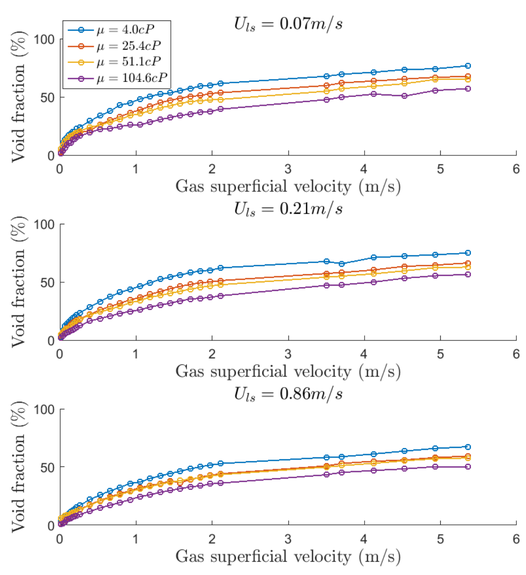

Spatio-temporal Images

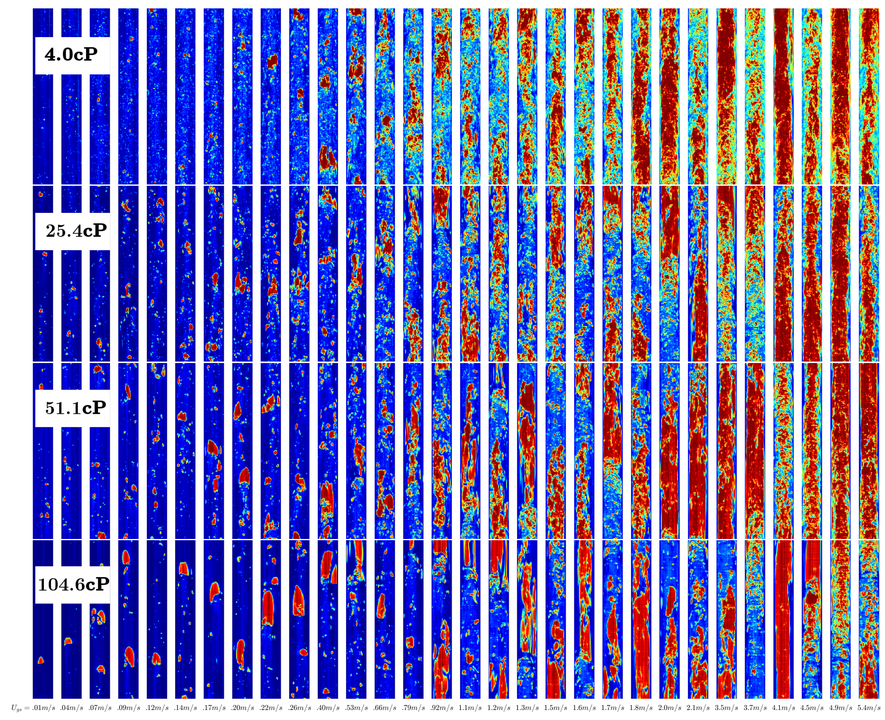

Pressure Gradient & Bubble Size

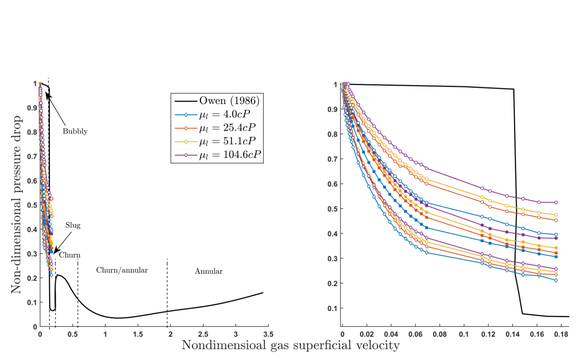

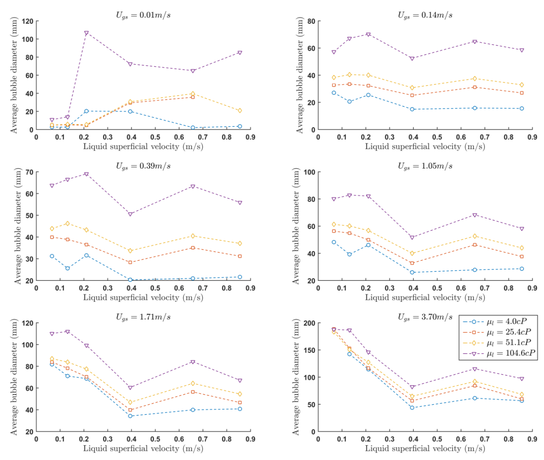

Outcome

- New unique data is generated for viscous flows in vertical large diameter pipes
- Improved closure models developed for various multiphase flow aspects

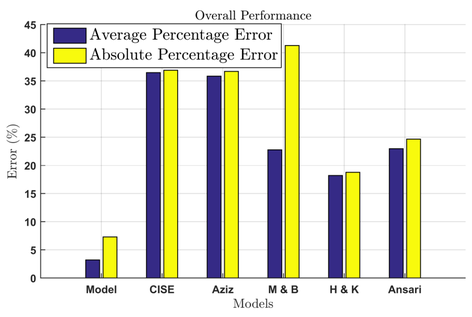

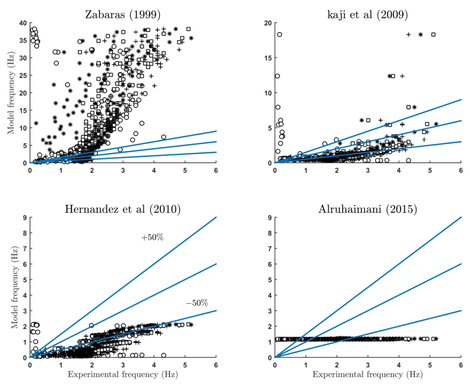

Acknowledgement

- This project was supported by Statoil company under the auspicious of TMF consortium and the Dean of Engineering Research Excellence.

Viscous Fingering in Deformable Systems

Jian H. Guan, Christopher W. MacMinn

Department of Engineering Science, University of Oxford

1. Classic viscous fingering

Viscous fingering (VF) is a classical hydrodynamic instability that occurs when a fluid is injected into a porous medium or Hele-Shaw cell containing a more viscous fluid[1] (Fig.1).

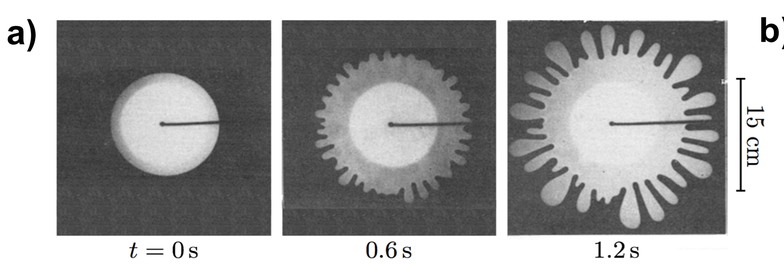

Fig.1: a) A classic example of viscous fingering in a Hele-Shaw cell[1]. b). Schematic of viscous fingering in a Hele-Shaw geometry.

2. Key parameters in VF

The extent of the fingering in a Hele-shaw geometry is dependent on three factors: flow rate, ***Q***, gap thickness, ***H***, and viscosity ratio between the invading (white)and defending fluid (blue), $\boldsymbol{\mu}$. (Fig.3)

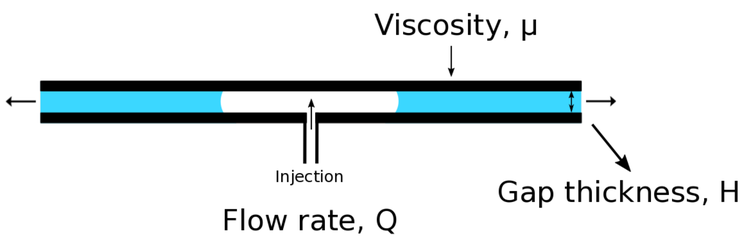

Fig. 3: Schematic showing the key variables in a VF experiment.

4. Volumetric Confinement → Gap gradient → Suppression of VF

In this work, we restrict the volumetric expansion of the flow area using a deformable elastic top boundary which is volumetrically confined. Any upward deformation near the injection will result in downward displacement else where. (Fig.6).

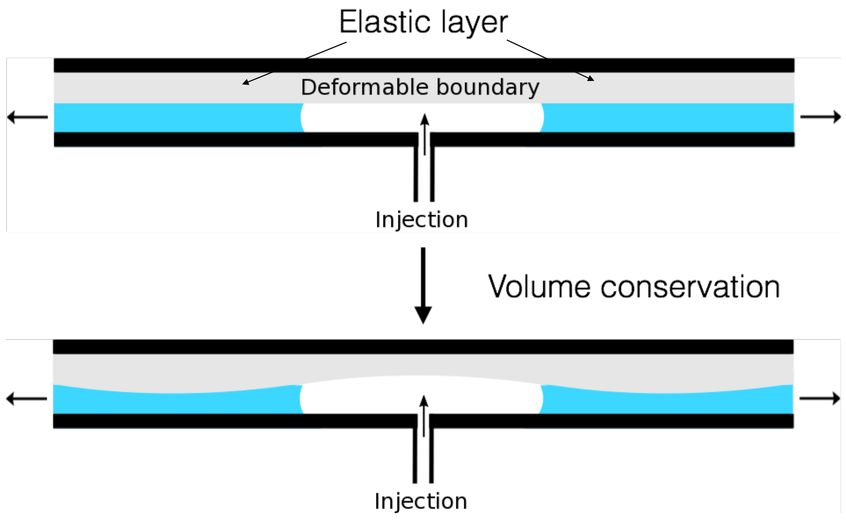

Fig. 6: Hele-Shaw cell with a deformable upper boundary allowing for a volumetrically confined flow area.

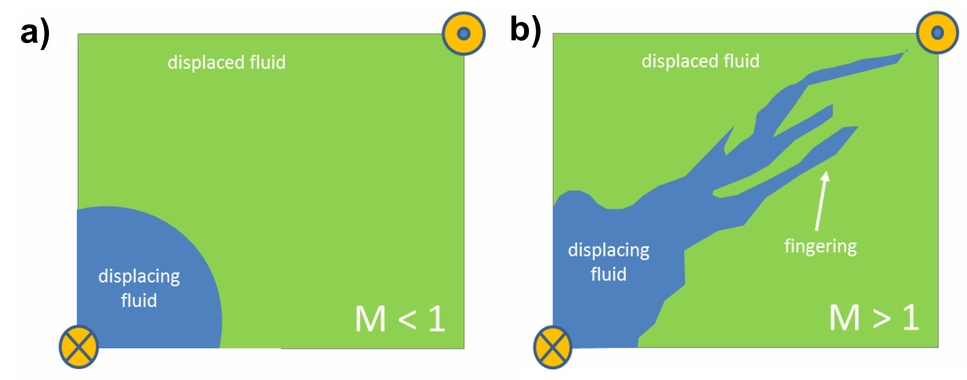

Fig.2: Illustrative cases for a) stable and b) unstable displacement of one fluid by another fluid where M is the mobility ratio.

Viscous fingering can be desirable in mixing in microfluidic devices but undesirable in oil recovery (Fig.2).

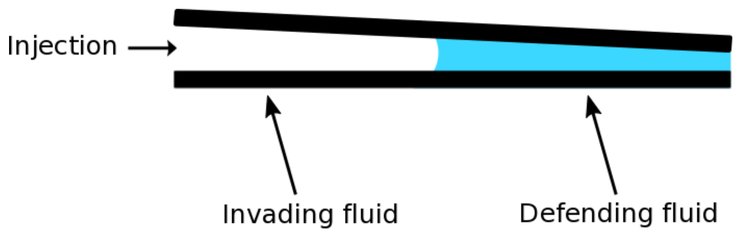

Fig. 4: Hele-Shaw cell with a negative gap gradient.

3. Supressing VF → Gap gradient → Volumetric expansion

It has been shown that viscous fingering can be supressed using a negative gradient in the gap thickness of the Hele-Shaw geometry[2] (Fig.4). It was further shown that, using a elastic top boundary, a negative gradient can be created by allowing for a volumetric expansion of the flow area[3] (Fig.5).

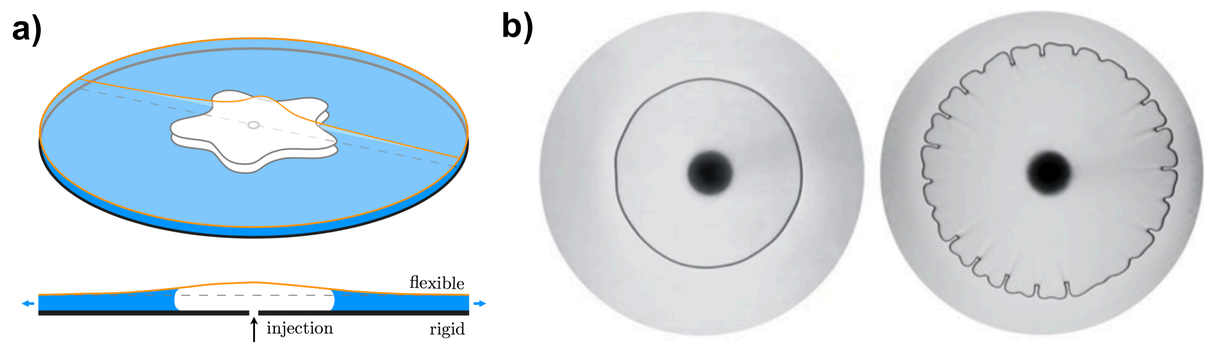

Fig. 5: a) Schematic of a Hele-Shaw cell with a elastic top boundary, b) Suppressed VF at different injection flow rate.

5. Non-monotonic behaviour

We find that softness does not simply suppress VF, but rather has a non-monotonic impact on VF (Fig.7a). We hypothesize that this results from the interplay between the wavelength of the deformation and the wavelength of the hydrodynamic instability (Fig.7b).

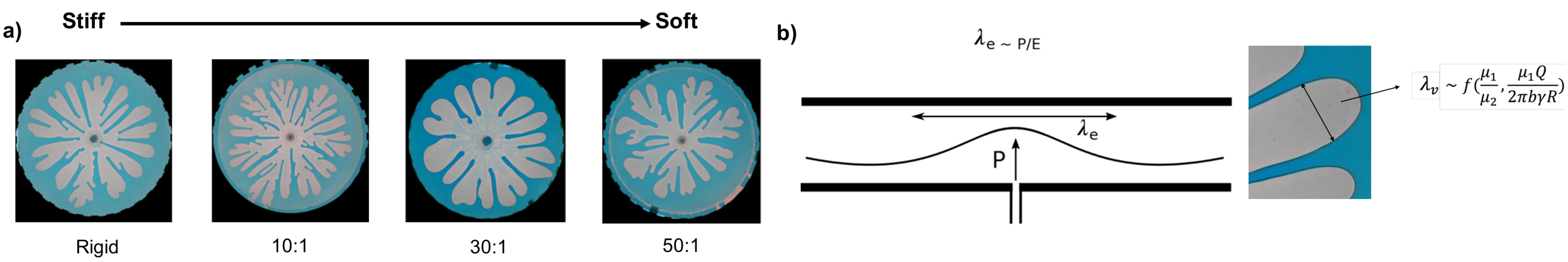

Fig. 7: a). Different final VF patterns in different Hele-Shaw cells of varying softness, b). Schematic showing the elastic and hydrodynamic length scales.

6. Summary

We show that a deformable but volumetrically confined system shows non-monotonic VF behaviours, which we suspect is a result of the interplay between elastic and hydrodynamic length scales.

References

1. T. Maxworthy. *Physical Review A*, 1989
2. Zhao *et al. Physical Review A, 1992*
3. Puzović *et al. Phys. Fluids, 2014*

Acknowledgements

JHG would like to acknowledge EPSRC for funding.

EPSRC

UNIVERSITY OF OXFORD

Heat and Mass Transfer of Cryogenic Solid-Liquid Flow

Yijian Li[1,2,*], Jun Xia[1], Junji Shinjo[3], Tao Jin[2], Tassos Karayiannis[1]
1. Brunel University London, UK; 2. Zhejiang University, China; 3. Shimane University, Japan.
yijian.li@brunel.ac.uk

◆Introduction

Cryogenic slurry is the low temperature two-phase fluid with solid particles suspended in the liquid, such as slush hydrogen and slush nitrogen. Slush hydrogen has been considered as a potential propellant for spacecraft in place of liquid hydrogen. Compared with subcooled liquid hydrogen, it increases density by 16-20%, which can help improve the tankage and thus reduce the dry weight of the vehicle.

◆Objectives

- Investigate the effect of flow velocity and solid fraction on the heat transfer and flow friction of slush nitrogen.
- Investigate the mechanism of interfacial heat and mass transfer.
- Provide the guidance for the design of HTS cooling system.

◆Experimental apparatus

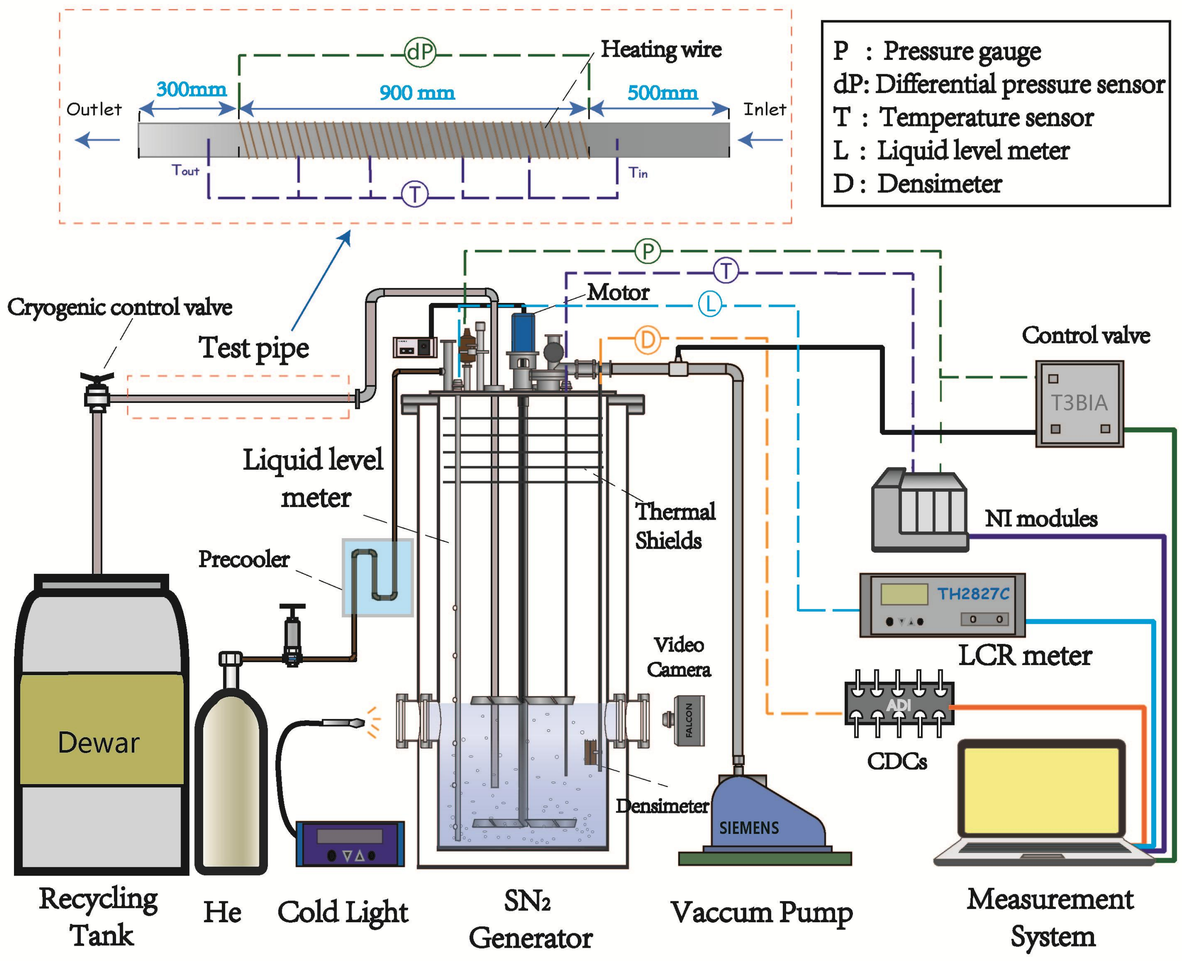

◆Experimental results

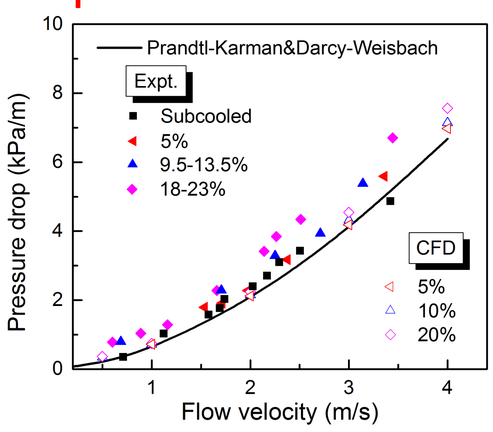

Pressure drop

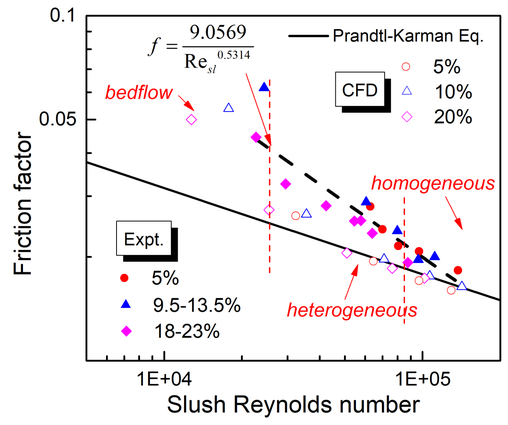

Friction factor

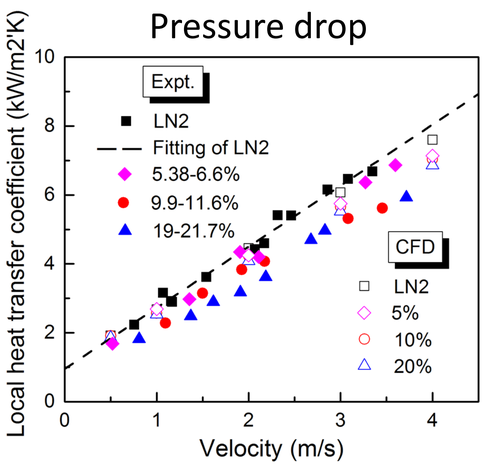

Heat transfer coefficient

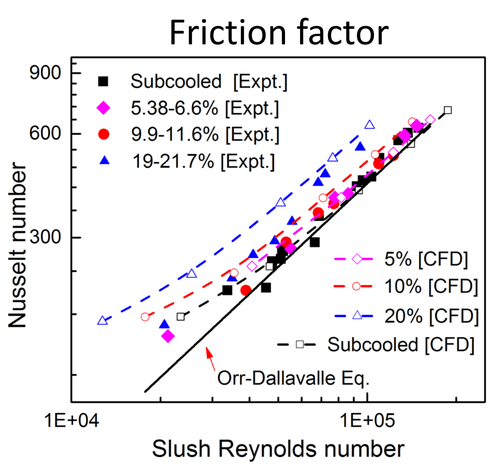

Nusselt number

Empirical correlations

$$f = \frac{9.0569}{\mathrm{Re}_{sl}^{0.5314}} \quad \left(2\times10^4 < \mathrm{Re}_{sl} < 1.5\times10^5\right)$$

$$Nu_{sl} = 0.086 Re_{sl}^{0.71} Pr_{sl}^{1/3} \left(\frac{\mu_l}{\mu_{lw}}\right)^{0.14} \quad \left(1.1\times10^4 < \mathrm{Re}_{sl} < 1.1\times10^5\right)$$

◆Numerical solver

- Governing equations: Navier-Stokes for liquid phase, Newton motion law for solid phase.
- Numerical methods: CIP for advective phase, CUP for source term [1].
- Surface capture: MARS (multi-interface advection and reconstruction solver) [1].
- Interphase interaction: embedded boundaries treatment [2].
- Validation: natural convection with a fixed particle [3].

◆Case set up

- 2-D Square domain (side length L=1.25x10^{-4} mm, grid numbers 100 x 100).
- Particle size: d=0.2 L, initial centre position: (50,20).
- Initial fluid velocity (u, v) = (0, 10 m/s) at y=0.
- Open boundaries.
- Properties of liquid and solid nitrogen:

	T (K)	ρ (kg/m^3)	Cp (J/kg/K)	μ (Pa·s)	k W/m/K	h_l (kJ/kg)
solid	63	1026.5	1.66	-	0.2	25.56
liquid	77	867.86	2.0	2.92e-4	0.162	-

◆Preliminary DNS results

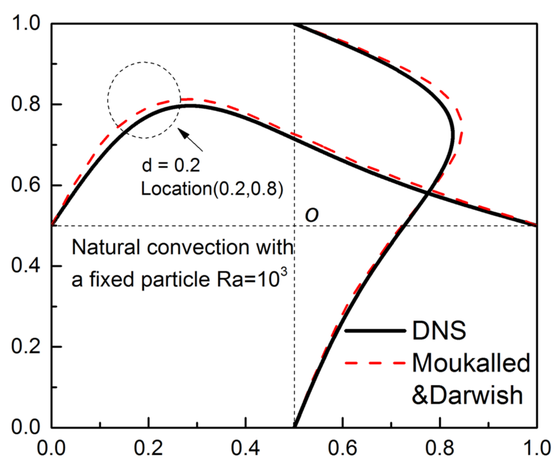

Validation: Temperature profiles on the vertical and horizontal centerlines

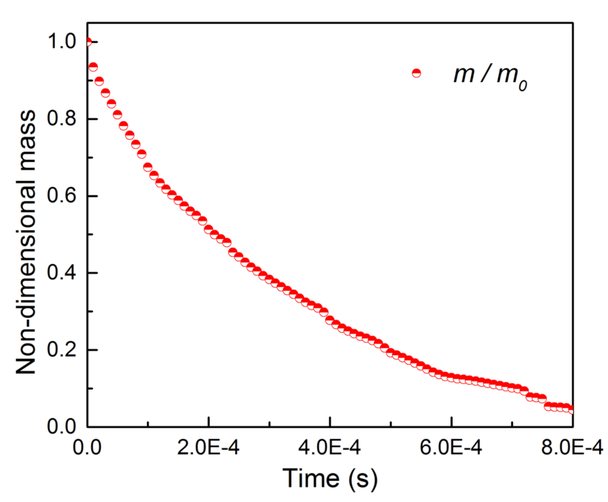

Decreasing mass of a fixed nitrogen particle melting in the LN_2 pool

Solid fraction & flow field

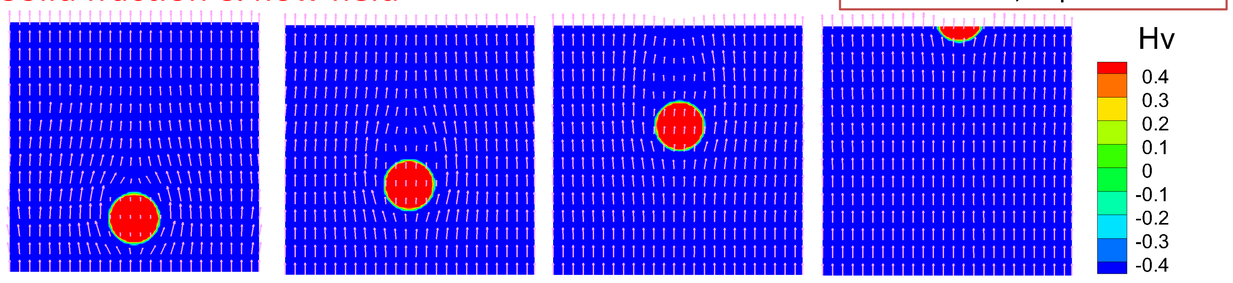

Temperature

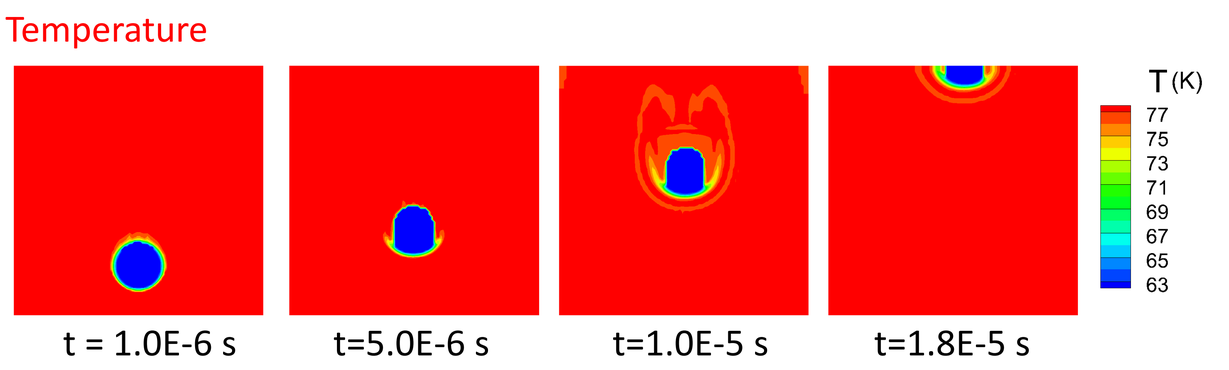

Time t = 1.0E-6 s t=5.0E-6 s t=1.0E-5 s t=1.8E-5 s

◆Future plans

➢Two-particle simulation (to consider particle-particle and particle-wall interactions)

➢A particle group under convective heating and compare with experimental data.

◆Acknowledgments

Financial support: China Scholarship Council & EPSRC.

◆Reference

1. Shinjo J, Xia J, Ganippa L C, et al., *J. Fluid Mech*., 2016, 793: 444-476.
2. Yabe T, Xiao F, Utsumi T, *J. Computational Physics*, 2001, 169(2):556-593.
3. Moukalled F, Darwish M, *Numerical Heat Transfer Part B Fundamentals*, 1997, 31(1):111-133.

Intensified extractions using "green solvents"

Dr Dimitrios Tsaoulidis and Prof Panagiota Angeli

Department of Chemical Engineering, University College London, WC1E 7JE, UK

e-mail: d.tsaoulidis@ucl.ac.uk ; p.angeli@ucl.ac.uk

Development of small scale extractors

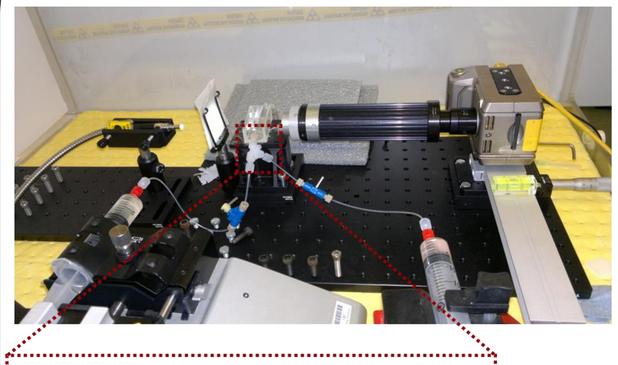

Experimental conditions:

- Channels sizes: 0.2-3.2 mm ID
- Channel material: Teflon and Glass
- Wide range of Q_{mix} and flow rate ratios
- Room temperature

Fluids:

- HNO_3/U(VI)solutions
- TBP/IL (30% v/v)

Techniques: *High-speed imaging, Shadowgraphy, Laser-based PIV, UV-Vis spectroscopy*

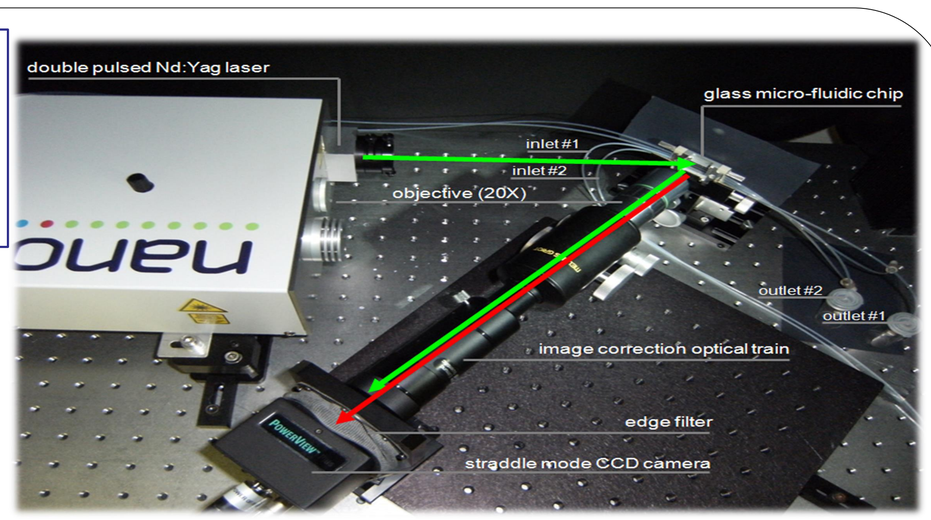

Advanced Particle Image Velocimetry techniques *are used to study flow and circulation patterns in the two-phase system.*

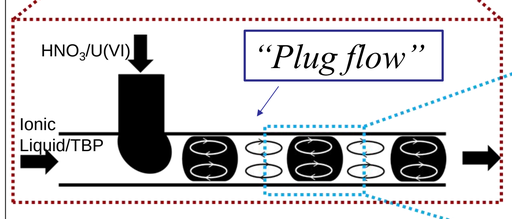

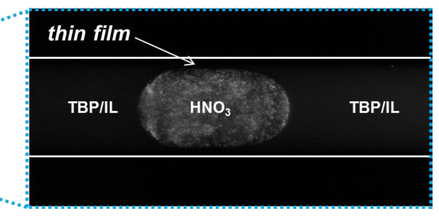

Velocity data are obtained for both phases

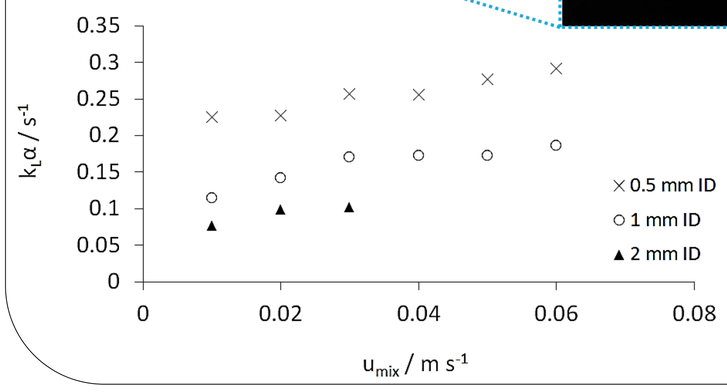

Mass transfer coefficients ***($k_L\alpha$)*** *in the small-scale systems were 1 to 2 orders of magnitude higher than in conventional contactors!!*

Velocity fields

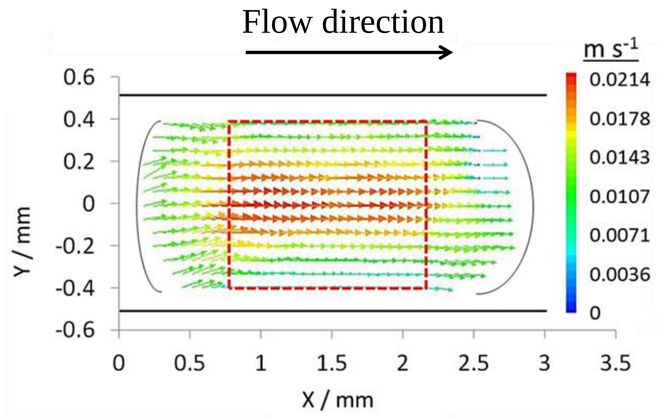

Velocity profiles

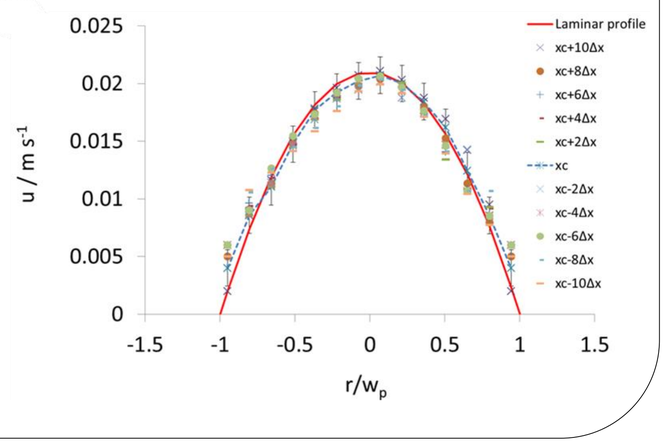

Lack of knowledge OR excess of fear...?

Nuclear Power…

- low-carbon technology with comparable emissions to other renewable forms of energy.
- reliable and safe; best safety records per unit of energy.

Public concerns...

- The management of the irradiated spent nuclear fuel, which can remain toxic for thousands of years and cannot be stored in containers due to corrosion issues.
- Weapon proliferation from the nuclear waste.

Solution…

Development of liquid-liquid Intensified Extraction Technologies for recovery of Uranium and Lanthanides to improve energy and material efficiency, and safety. The intensified technologies will also benefit from the application of environmentally friendly solvents (**IONIC LIQUIDS**)

- ✓ **Negligible volatility & flammability**
- ✓ **High resistance to radiation**
- ✓ **High distribution coefficients**

Development of intensified impinging jet-mixers

- $\mathbf{d_j}$: Internal diameter of nozzle= 0.25-0.5 mm
- **D**: Internal diameter of channel= 2- 3.2 mm

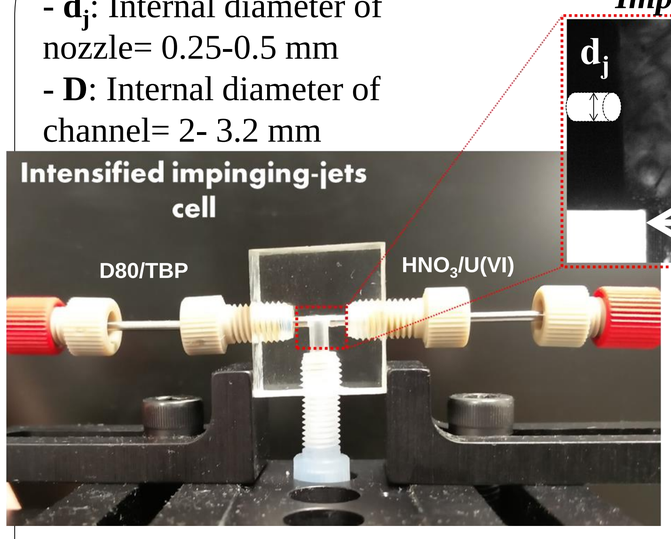

- High energy dissipation in the impingement zone

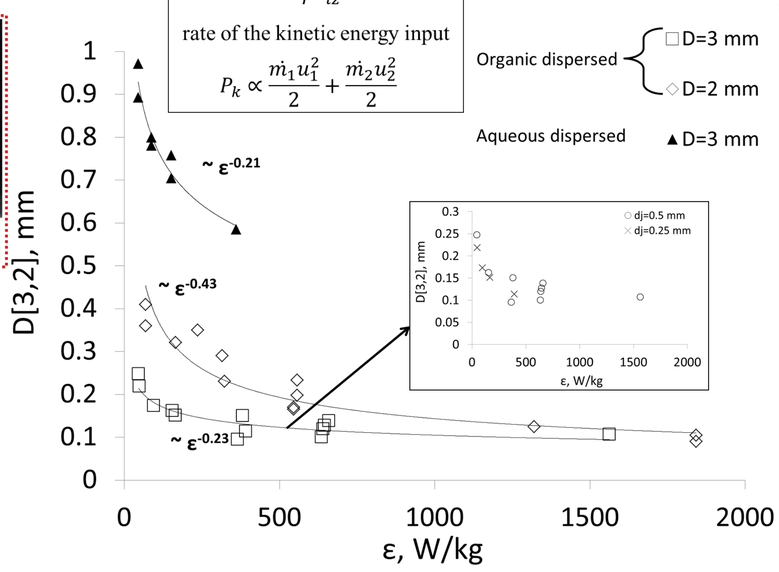

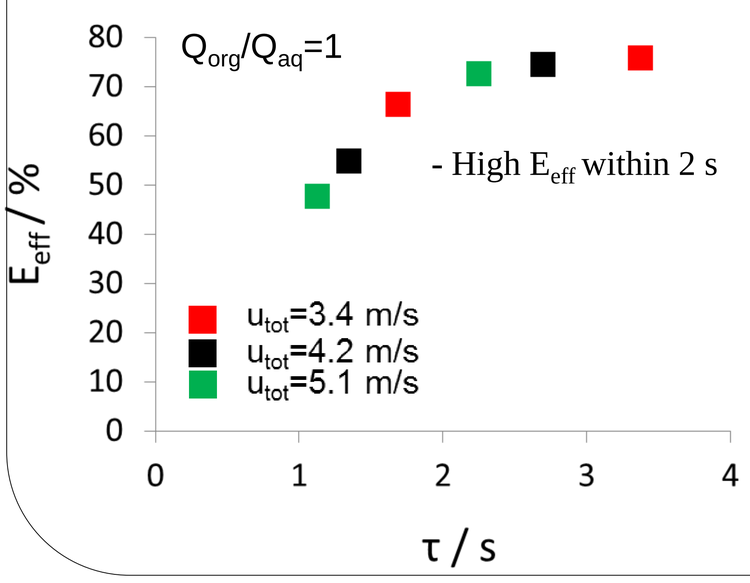

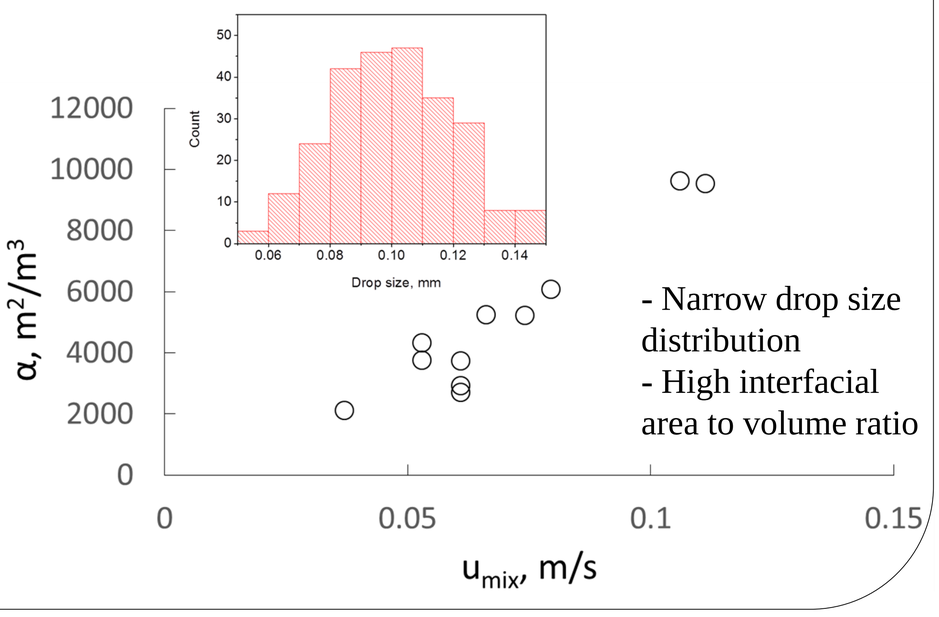

- Narrow drop size distribution
- High interfacial area to volume ratio

Modelling and flow process optimization

 # Development of 2-D model to predict hydrodynamics and mass transfer in the liquid-liquid systems

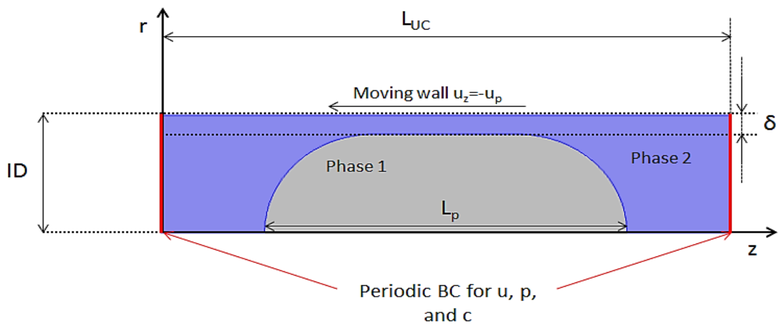

Concentration profile

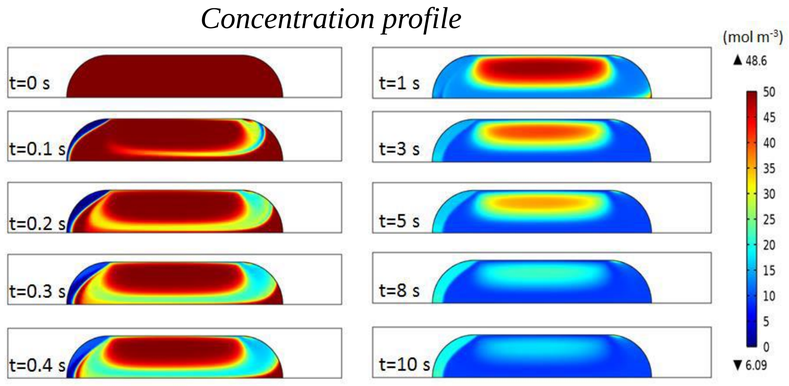

 # Development of mathematical models for multicomponent extractions in small channels, relevant to SNF reprocessing

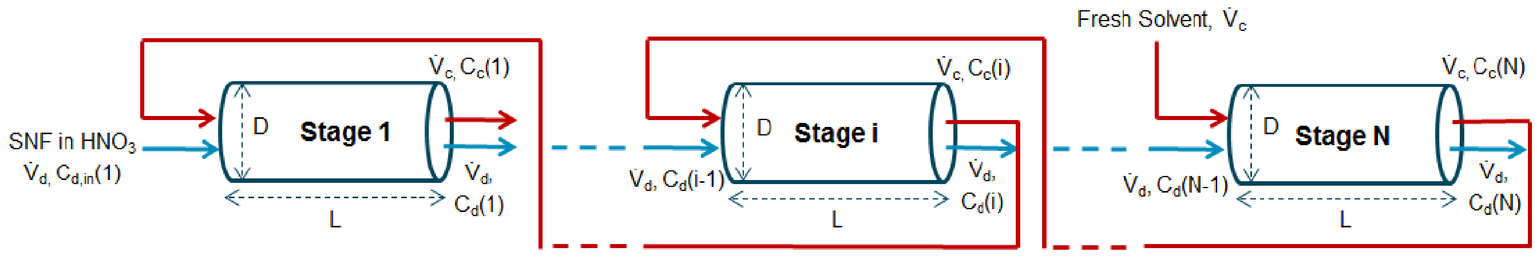

 # Development of scaling up aspects - manifolds

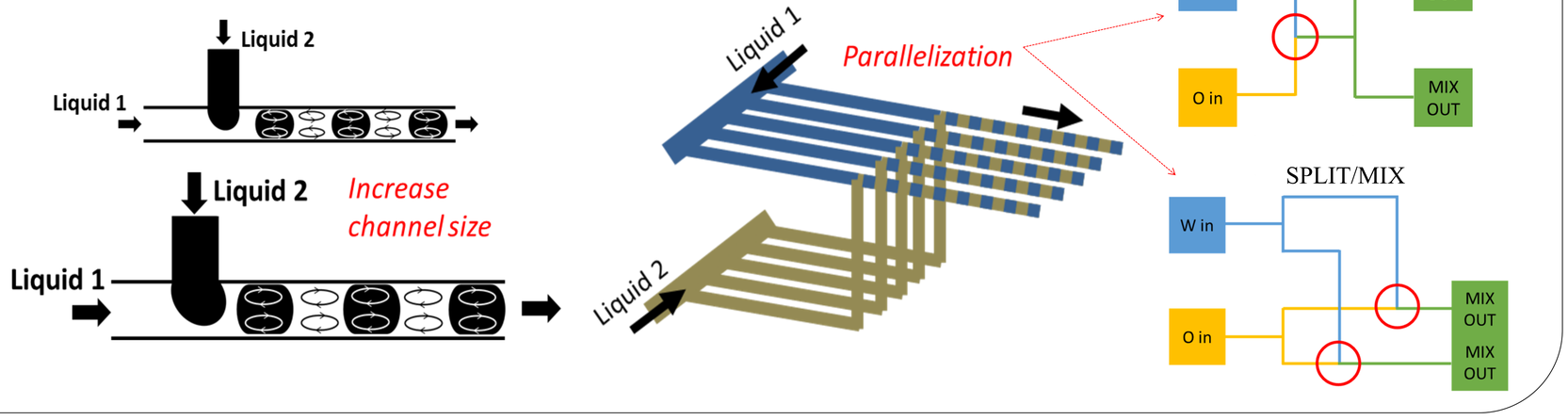

THE UNIVERSITY of EDINBURGH

EPSRC Pioneering research and skills

Liquid Distribution and Fraction Measurement in Counter Flow Packed Column by Electrical Tomography

Yunjie Yang, Hao Wu, Jiabin Jia, Bill Buschle and Mathieu Lucquiaud

Agile Tomography Group, School of Engineering, The University of Edinburgh, Email: jiabin.jia@ed.ac.uk

Introduction

- Random or structured packing materials are used in gas separation/carbon capture applications to prolong reaction time and increase contact areas.
- Quantifying and modifying the effectiveness of the packing (i.e. wetted area) is challenging, especially at full scale off-spec conditions.
- This work investigates the potential of Electrical Tomography as an ***in-situ*** monitoring and analysis tool for gas separation and carbon capture applications.

Electrical Capacitance & Resistance Tomography

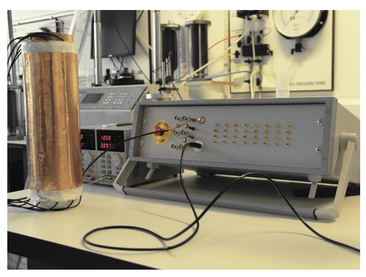

ECT System

ERT System

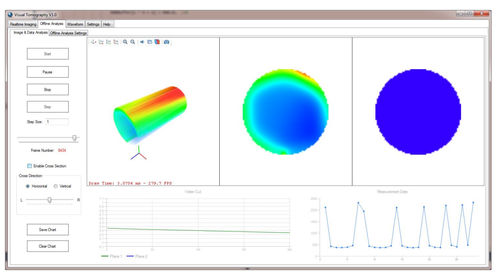

Visual Tomography

ECT system: 200 kHz, 1000 fps; ERT system: 10 kHz, 625 fps; Visual Tomography: Real-time 3D Imaging Software.

Method & Model

Measurement principle of ECT

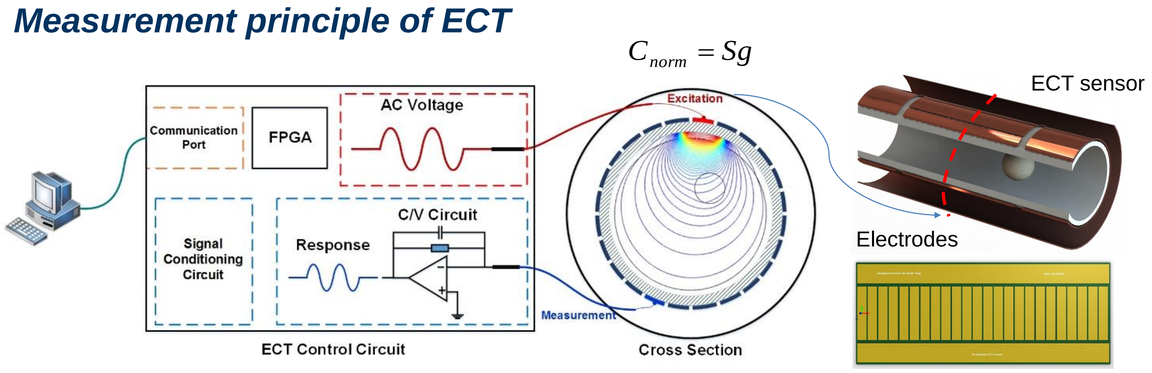

Liquid fraction calculation model

$$C_{norm} = \frac{C_{mea(j)}}{C_{ref(j)}}, \quad j = 1,2,\ldots,P$$

$$\frac{C_{mea(j)}}{C_{ref(j)}} \approx \frac{\sum_{k=1}^{w} \varepsilon_{mea(k)} s_{j,k}\left(\varepsilon_{mea(k)}\right)}{\sum_{k=1}^{w} \varepsilon_{ref(k)} s_{j,k}\left(\varepsilon_{ref(k)}\right)}$$

$$\frac{\varepsilon_{mea(k)}}{\varepsilon_{ref(k)}} \approx \frac{\sum_{j=1}^{P} \frac{C_{mea(j)}}{C_{ref(j)}} s_{j,k}\left(\varepsilon_{ref(j)}\right)}{\sum_{j=1}^{P} s_{j,k}\left(\varepsilon_{ref(j)}\right)}$$

$$LMR \approx \frac{\varepsilon_{mea(k)} - \varepsilon_{ref(k)}}{\varepsilon_{mea(k)} + 2\varepsilon_{ref(k)}} = \frac{\varepsilon_{mea(k)} / \varepsilon_{ref(k)} - 1}{\varepsilon_{mea(k)} / \varepsilon_{ref(k)} + 2}$$

⇨ *Liquid in Mixture Ratio*

Calculation procedure for ECT measurement in packed column

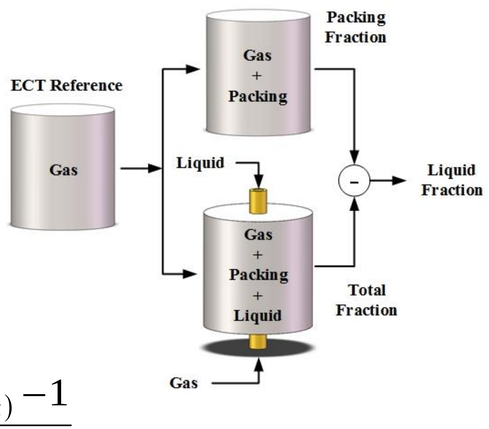

FEM Simulation

2D simulation models with different packing structure (two-phase)

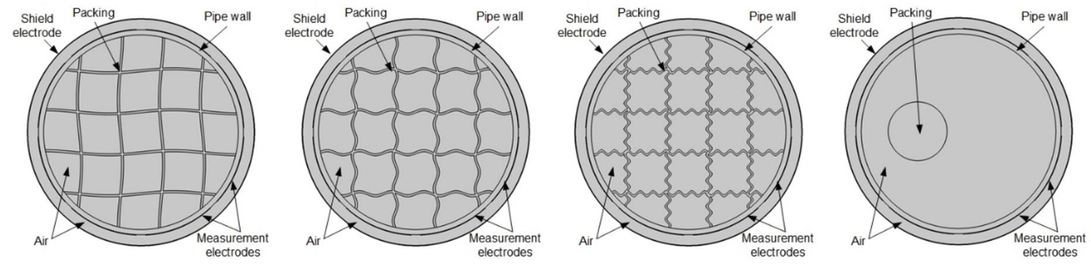

Tab.1. Calculation results for 2D simulation model

Packing structure	a	b	c	d
Packing area (mm^2)	2596	2596	2601	2596
Packing fraction	9.156%	9.156%	9.173%	9.156%
Calculated packing fraction	7.80%	7.57%	7.88%	7.81%
Calculation error	1.356%	1.586%	1.293%	1.356%

3D simulation model of packed column (three-phase)

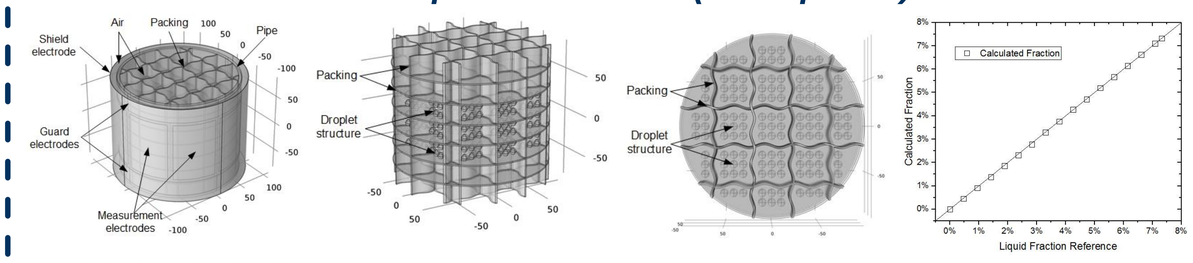

Model of packed column *Packing and liquid droplets in simulation* *Calculated liquid fraction*

Experiment Results

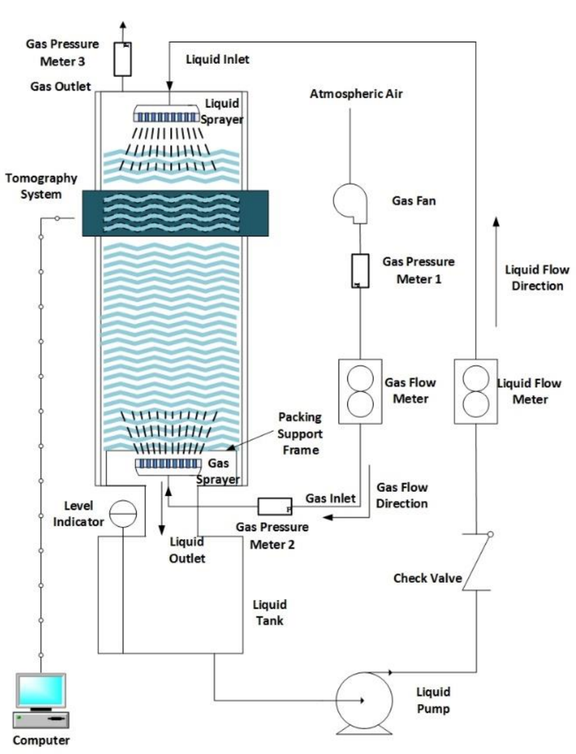

Pilot scale experimental flow loop

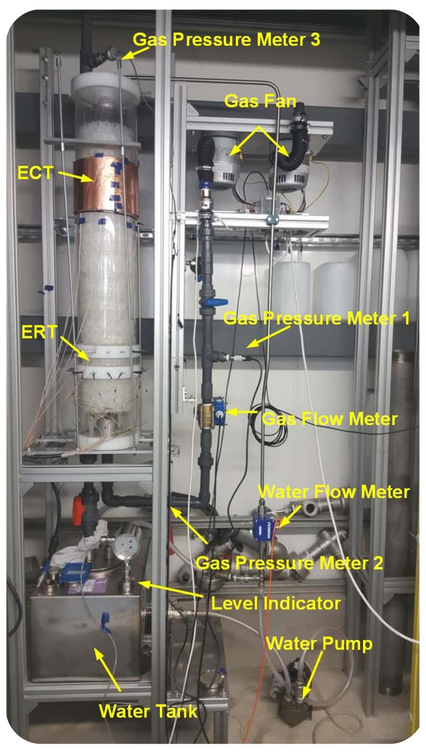

Sulzer Mellapak 250Y structured packing

Liquid sprayer

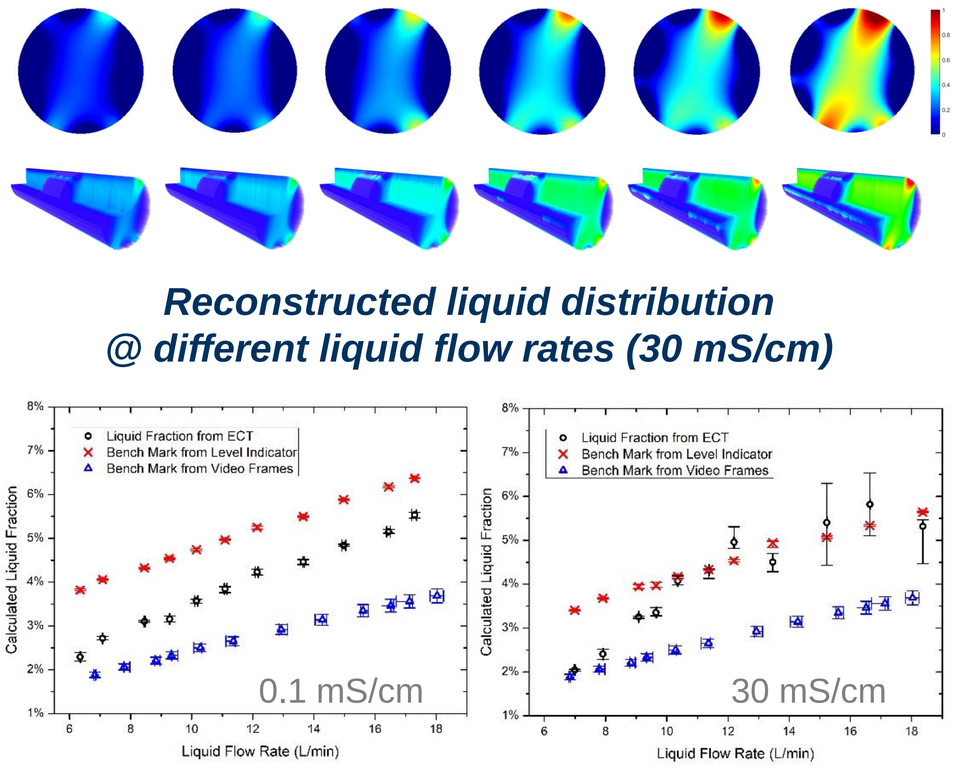

Reconstructed liquid distribution @ different liquid flow rates (30 mS/cm)

Calculated liquid fractions by ECT vs. reference

Conclusions and Future Work

- Simulation and experiments verified that electrical tomography together with the developed calculation method and model could be used to measure the liquid fraction quantitatively and reconstruct the gas-liquid distribution qualitatively in the counter flow packed column.

References

- Wu. H, Yang. Y, Jia, J., etc. (2017). Liquid Fraction Measurement in Counter Current Flow Packed Column by Electrical Capacitance Tomography. Submitted to *Chemical Engineering Journal*.

Microwave Sensor For Watercut in Multiphase Flow

Prafull Sharma
PhD Supervisor: Dr Liyun Lao, Prof Gioia Falcone
SWEE, Cranfield University

Cranfield UNIVERSITY

Introduction

The objective of this project is to develop a sensor for Watercut measurements in three phase flow in Oi & Gas production

Watercut measurement technology in multiphase flow by incorporating effect of salinity and hydrate inhibitors. Liquid film thickness in wetgas is also feasible. The technology can be a part of Multiphase flow meter or a stand alone watercut meter

Commercialization: Cranfield university is looking for industry support in form of sponsorship, field tests, data sharing.

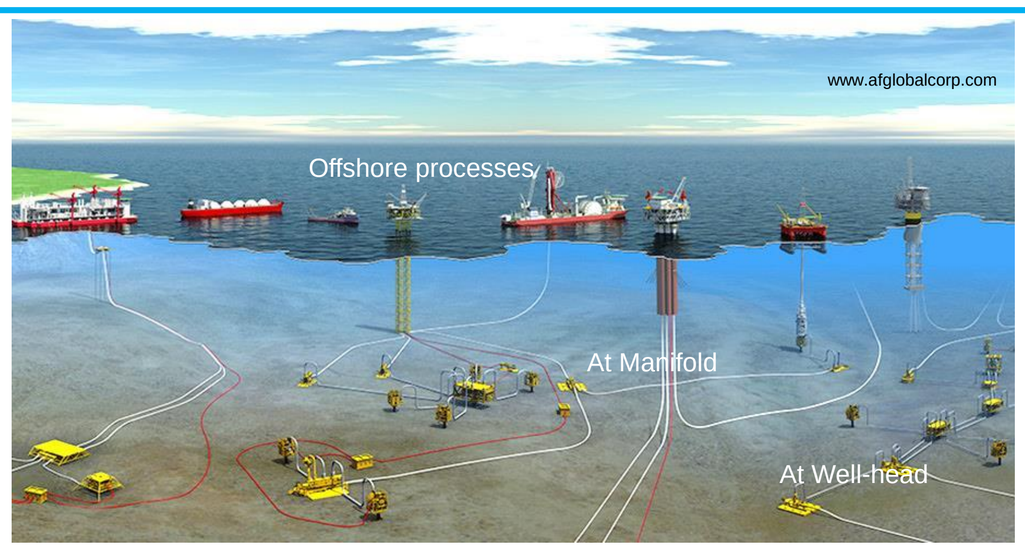

Measurement principle

Why microwaves ? Dielectric contrast between oil and water (2.3 : 80)

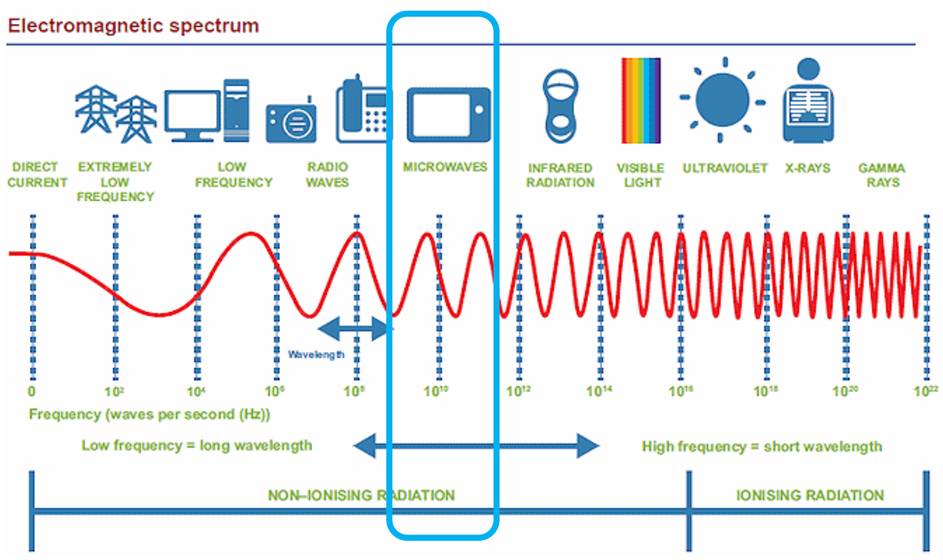

Operating frequency 1 GHz-5 GHz

Transmission attenuation and phase is affected by the permittivity of oil and water mixture

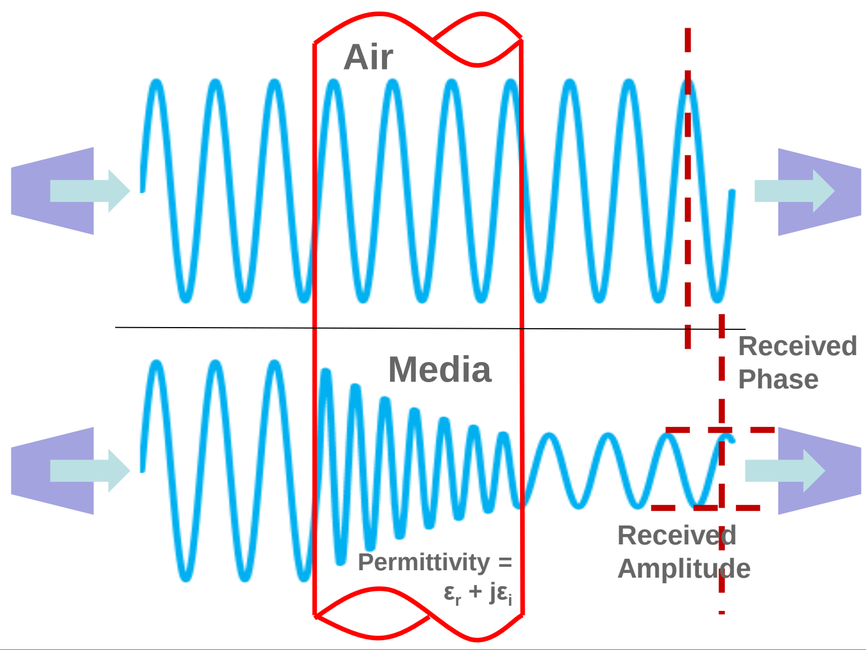

Estimation Steps

Based on fluid properties for robustness

Oil and water permittivity are affected by their constituents. Accounting for hydrate inhibitors and salts promises to improve the accuracy of measurements

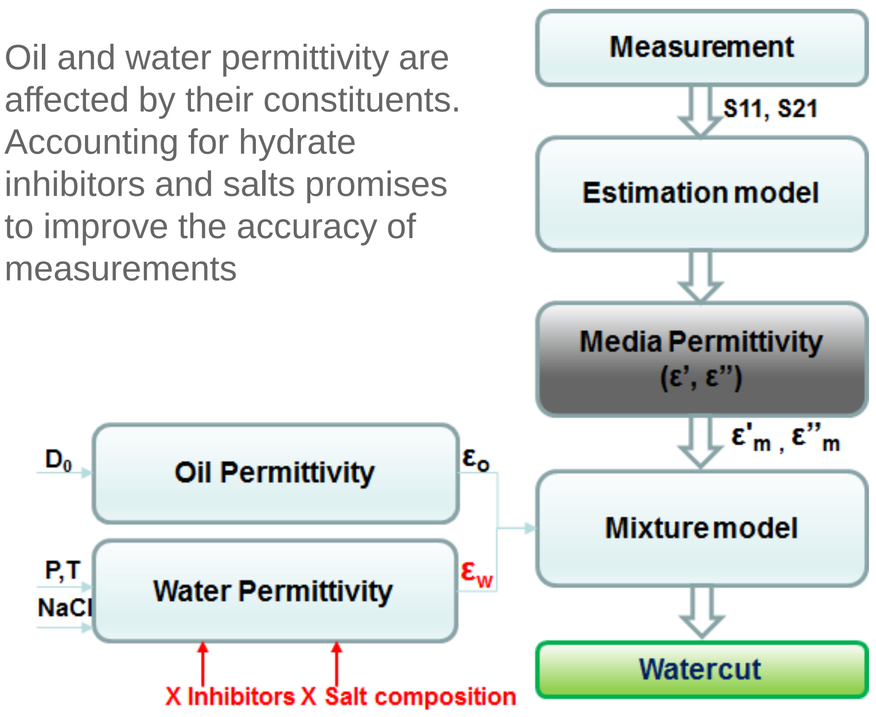

From Physics to Prototypes

Design iterations using simulations and experiments

➢ Concept

Current design can hold upto 30 bars

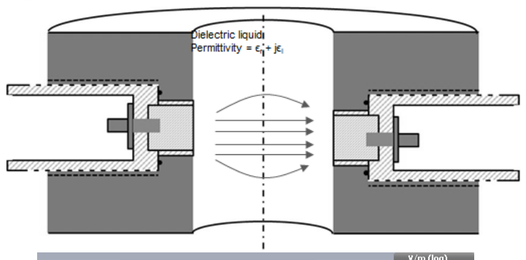

➢ EM simulations

Microwave frequency simulations to improve sensor design

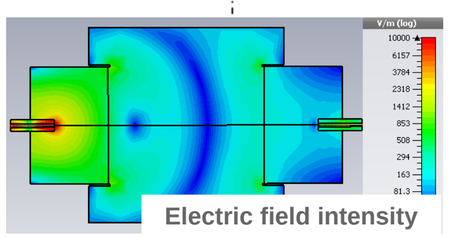

➢ Prototype

Initial prototype is being evaluated

Improve watercut and salinity measurement sensor technologies

www.cranfield.ac.uk

Contact:
prafull.sharma@cranfield.ac.uk
l.lao@cranfield.ac.uk

Front-Tracking Simulations of Stratified Wavy Air-Water flows using code BLUE

Dr. Aditya Karnik, Prof. Omar K. Matar
Department of Chemical Engineering, Imperial College London, United Kingdom

Introduction

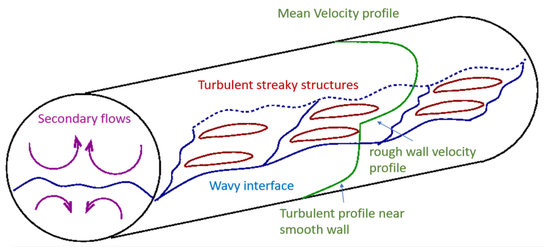

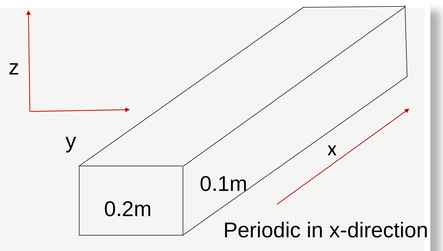

- Turbulent multiphase flows involving large-scale interfaces
- Deliver reliable numerical solutions within a reasonable time-scale
- Characterise the wave patterns
- Capture the turbulent structures residing on both sides of the interface

- Horizontal stratified co-current air-water flow
- Both phases are turbulent
- Stratified wavy regime

Code BLUE: a front-tracking code

- Highly accurate mass conservation
- DNS and LES capability
- Scalable to large number of cores

Blue setup

- Uniform grid in all directions
- Smagorinsky LES model

$$\mu_{sgs}^{k} = \rho^{k}(C_s\Delta)^2|\tilde{S}^{k}|$$

$C_s = 0.1$

Description of test cases

	CASE A	CASE B	CASE C
Air superficial velocity (m/s)	2.27	3.77	5.94
Water superficial velocity (m/s)	0.15	0.15	0.15
Mean Interface height (m)	0.038	0.0315	0.0215
Experimental Pressure drop (Pa/m)	2.1	6.7	14.8
Reynolds number (Air)	22,200	36,000	54,600
Reynolds number (Water)	48,800	51,200	55,400

Result and Discussion

Case A - Preliminary Results – Flow properties

$\Delta x^+ = \Delta y^+ = \Delta z^+ = 11$
(based on the air friction velocity at interface)

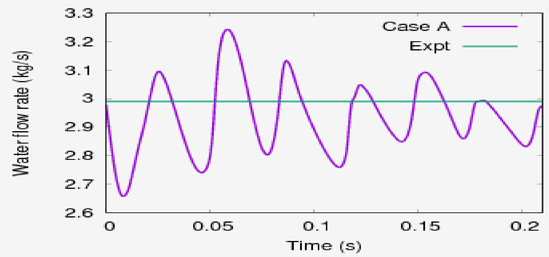

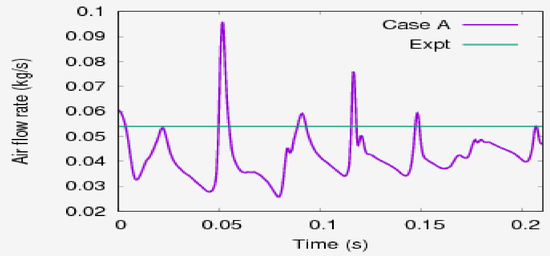

Case A - Preliminary Results – Mean velocity

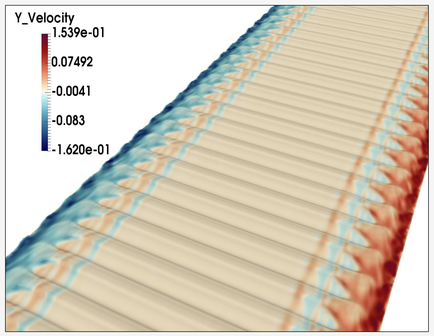

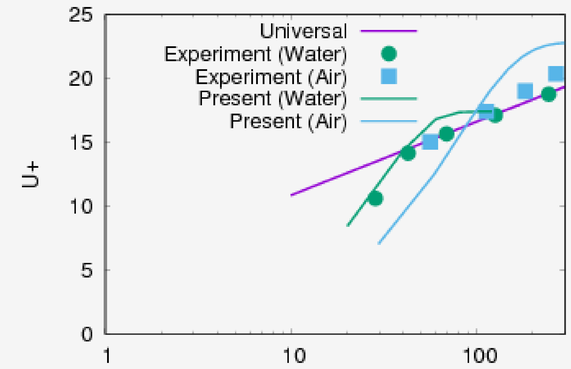

Case B - Preliminary Results – Flow properties

$\Delta x^+ = \Delta y^+ = \Delta z^+ = 23.5$
(based on the air friction velocity at interface)

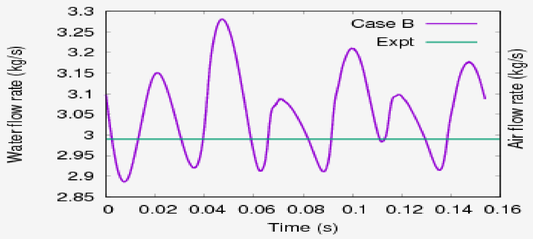

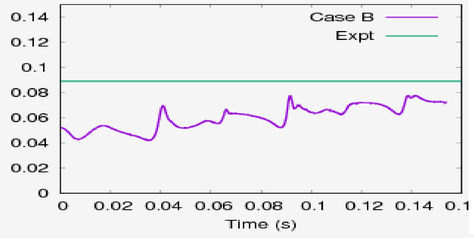

Wave amplitudes and roughness

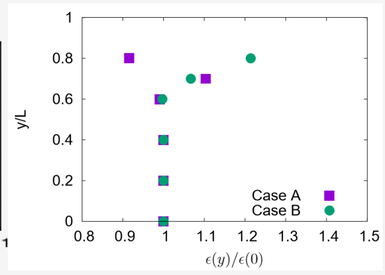

Summary

- Capture the secondary flows in the Y-Z plane
- Estimate average interfacial shear stress.
- Measure span-wise variation of wall shear stress

Acknowledgement

We would like to acknowledge the support of the Engineering and Physical Sciences Research Council, UK, through the Programme Grant MEMPHIS (EP/K003976/1).

References

- Fabre, Masbernat, Suzanne, Multiphase Science Technology, 3, 1987, 285-301.
- Yang, J., Narayanan, C., Lakehal, D. Nucl. Eng. Des., 2016.

Study of suspension fluid dynamics in complex oral health products (CORAL)

Rashid Jamshidi [a], Panagiota Angeli [a], Luca Mazzei [a], Stavroula Balabani [b], Manish Tiwari [b], Helen Wilson [c]

[a] Chemical Engineering, [b] Mechanical Engineering, [c] Mathematics, University College London

1. Introduction

Aim

This research aims to provide new fundamental insights into complex oral health formulations. Computational Fluid Dynamics (CFD), mathematical modelling and experimental studies are the tools used to tackle the associated challenges.

Objectives

- Characterization of the rheological behaviour of the suspensions involved in the process via experimentation and mathematical modelling.
- Derivation of rheological constitutive equations for these complex fluids.
- Formulation of a continuum model for the description of the suspension fluid dynamics and experimental validation of the numerical results.
- Scale-up and manufacturing issues. Development of continuous manufacturing strategies.

2. Rheological characterization

Spherical glass particles are suspended in glycerine. Shear thinning behaviour is observed at high solid concentrations.

The CFD model requires a shear and solid concentration dependent closure equation for the suspension viscosity.

Measurements such as those reported in this figure are essential for predicting the flow of non-Newtonian suspensions.

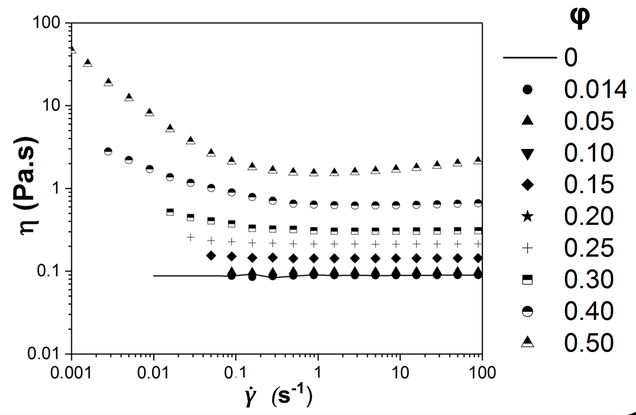

UCL Mechanical Engineering

3. Mathematical modelling

Analysis of the flow of Newtonian and non-Newtonian fluids around an isolated spherical particle. This study is required to investigate the fluid-particle interaction.
The cell model is adopted in this analysis.

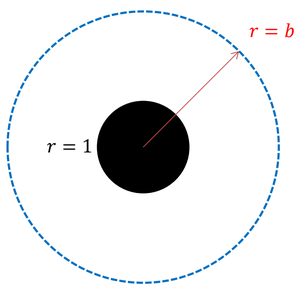

The model predicts the effective viscosity of a dilute suspension as a function of the solid concentration for 2nd order fluids.

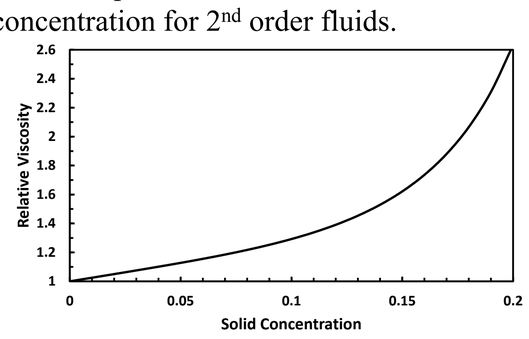

Study of the fluid dynamic interaction between two spherical particles in Newtonian and non-Newtonian fluids. This study is required to investigate particle-particle interactions.

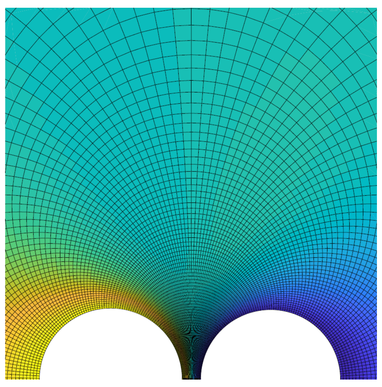

Velocity field around two approaching spherical particles in a 2nd order fluid.

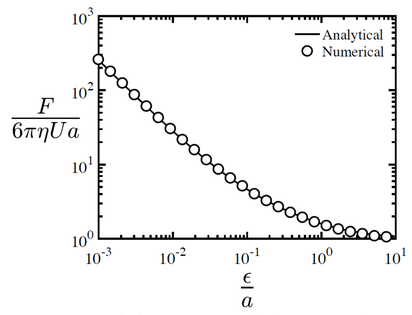

Force exerted by a particle on the other as a function of distance between them.

UCL Mathematics

4. CFD simulations

CFD can successfully predict the suspension flow characteristics, if satisfactory closures are adopted for the stress tensors of the phases and the fluid-particle interaction forces.
We use mixture modelling approach.

Continuity: $\partial_t \rho_m + \partial_{\boldsymbol{x}} \cdot (\rho_m \boldsymbol{u}_m) = 0$

Momentum: $\partial_t (\rho_m \boldsymbol{u}_m) + \partial_{\boldsymbol{x}} \cdot (\rho_m \boldsymbol{u}_m \boldsymbol{u}_m) = -\partial_{\boldsymbol{x}} \cdot (\boldsymbol{\sigma}_e + \boldsymbol{\sigma}_s + \boldsymbol{\sigma}_a) + \rho_m \boldsymbol{g}$

Diffusion stress: $\boldsymbol{\sigma}_a = \rho_m \omega_e \omega_s (\boldsymbol{u}_e - \boldsymbol{u}_s)(\boldsymbol{u}_e - \boldsymbol{u}_s)$

Slip velocity: $\boldsymbol{u}_e - \boldsymbol{u}_s = (1/\beta)[\varepsilon_e \partial_{\boldsymbol{x}} \cdot \boldsymbol{\sigma}_s - \varepsilon_s (\rho_s - \rho_m)(\boldsymbol{g} - D_t \boldsymbol{u}_m)]$

Test case 1:
Laminar flow of a dilute suspension in a pipe.

We predict pressure drop correctly when the mixture viscosity obtained from experiments is used in the model.

$$\tau(\varphi) + k(\varphi)\dot{\gamma}^{n(\varphi)-1}$$

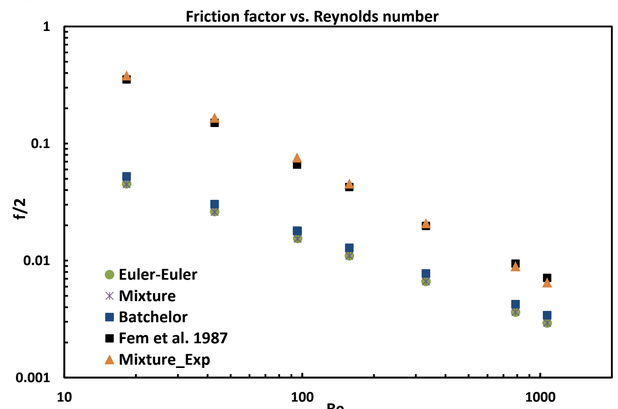

Test case 2:
Laminar flow of a dense suspension through an abrupt expansion.

The model captures the non-uniform profile of solid concentration in complex geometries.

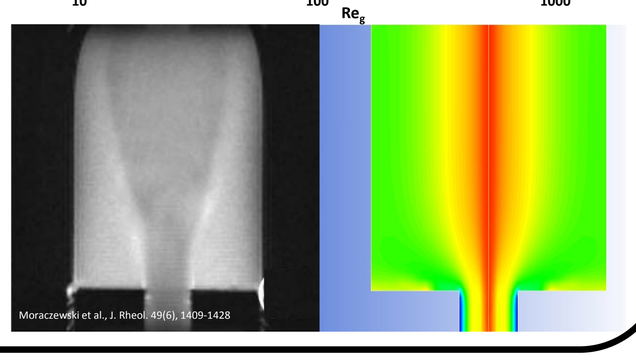

UCL Chemical Engineering

5. Experiments

Taylor-Couette flow.

The flow between two concentric cylinders is characterized via PIV and measurements of the torque.

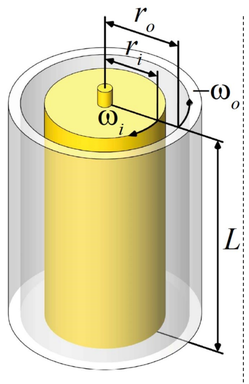

Flow Structure for a Newtonian Fluid

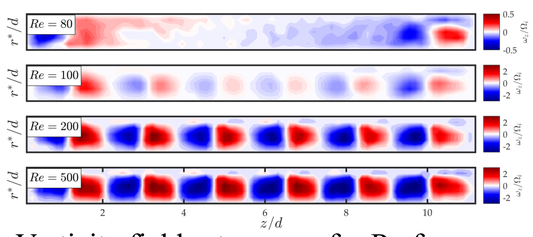

Vorticity fields at a range for Re for distilled water.

Flow Structure for a Shear-thinning Fluid

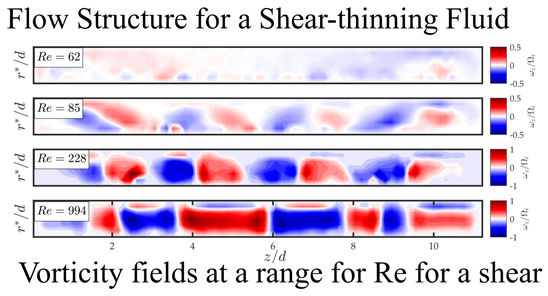

Vorticity fields at a range for Re for a shear thinning solution of xanthan gum in water.

Stirred tank flow.

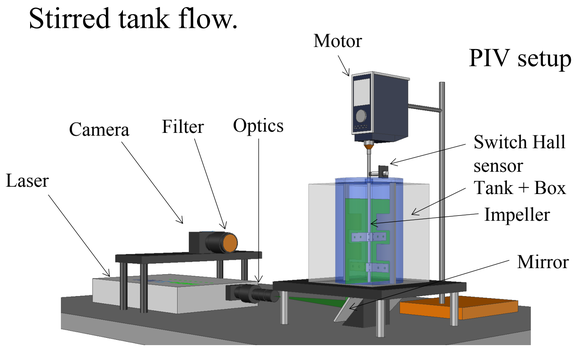

So far, the flow of a non-Newtonian fluid without particles has been studies. The CFD results agree with PIV measurements. The next step will be running similar experiments on the same fluid containing particles.

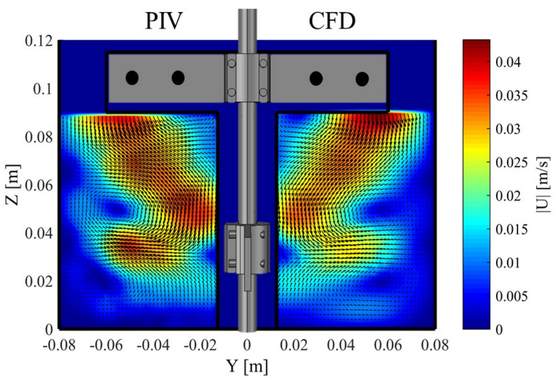

Velocity field in a stirred tank obtained by PIV and calculated by CFD.

UCL Mechanical Engineering

UCL Chemical Engineering

6. Continuous manufacturing

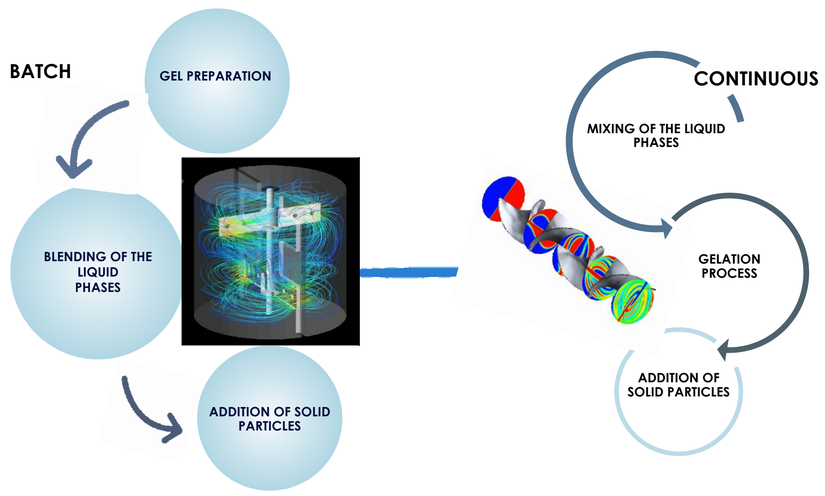

- Higher compactness
- Shorter operating times
- Lower viscosity ratio
- Lower operating temperature

Design criteria

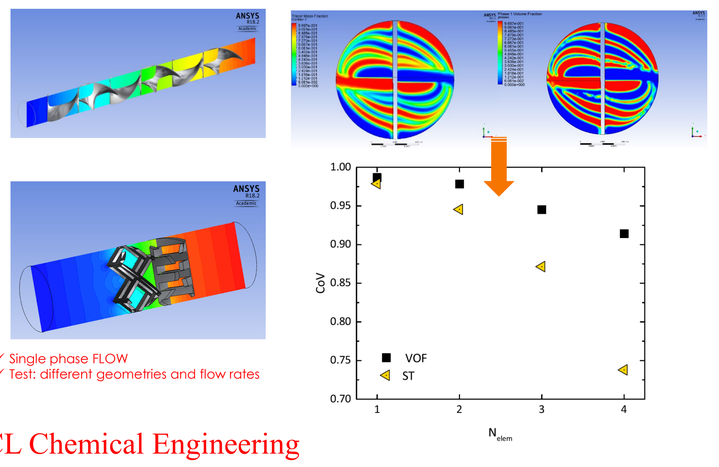

✓ Single phase FLOW
✓ Test: different geometries and flow rates

Next step

Experimental characterization of the flow of non-Newtonian fluids and suspensions in static mixers.

ALTERNATIVE GEOMETRY

UCL Chemical Engineering

Researchers involved in the project:
Jurriaan Gillissen, Neil Cagney, Wehliye Hashi Wehliye, Yao Lu, Marti Cortada Garcia, Simona Migliozzi, Anastasia Papadopoulou, Liam Escott, Giovanni Meridiano

Working research codes into fluid dynamics education: A science gateway approach

Lachlan R. Mason,[a] James Hetherington,[b,c] Martin O'Reilly,[b] May Yong,[b] Radka Jersakova,[b]
Stuart Grieve,[c] David Perez-Suarez,[c] Roman Klapaukh,[c] Richard V. Craster,[a] Omar K. Matar[a]

[a] Imperial College London, [b] The Alan Turing Institute, [c] University College London

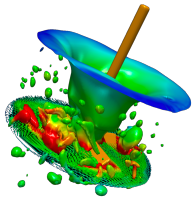

Imperial College London

The Alan Turing Institute

UCL

Rationale

Abstract

We have created a science gateway for the BLUE [1] fluid dynamics code. Students can use this gateway, in the form of a web application, to run simulations either in the cloud or on their local university computing infrastructure.

Introduction

Research codes are effective for illustrating complex concepts in educational fluid dynamics courses, compared to textbook examples, an interactive three-dimensional visualisation can bring a problem to life! Various barriers, however, prevent the adoption of research codes in teaching; codes are typically created for highly-specific 'one-off' calculations and, as such, have no user interface and a steep learning curve.

Science gateways enable novice users, be it undergraduate students or the general public, to run high-performance simulations through a familiar web interface [2]. Users can focus the majority of their time on solving the problem at hand, rather than learning a conventional scientific programming workflow and the intricacies of its computing infrastructure. While gateways are emerging in many research domains, such as astrophysics [2] and the life sciences [3], a need exists for a platform tailored to the requirements of the fluid dynamics community.

Our project allows academics to rapidly work research codes into their teaching via a minimalist science gateway framework. The gateway (Figure 1) is a simple, yet flexible, web interface allowing students to construct and run simulations, as well as view and share their output (Figure 2). Behind the scenes, the common operations of job configuration, submission, monitoring and post-processing are customisable at the level of shell scripting.

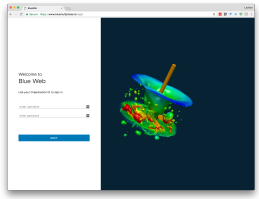

Figure 1: A science gateway web application to the BLUE fluid dynamics code [1]. Students login to the web application to access and run their simulations.

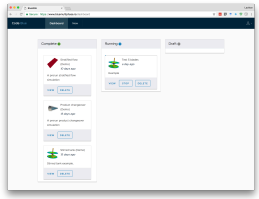

Figure 2: The simulation dashboard. Students can quickly see an overview of their work; 'completed' and 'running' simulations are displayed separately, making it simple to monitor their progress.

Design

Usage

To reduce complexity, we supply 'cases' to the user – a case represents a specific problem, such as laminar Poiseuille flow or a generic stirred tank, with a limited number of configurable parameters (Figure 3). Students can select parameters via HTML sliders, keep a record of notes, or save a case for later use. Once finalised, the case can be submitted to cloud computing infrastructure directly from the browser.

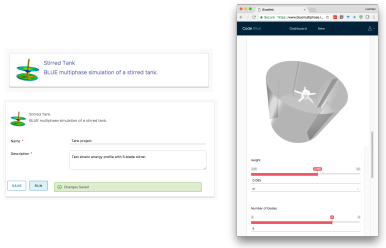

Figure 3: Example 'case' for a stirred tank simulation. Students can configure a range of parameters via HTML sliders. Cases can be used to store notes on parameter choices and their effects on simulation results.

Implementation

Technologies

We use a modular architecture for maximum flexibility. The implementation consists of three interacting components (Figure 4):

- a front-end web application (Google Angular 4 framework)
- a middleware layer for simulation data management (Python Flask micro-services)
- a high-performance computer or cloud resource (local cluster or Microsoft Azure)

All components can be deployed locally on a university network, or alternatively outsourced to cloud infrastructure providers such as Amazon AWS or Microsoft Azure.

We are a multidisciplinary development team, with backgrounds in conventional chemical engineering, mathematics and research software engineering. To ensure maximum efficiency, transparency and learning, we make use of version control (GitHub) and automated testing (Travis CI).

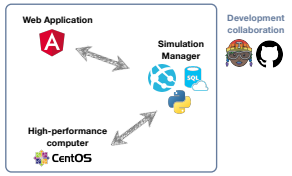

Figure 4: Modular design of gateway components. For maximum flexibility and development speed, we use a system of three interacting components. Development collaboration between multiple institutions is possible via distributed version control.

Usage

Data monitoring

High-performance simulations generate an overwhelming amount of numerical information. In practice, only a subset of the total dataset may be required. To address this, we enable students to visualise key diagnostic metrics and time series charts without leaving the browser (Figure 5). The data can be monitored in real time, while the simulation is running.

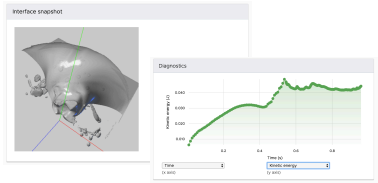

Figure 5: Key metrics and time series charts can be monitored in real time without leaving the browser.

Simplicity

Workflow

A gateway approach reduces the entrance 'barrier' to running high-performance fluid dynamics simulations. Each action in a conventional scientific workflow is replaced by an automated feature in the web application (Figure 6).

	Conventional workflow	Gateway workflow
Setup	Edit Fortran 'name list' file	Adjust parameter sliders
Configuration	Edit GNU Make 'Makefile'	Adjust configuration sliders
Submission	Edit submission script, connect to cluster via SSH, submit job using PBS 'qsub' command	Click 'Submit' button
Monitoring	Manually determine compute node, SSH into compute node, run bash 'tail' command on output data file	See live results in 'Dashboard'
Data access	Copy files to local computer using terminal and 'scp' commands	Click on 'Download' links
Data visualisation	Open files in VTK software (Paraview, Visit)	View outputs in browser
Version control	Keep track of directory names, use 'git' commands (…or maybe not at all!)	Automated version control
Distribution	Copy files using 'scp' and public SSH keys (…or external hard drives!)	'Share' a simulation

Figure 6: Conventional workflow (left) using a terminal connection directly into a high-performance computer, and gateway workflow (right) showing simplified actions for simulation control (view, stop, delete).

Extensibility

Educational use

Gateway cases can be configured to target components of a fluid dynamics course: we are currently testing with student users in an undergraduate fluids laboratory. Student feedback will be integrated directly into the application as part of its continuous development cycle.

Data export

Our fluid dynamics gateway is general and extensible, meaning that it can be connected to generic fluid dynamics solvers (including open-source options). Simulation data remains 'open' in that it can be exported for external post-processing and analysis (Figure 7). Links are provided for direct download of output data from cloud hosted storage. A summary report of all simulation parameters can be used for later reference and to encourage the practice of reproducible research.

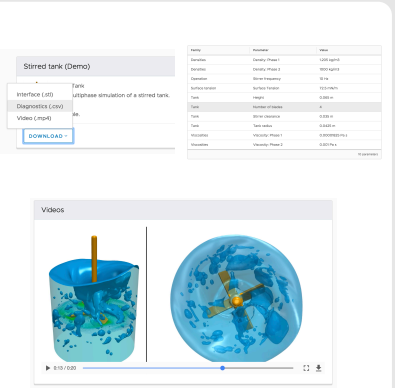

Figure 7: Simulation data can be exported from the web application for further post-processing and analysis. A report of all simulation parameters aids reproducibility.

References

[1] S. Shin, J. Chergui, and D. Juric. A solver for massively parallel direct numerical simulation of three-dimensional multiphase flows. Journal of Mechanical Science and Technology, 31(4):1739–1751, 2017.

[2] U. Becciani, E. Sciacca, A. Costa, P. Massimino, C. Pistagna, S. Riggi, F. Vitello, C. Petta, M. Bandieramonte, and M. Krokos. Science gateway technologies for the astrophysics community. Concurrency and Computation: Practice and Experience, 27(2):306–327, 2015.

[3] M. A. Miller, T. Schwartz, B. E. Pickett, S. He, E. B. Klem, R. H. Scheuermann, M. Passarotti, S. Kaufman, and M. A. O'Leary. A RESTful API for access to phylogenetic tools via the CIPRES science gateway. Evolutionary Bioinformatics Online, 11:43, 2015.

Lubrication model for evaporating binary sessile drops

A. G. L. Williams[1], G. Karapetsas[2], O. K. Matar[3], K. Sefiane[1], P. Valluri[1]

[1] *University of Edinburgh, Institute of Multiscale Thermofluids*

[2] *University of Thessaloniki, School of Chemical Engineering*

[3] *Imperial College London, Department of Chemical Engineering*

Motivation

- Experiments have revealed that the evaporation of sessile drops consisting of binary mixtures is a highly dynamic and complex process.
- For example, heptane/octane drops have been seen to be unstable in complete wetting scenarios:

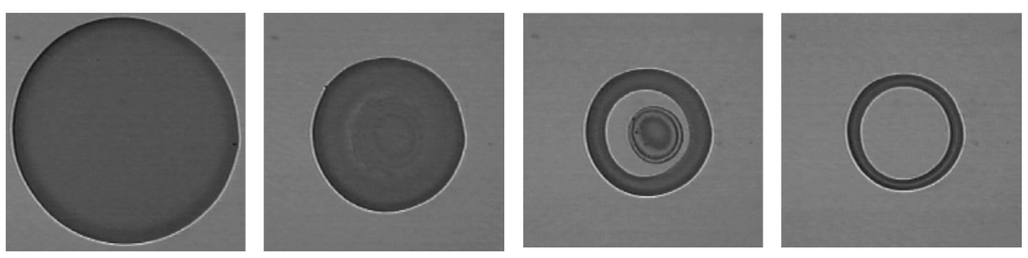

Ariel view of a 0.6 μL wetting droplet consisting of a heptane/octane mixture. Initial concentration: 15% of heptane in octane. Guena et al, 2007

- The central part of the drop evaporates first, leaving an outer ring.
- We use the Lubrication approximation and the assumption to develop and finite-element model for a wetting drop.

Problem Formulation

- Ideal miscible Newtonian mixture consisting of liquids A and B.
- Droplet deposited into precursor film, assume that $\varepsilon = \frac{\hat{H}_o}{\hat{R}_o} \ll 1$.

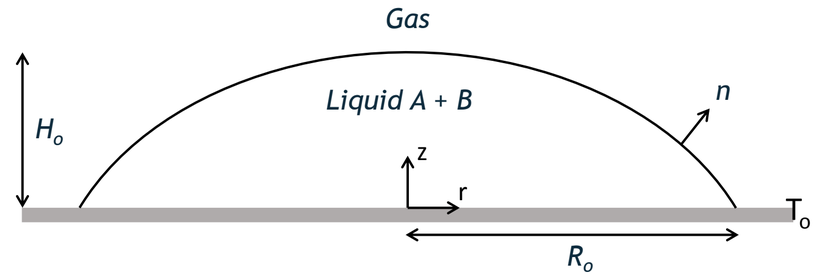

- Mixture properties (φ) calculated with mixing rule:

$$\varphi = \chi_A + (1 - \chi_A)\frac{\hat{\varphi}_B}{\hat{\varphi}_A}$$

- Surface tension (σ) dependant on temperature and concentration:

$$\sigma = \chi_A(1 - Cn\,T) + (1 - \chi_A)\left(\frac{\hat{\varphi}_B}{\hat{\varphi}_A} - \gamma\, Cn\, T\right)$$

Equations

Dimensionless numbers

$$\varepsilon = \frac{\hat{H}_o}{\hat{R}_o} \qquad Re = \frac{\varepsilon\hat{\rho}\hat{\gamma}_A\Delta\hat{T}\hat{H}_o}{\hat{\mu}_A^2} \qquad Pr = \frac{\hat{\mu}_A\hat{C}_{p,A}}{\hat{k}_A} \qquad Pe = \frac{\hat{\gamma}_A\Delta\hat{T}\hat{H}_o}{\hat{\mu}_A\hat{D}_A} \qquad Ma = \frac{\hat{\gamma}_A\Delta\hat{T}}{\hat{\sigma}_{A,o}}$$

$$E = \frac{\hat{k}_A\hat{\mu}_A}{\varepsilon^2\hat{\rho}\hat{\gamma}_A\hat{H}_o\hat{L}_{v,A}} \qquad \delta = \frac{\hat{T}_g\hat{\mu}_A}{\hat{\rho}\hat{H}_o\hat{L}_{v,A}} \qquad K = \frac{\hat{k}_A\left(2\pi\hat{R}_g^3\hat{T}_g^5\right)^{\frac{1}{2}}}{\hat{H}_o\hat{L}_{v,A}^2\hat{P}_A^o\hat{M}_A^{\frac{3}{2}}} \qquad \mathrm{A} = \frac{\hat{A}}{6\pi\hat{\gamma}_A\Delta\hat{T}\hat{H}_o^2}$$

Governing equations

Mass: $$\nabla\cdot\boldsymbol{u} = 0$$

Momentum: $$\varepsilon Re\left(\frac{\partial\boldsymbol{u}}{\partial t} + \boldsymbol{u}\cdot\nabla\boldsymbol{u}\right) + \nabla P - \mu\nabla^2\boldsymbol{u} = 0$$

Energy: $$\varepsilon RePrC_p\left(\frac{\partial T}{\partial t} + \boldsymbol{u}\cdot\nabla T\right) - \nabla\cdot(k\nabla T) = 0$$

Ad-vec: $$Pe\left(\frac{\partial X_A}{\partial t} + \boldsymbol{u}\cdot\nabla X_A\right) - \nabla^2 X_A = 0$$

Normal stress BC

$$P = P_v - \frac{\varepsilon^2}{Ca}\sigma\left(\frac{1}{r}\frac{\partial}{\partial r}\left(r\frac{\partial h}{\partial r}\right)\right) - \frac{A}{h^3}$$

Evaporative flux

$$J_A = \frac{X_A}{K}(\delta(P - P_A^o) + T_h) \qquad J_B = \frac{(1 - X_A)\alpha\beta^{\frac{3}{2}}}{K}(\delta(P - \alpha P_A^o) + \Lambda T_h)$$

Dimensionless values for ethanol/water drop, R = 1 mm

$\boldsymbol{\varepsilon}$	0.2	$\boldsymbol{E}$	3.9×10^{-4}	$\boldsymbol{\sigma_o}$	3.20	$\boldsymbol{\mu_R}$	0.84
$\boldsymbol{Re}$	0 – 9	$\boldsymbol{K}$	1.3×10^{-3}	$\boldsymbol{\gamma}$	1.81	$\boldsymbol{C_{pR}}$	1.7
$\boldsymbol{Pr}$	16.1	$\boldsymbol{\delta}$	1×10^{-5}	$\boldsymbol{\alpha}$	0.40	$\boldsymbol{\beta}$	0.39
$\boldsymbol{Pe}$	5×10^{4}	$\boldsymbol{A}$	1×10^{-4}	$\boldsymbol{k_R}$	3.36	$\boldsymbol{\Lambda}$	2.38
$\boldsymbol{Ma}$	0.18						

Results

Ethanol/water, R = 1mm, initial 2% ethanol

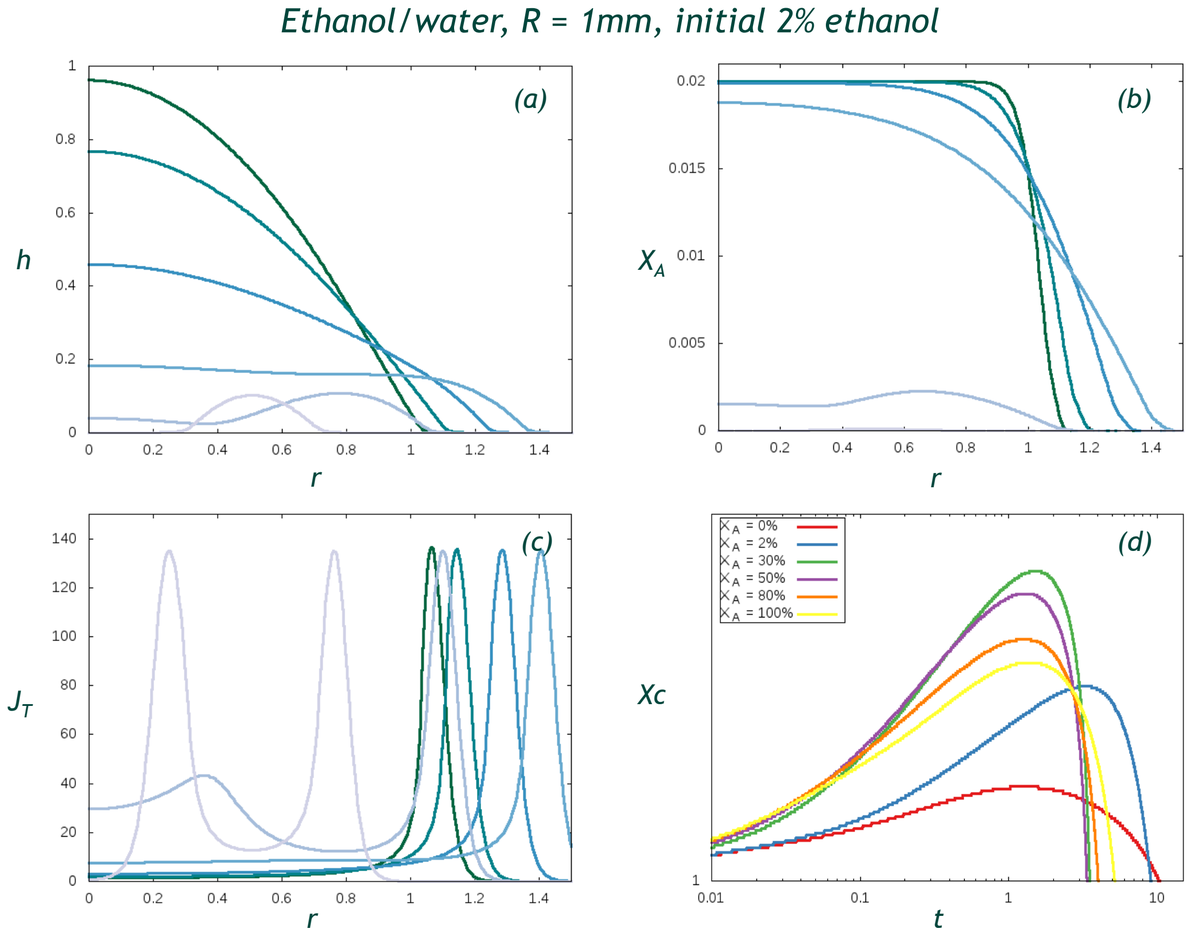

(a) - (c) show quantities along r in distinct snapshots in drop life time. (a) Drop interface profile, (b) Mass fraction of ethanol, (c) Total evaporative flux of ethanol + water, (d) Contact line position over drop life time for various initial concentrations of ethanol.

Comparison with Guena et al

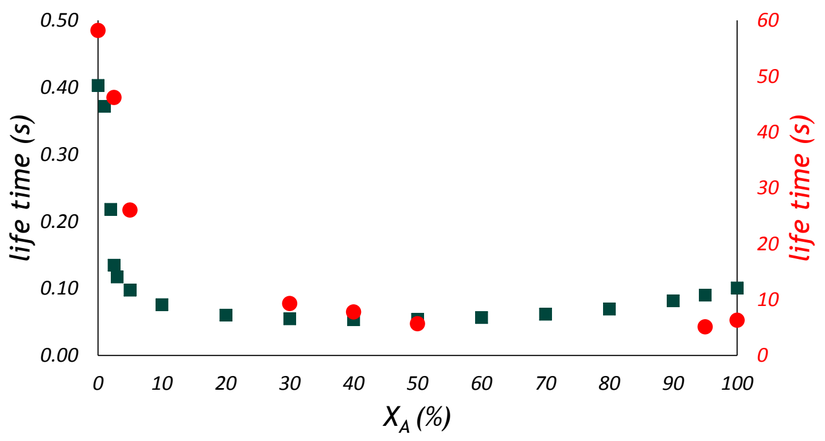

THE UNIVERSITY of EDINBURGH

EPSRC Engineering and Physical Sciences Research Council

Leidenfrost rotation: Fluid dynamics on turbine-like surfaces

Prashant Agrawal[$], Gary G. Wells[$], Rodrigo Ledesma-Aguilar[$], Khellil Sefiane[†], Glen McHale[$*]

[$]Smart Materials & Surfaces Laboratory, Northumbria University, UK

[†] School of Engineering, The University of Edinburgh, UK

*glen.mchale@northumbria.ac.uk http://www.naturesraincoats.com/

Introduction

When a droplet interacts with a substrate heated at temperatures significantly higher than the droplet's boiling point, a cushion of the evaporating liquid causes the droplet to levitate over the substrate. This phenomenon is called the Leidenfrost effect[(1)]. The vapour layer acts as a virtually frictionless surface on which the droplet can translate. Furthermore, by rectifying the flow of vapour from the evaporating liquid (or a sublimating solid), directed motion of Leidenfrosting liquids and solids can be achieved[(2,3)] (Figure 1).

Here we demonstrate that by employing asymmetrically textured, turbine-like, substrates the Leidenfrost effect can be used to rotate dry ice blocks and liquid droplets[(4)]. An understanding of the dynamics of rotation of these Leidenfrosting solid and liquid components, opens up possibilities of developing heat engines for power generation at millimetre and sub-millimetre scales. Furthermore, the use of alternative solid and liquid fuels e.g. carbon dioxide and methane, can be explored for power generation in extreme environments for space and planetary exploration, where they might be naturally available.

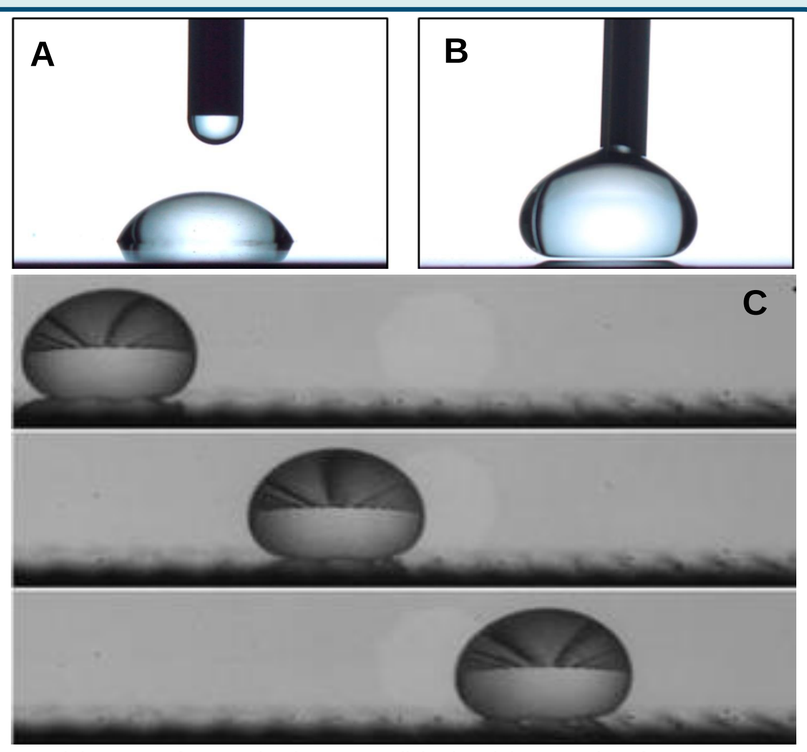

Figure 1 – (A) Image of water droplet on a polished stainless steel surface at $T = 20\,°C$[(5)]. (B) Image of water droplet on a polished stainless steel surface at $T = 250\,°C$[(5)]. (C) Side view of translation of a 60 µl water droplet placed on a ratchet at $T = 85\,°C$[(2)].

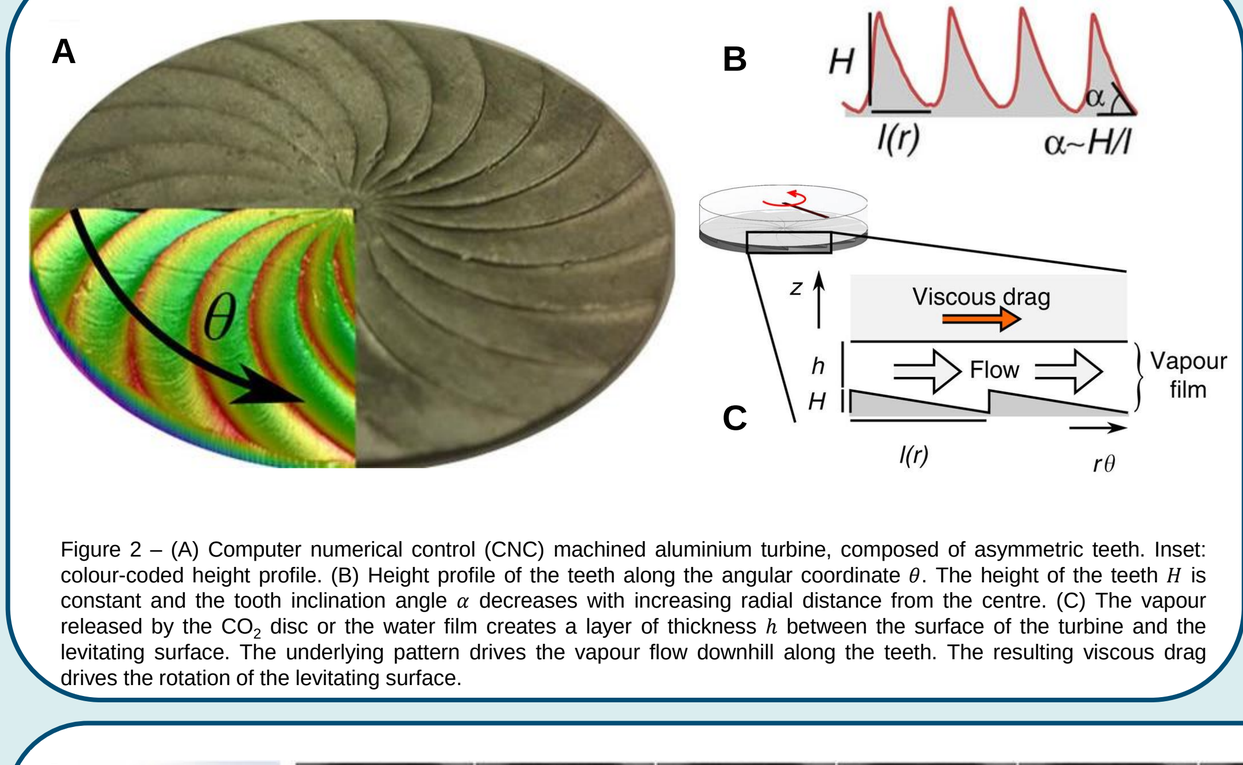

Figure 2 – (A) Computer numerical control (CNC) machined aluminium turbine, composed of asymmetric teeth. Inset: colour-coded height profile. (B) Height profile of the teeth along the angular coordinate θ. The height of the teeth H is constant and the tooth inclination angle α decreases with increasing radial distance from the centre. (C) The vapour released by the CO_2 disc or the water film creates a layer of thickness h between the surface of the turbine and the levitating surface. The underlying pattern drives the vapour flow downhill along the teeth. The resulting viscous drag drives the rotation of the levitating surface.

Rotation on turbine-like textured surfaces

Turbine like structures were machined on aluminium plates using CNC to redirect vapour flow from an evaporating liquid droplet or a sublimating dry ice block (Figure 2). The asymmetric shape of the teeth redirects the vapour flow in the θ direction and the resulting viscous drag produces a torque on the levitating rotor. Consequently, a dry ice block, or a metal plate supported on a water pool, is seen to rotate in Figures 3A and 3B.

An analytical model is developed to investigate the mechanism behind this Leidenfrost rotation. Assuming an incompressible flow, the viscous friction dominated flow in the vapour film is modelled using the lubrication approximation. The estimation of a critical mass, that ensures levitation of the rotor, and torque obtained from the model agrees well with experiments (Figures 3C and 3D).

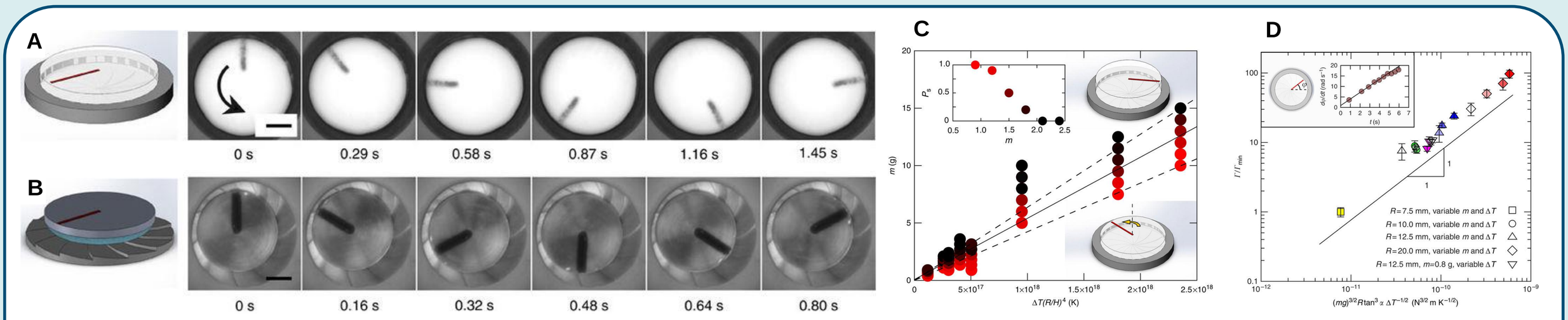

Figure 3 – (A) Time-lapse of rotation of a dry ice disc placed on the hot turbine-like surface ($T \sim 500\,°C$). (B) Sequence of rotation of a drop of water supporting a metal plate placed on the top of the turbine. The length of the scale bars is 1 cm. (C) Critical mass for levitation of a dry-ice block. The transition is quantified in terms of the probability of a rotating load, P_s, which decreases with increasing mass (for example, the inset figure shows the probabilities P_s for the data points corresponding to $\Delta T(R/H)^4 = 3e7$ K in the main figure). The critical mass, indicated by the solid line, scales linearly with $\Delta T(R/H)^4$ as predicted by the theory. The dotted lines correspond to 90% confidence intervals extracted from the probability distributions. (D) The variation of torque τ for a wide range of the disc radii R, temperature difference ΔT, mass m and teeth angle α. The shade intensity within each set of symbols indicates increasing ΔT. The torque has been normalized by the minimum torque measured, $\tau_{min} = 0.0109$ µNm.

Design optimization and liquid fuels

To further explore the possibilities of a Leidenfrost rotation based heat engine, we extend the study to explore the dynamics of rotation of a liquid pool on these substrates.

The process involves numerically simulating the flow of vapour over different turbine geometries to ascertain the optimum turbine design for maximum rotation speed (Figure 4A). An axisymmetric model is then used to model the unsteady rotation of a metal plate on a liquid pool. Initial results show a promising agreement with experiments in Figure 4B.

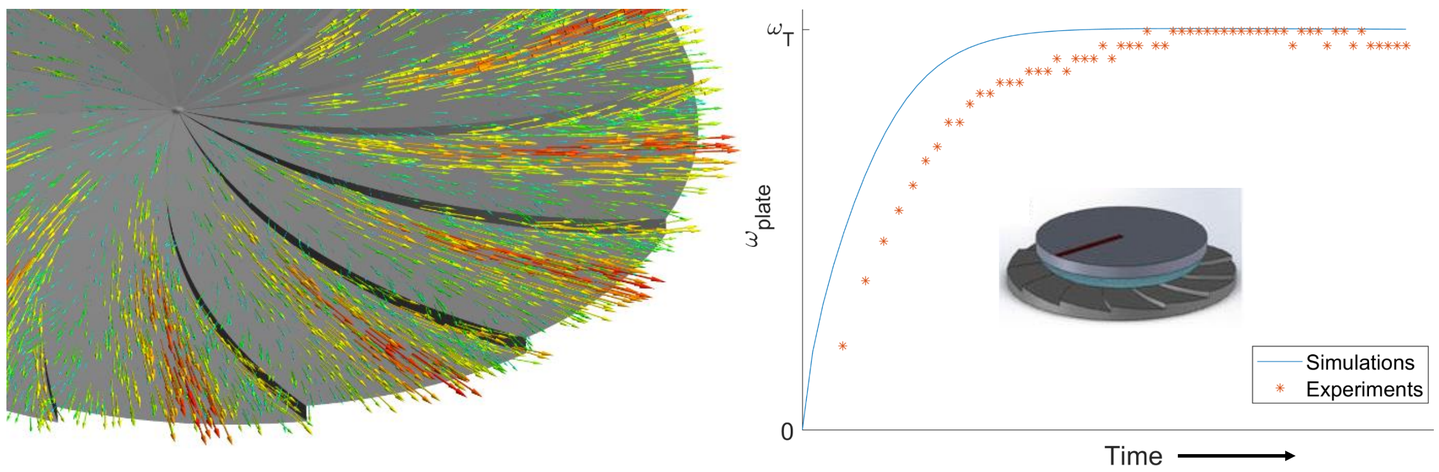

Figure 4 – (A) Depiction of flow obtained from a 3D simulation of vapour flow over the teeth of the turbine-like substrate. (B) The variation of rotation speed of a plate kept over a Leidenfrosting water pool (inset) over the heated turbine-like substrate. The plot shows a comparison of the rotation speed of the plate obtained from experiments and simulations; ω_T represents the terminal angular velocity of the plate.

References:

(1) Leidenfrost, J. G. De Aquae Communis Nonnullis Qualitatibus Tractatus, Duisburg, 1756.
(2) Dupeux, G. et al. Propulsion on a superhydrophobic ratchet, Scientific Reports 4 (5280), 2014.
(3) Soto, D. et al. Surfing on a herringbone, Phys. Rev. Fluids 1, 013902, 2016.
(4) Wells, G. G. et al. A sublimation heat engine, Nature Communications 6 (6390), 2015.
(5) Geraldi, N. R. et al. Leidenfrost transition temperature for stainless steel meshes, Materials Letters, Vol. 176, 205-208, 2016.

Acknowledgements

The authors would like to acknowledge the UK EPSRC grants EP/P005896/1 and EP/P005705/1.

Chaotic Orbits of Tumbling Ellipsoids

Erich Essmann, Pei Shui*, Rama Govindarajan† , Stephane Popinet‡ & Prashant Valluri**
**School of Engineering, The University of Edinburgh, UK †TIFR International Centre for Theoretical Sciences, Bangalore, India ‡Université Pierre et Marie Curie, France*

THE UNIVERSITY of EDINBURGH

Introduction

Direct Numerical Simulations are used to solve 3D flow equations (conservations of mass and momentum) coupled with 3D immersed solid 6 Degree-of-Freedom (DoF) motions . The solver is named Gerris Immersed Solid Solver (GISS).

Fluid governing equations in **Eulerian** **coordinates**

Eq. Continuity

$$\nabla \cdot \mathbf{u} = 0$$

Eq. Momentum

$$\rho \frac{D\mathbf{u}}{Dt} = -\nabla p + \mu \nabla^2 \mathbf{u} + \mathbf{f}$$

Interfacial elements

Implicit coupling

$$\mathbf{f} = \rho a(\mathbf{U_s} + \mathbf{r} \times \boldsymbol{\Omega_s} - \mathbf{u})/Dt$$

$$\mathbf{F} = \boldsymbol{\sigma}(\mathbf{u}, \mathbf{p}, f) \otimes \mathbf{A}$$

$$\mathbf{A} = \mathbf{A}(a, s_d, h)$$

$$\sigma_{ij} = -p\delta_{ij} + \mu\left(\frac{\partial u_i}{\partial x_j} + \frac{\partial u_j}{\partial x_i}\right)$$

Solid governing equations in **Lagrangian** coordinates

Eq. Momentum

$$m \frac{d\mathbf{U_s}}{dt} = \sum \mathbf{F}$$

Eq. Angular Momentum

$$I \frac{d\boldsymbol{\Omega_s}}{dt} = \sum \mathbf{r} \times \mathbf{F}$$

Contact and Collision Model

Composite Contact Model using Force Field and LCP constraint based approaches

Figure 1 - *Summary of the internal structure of the GISS project, Shows the two major modules and the linking equations.*

Here, we study the motion of a tumbling ellipsoid in an inviscid fluid. The equations governing such motion were shown to be non-integrable by Kozlov & Oniscenko (1982) for a general ellipsoid. The ensuing chaotic motion would is the ultimate validation test case for the GISS solver.

Methodology

Under the conditions of inviscid flow and rigid body motion the equations are simplified into a set of ODE's (Kirchoff Equations). This, therefore, allows us to compare GISS to previous work (Aref & Jones, 1993) and to solutions of the Kirchoff equations produced in-house.

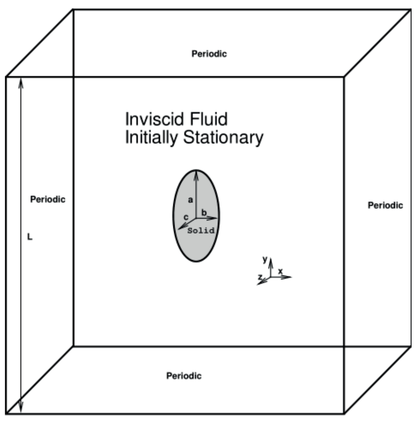

Figure 2-- - *Schematic of GISS initial conditions and simulation volume*

- Key parameters to simulations:

$$\sigma = \frac{\rho_{fluid}}{\rho_{solid}}$$ Fuild-Solid Density Ratio

$$E = \frac{k_t}{k_r} = \frac{mV^2}{I\Omega^2}$$ Translational-Rotational Kinect Energy Ratio

$$Re_p = \frac{2Va}{\nu}$$ Praticle Reynold's Number

The orbits traced by the ellipsoid and the chaotic behaviour are quantified by Recurrence Quantification Analysis (RQA). RQA allows us to perform the following analysis:

- Recurrence Rate (RR) is used to classify the system's behaviour
- We can use the plot to calculate the DET Determinism of the system.
- The Lyapunov exponent and Rényi Entropy of the system encoded in recurrence plot.

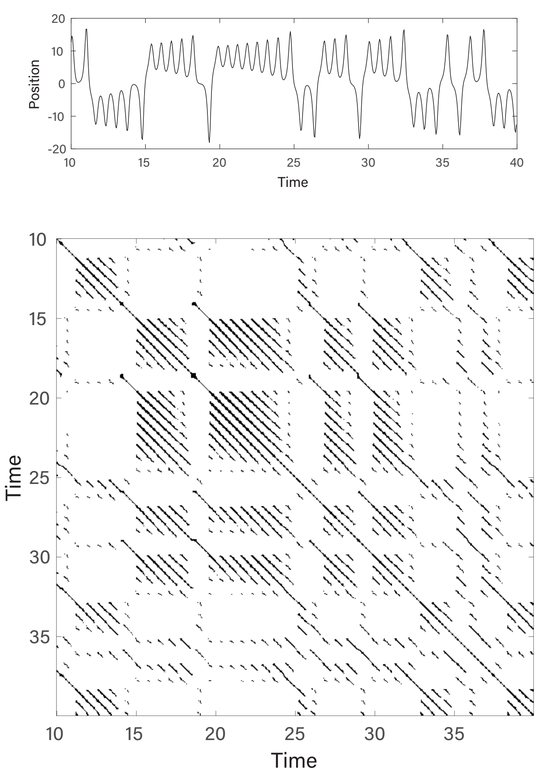

Figure 3 - *Recurrence Plot of the time series of a chaotic orbit*

RQA allows the creation of a map of the different dynamical regimes

Validation

The DNS results from the GIS solver are in very strong agreement with the results from Aref & Jones (1993) and the analytical solution. The orbits become more more chaotic as the density ratio increases, concurring with Aref & Jones.

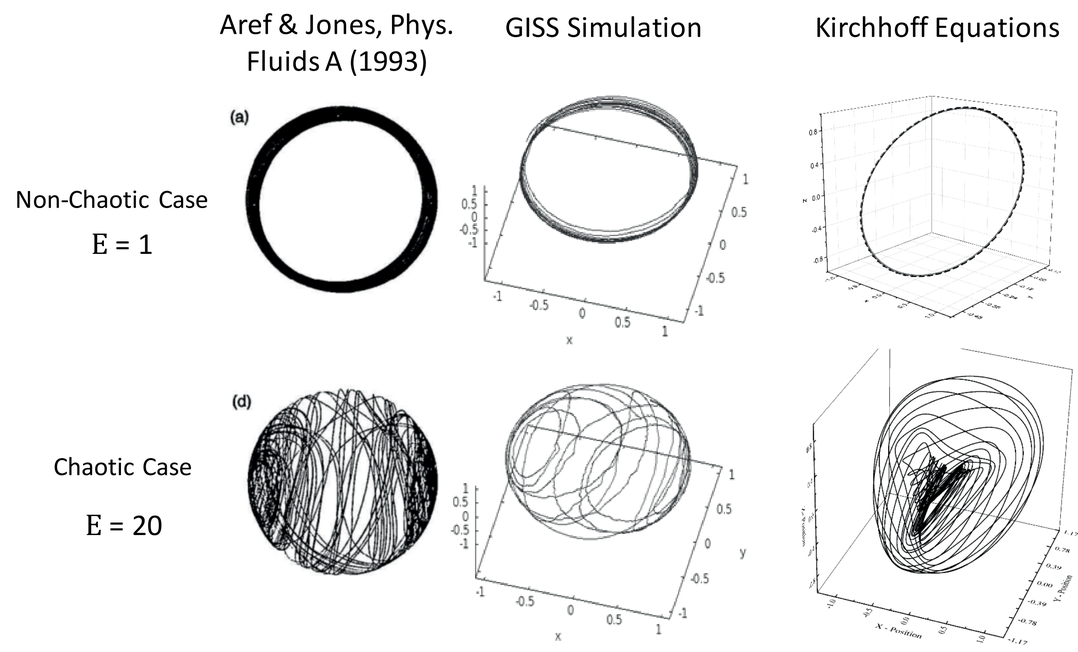

Figure 4 - *The ratio of rotational to translational kinetic energy, E, determines whether the system behaves chaotically. The graphs show the position of the marker point on the ellipsoid as it orbits over time. As can be seen the results from GISS match those from previous work very well.*

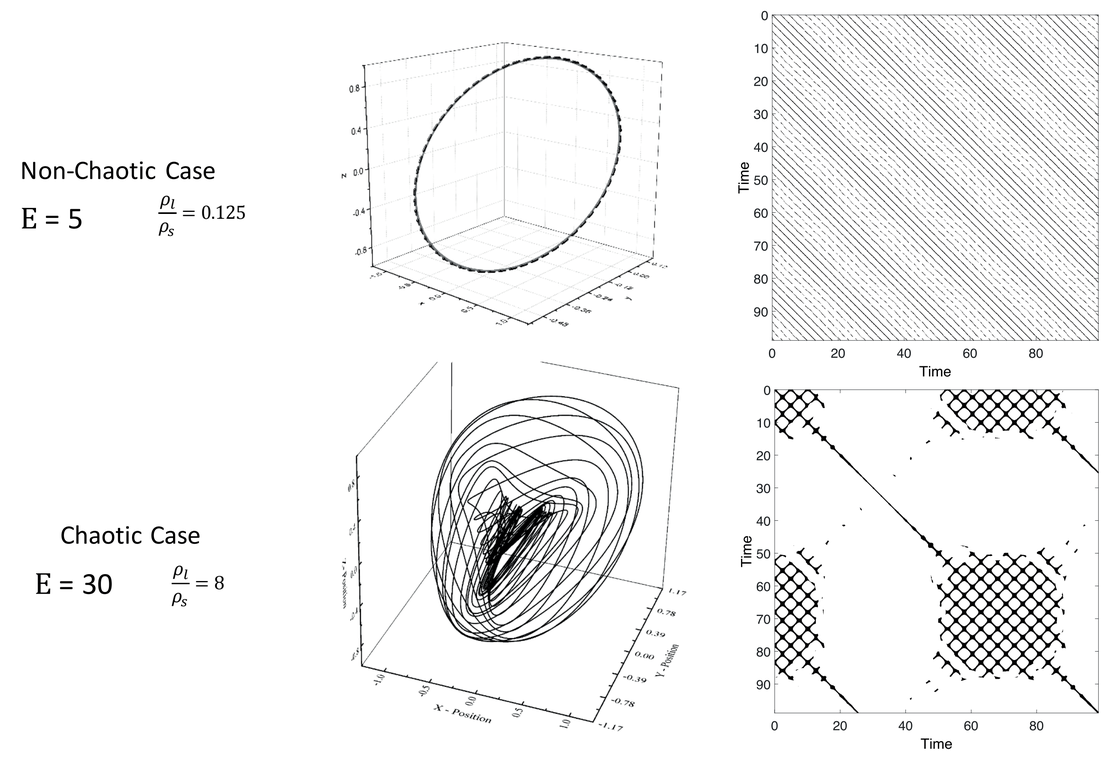

Figure 5 - *Comparing a chaotic system to a periodic system, it becomes clear that Recurrence Plots are very powerful tools; since they can be used to easily classify the behaviour of systems*

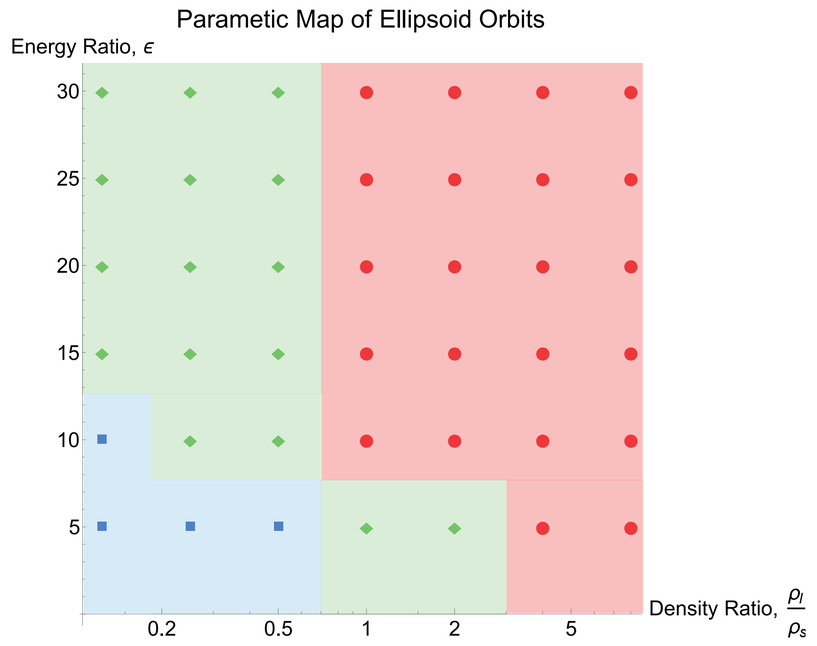

Figure 6 - *Map supports the trend found by (Aref & Jones, 1993) that chaos increases with density ratio and lower density region's behaviour better described as quasiperiodic*

Future Work

Understanding orbital behaviour in the presence of

- Viscosity
- Geometric symmetry
- Temperature gradients (viscosity gradients)

NCRST
National Commission On Research Science & Technology

Department of Mechanical and Aerospace Engineering

Brunel University London | Institute of Energy Futures

Flow Boiling and Condensation in Multi-Microchannels: Design of an Integrated High Heat Flux Thermal Management System

Ali Al-Zaidi, Tassos G. Karayiannis*, Mohamed Mahmoud, Luiz Wrobel

* Corresponding author: tassos.karayiannis@brunel.ac.uk

• Introduction and Project Objectives

New methods of cooling computer chips and high heat flux electronic devices are currently considered by the scientific and industrial community. This was motivated by the limitation of the currently adopted cooling techniques, i.e. they cannot meet some of the current and future thermal loads in these devices, which are expected to reach about 10 MW/m^2 with higher rates at the hot spots that can exist. Two-phase flow in microchannels is one of the proposed heat transfer systems that can achieve high heat transfer rates and hence be suitable for these applications. In such systems the final dissipation of the thermal load to the ambient can be equally challenging. This study aims to investigate experimentally flow boiling and condensation heat transfer in copper multi-microchannel configurations and lead and concluded with a design of a fully-integrated thermal management system for transferring high and ultra-high heat fluxes. HFE-7100 was chosen as the test fluid due to its environmentally friendly nature and high dielectric strength.

• Experimental system

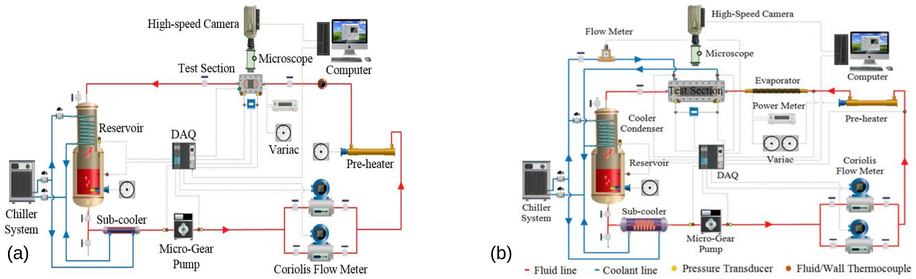

Fig.1 Schematic diagram of the experimental facility (a) flow boiling experiments (b) flow condensation experiments.

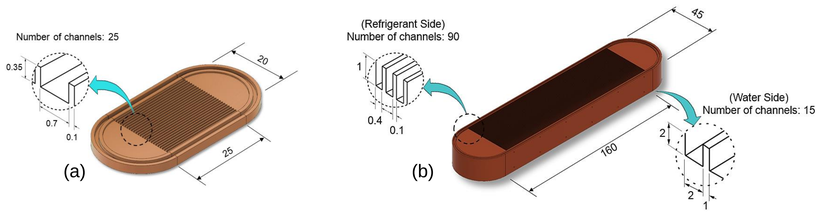

Fig.2 Test section dimensions (a) microchannel evaporator (b) microchannel condenser (all dimensions are in mm)

Flow boiling results

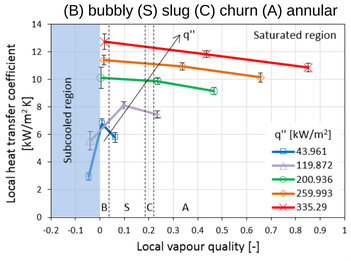

Fig.3 Effect of heat flux on the heat transfer coefficient at a mass flux of 250 kg/m^2 s

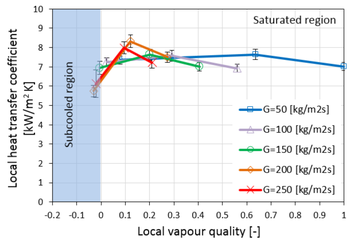

Fig.4 Effect of mass flux at a heat flux of 100 kW/m^2

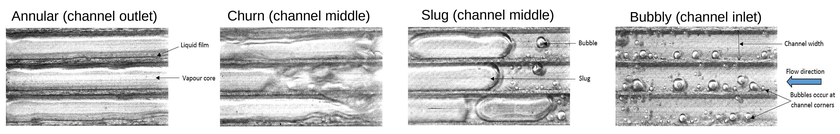

Fig.5 Observed flow patterns at a heat flux of 51.1 kW/m^2 and mass flux of 50 kg/m^2 s

- The observed regimes were bubbly, slug, churn and annular flow.
- The heat transfer coefficient increased with increasing heat flux.
- There was no a clear effect of mass flux, in the range studied.
- The local heat transfer coefficient decreased with increasing local quality.

Flow condensation results

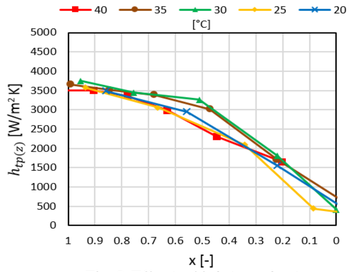

Fig.6 Effect of inlet coolant temperature on the heat transfer coefficient at a mass flux of 86 kg/m^{2}s and coolant flow rate of 0.5 L/min

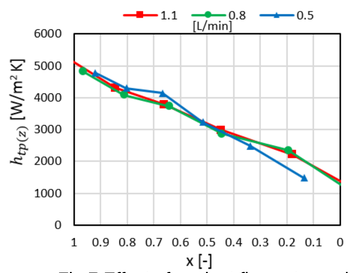

Fig.7 Effect of coolant flow rate on the heat transfer coefficient at a mass flux of 126 kg/m^{2}s and inlet coolant temperature of 30 °C

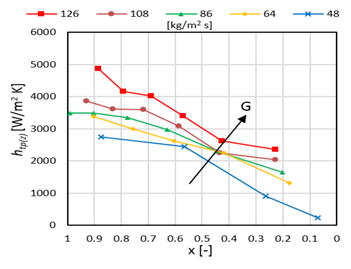

Fig.8 Effect of refrigerant mass flux and local quality on the heat transfer coefficient at coolant flow rate of 0.5 L/min and inlet coolant temperature of 40 °C

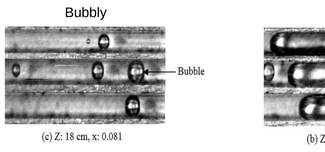

Fig.9 Observed flow patterns at a mass flux of 108 kg/m^{2}s, coolant flow rate of 0.8 L/min and inlet coolant temperature of 25 °C.

- The observed regimes were annular, slug and bubbly flow.
- There was no a clear effect of the coolant side conditions, in the range studied.
- The heat transfer coefficient increased with increasing refrigerant mass flux and decreased with decreasing local quality indicating dominance of interfacial shear stress.

Flow boiling results

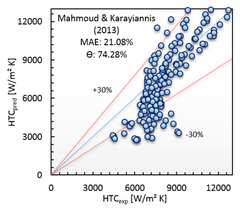

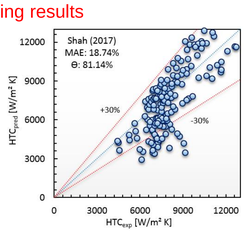

Flow condensation results

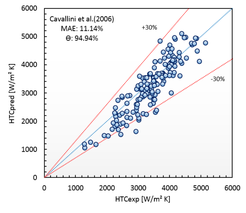

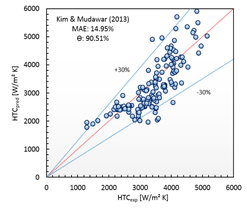

Fig.10 Comparison with existing two-phase heat transfer correlations.

• Conclusions

- The observed flow patterns:
  - Flow Boiling: bubbly, slug, churn and annular flow.
  - Flow Condensation: annular, which is the prevalent regime, slug and bubbly flow.
- The flow boiling heat transfer coefficient increases with increasing heat flux.
- There is a negligible effect of mass flux, while, in most experiments, the local flow boiling heat transfer coefficient decreases with increasing local quality.
- The coolant side has a negligible effect on the condensation heat transfer coefficient.
- In the condensation experiments, the heat transfer coefficient increased with increasing mass flux and decreased with decreasing local quality; the interfacial shear stress is the dominant regime at this scale and with this particular fluid.
- Correlations by Mahmoud & Karayiannis (2013) and Shah (2017) predict the flow boiling experimental data with a MAE of 21.08% and 18.74%, respectively.
- Correlations by Cavallini et al. (2006) and Kim & Mudawar (2013) predict the condensation experimental data with a MAE of 11.14% and 14.95%, respectively.
- The present multi-microchannel water-cooled condenser could achieve a cooling capacity of 520 W at a low coolant flow rate and standard coolant temperature. This corresponds to a heat flux of 1 MW/m^2 for a chip die size of 20 mm × 25 mm (500 mm^2) when such a condenser forms part of an integrated small-scale thermal management system for high heat flux devices.

Enhanced Flow Boiling Integrated System for Cooling High-Flux Electronics

Vivian Lee, Tassos G. Karayiannis*, Gary Henderson, Jun Xia
*Corresponding author: *tassos.karayiannis@brunel.ac.uk*

Brunel University London | Institute of Energy Futures
Dept. of Mechanical & Aerospace Engineering

TMD

INTRODUCTION

Technology scaling resulted in high power densities & thermal challenges in base heat flux and hotspots.

- Power electronics, for eg. microwave devices and radars exceed **10 MW/m²** – **10 x the air cooling limit**, while hotspots may be **6 – 10 x** the average heat flux**.**
- Flow boiling in microchannel heat sinks have proven effective for heat fluxes up to **10 MW/m²** [1].

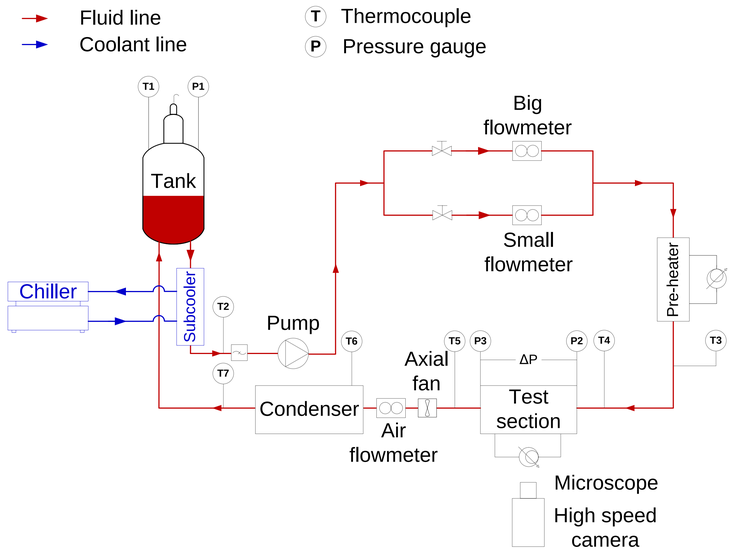

Test facility to study flow boiling in multi microchannels suitable for cooling micro-electronics. Working fluid: HFE 7200.

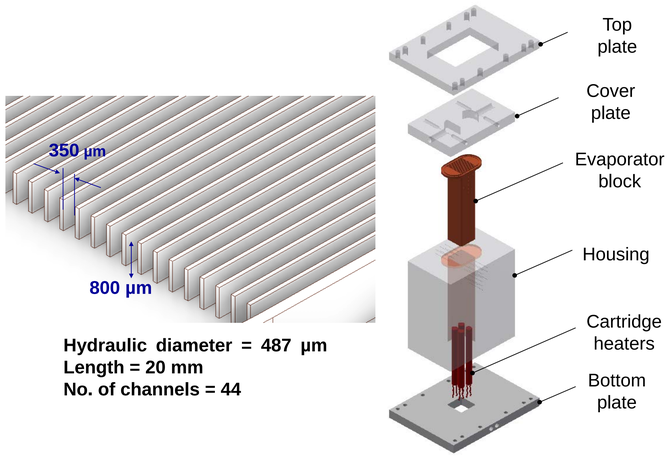

Hydraulic diameter = 487 µm
Length = 20 mm
No. of channels = 44

Base experiments using a microchannel module of footprint area 20 mm x 20 mm with plain parallel channels.

Despite the benefits of two-phase microchannel heat sinks, its implementation is challenged by several issues.

TECHNOLOGY CHALLENGES

- Possible high wall superheat at boiling incipience.
- Possible dryout, hence low heat flux for part of the channel.
- Flow reversal and instabilities.
- Appropriate general design correlations

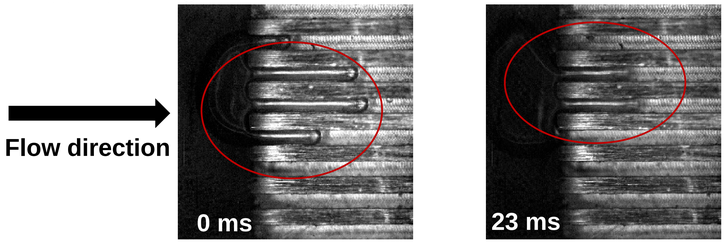

Flow reversal in rectangular microchannels with R134a [2]

PINS / CAVITIES

Micro-pin structures or **artificial cavities** influence bubble dynamics that potentially:

- Eradicate flow instabilities
- Lower surface temperatures
- Enhance heat transfer rates

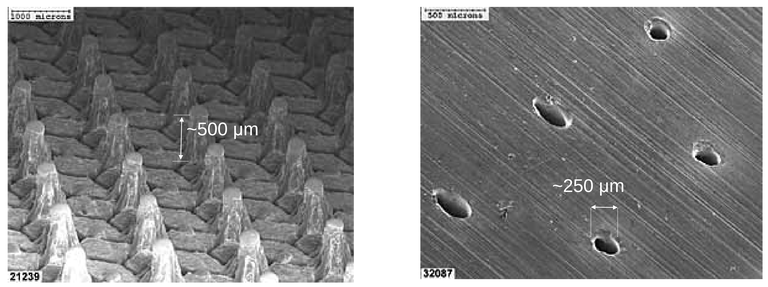

Microstructure-enhanced surfaces along the channel floor, to be provided by TWI

- Cylindrical cavities of size diameter & depth 50 µm with 1 mm spacing are designed based on Hsu's model for nucleation [3].

COATINGS

Nano-coatings increase roughness (nucleation site density), heat transfer area and alter the wettability characteristics of the surface.

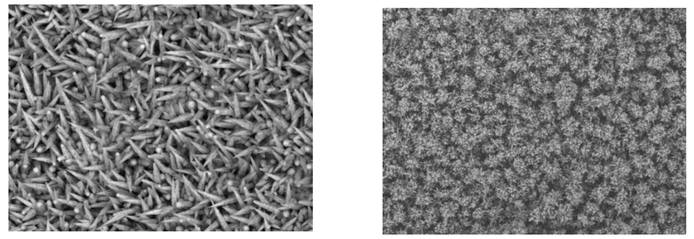

Nano-coatings, to be provided by Oxford nanoSystems Ltd.

SPECIFIC PROJECT APPLICATIONS: MODULAR DESIGN

** Images adapted from munich-aviation.de and gettyimages.co.uk*

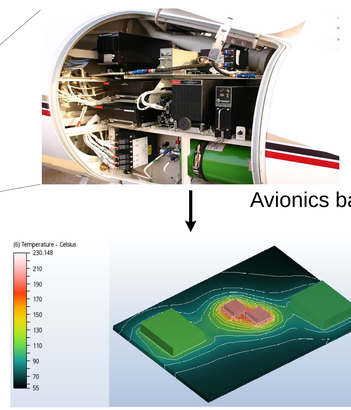

Simple thermal map of a package

In the aerospace context, thermal management solutions must be compact, modular and reliable for harsh environmental operating conditions **(- 40 °C** to **+70 °C)**.

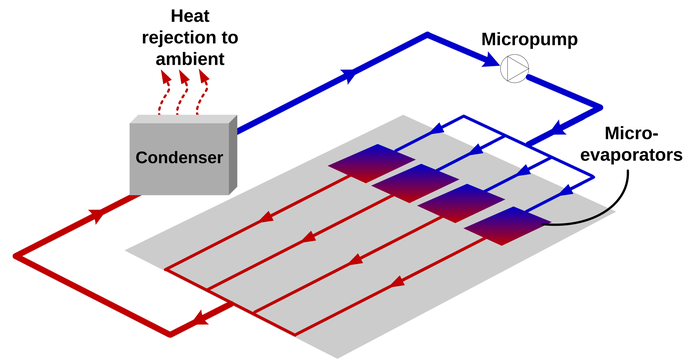

Close-looped two-phase cooling for electronic packages, micro-evaporators integrated on chips.

Condenser Design: Significant challenges remain in the design of small scale air-cooled condensers needed for integrated thermal management systems.

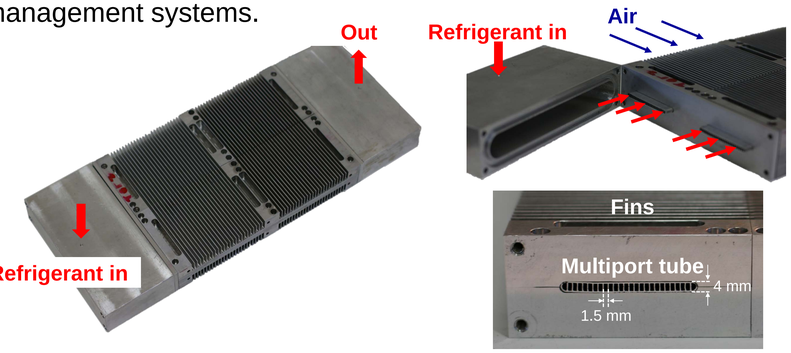

Compact liquid-to-air heat exchanger, designed for 2 kW capacity with 200 cfm airflow

1. T.G. Karayiannis, M.M. Mahmoud, *Flow boiling in microchannels: Fundamentals and applications*, Applied Thermal Engineering, Volume 115, 2017, pp. 1372-1397.
2. E.M. Fayyadh, M.M. Mahmoud, K. Sefiane, T.G. Karayiannis, *Flow boiling heat transfer of R134a in multi microchannels*, International Journal of Heat and Mass Transfer, Volume 110, 2017, pp. 422-436
3. Y.Y. Hsu, *On the size range of active nucleation cavities on a heating surface*, J. Heat Transfer, 84, 1962, pp. 207-215

An Experimental Study on the Effect of Surfactants on Drop/interface Partial Coalescence

Teng Dong, Weheliye Hashii Weheliye, Panagiota Angeli
ThAMeS Multiphse, Department of Chemical Engineering, UCL

Introduction

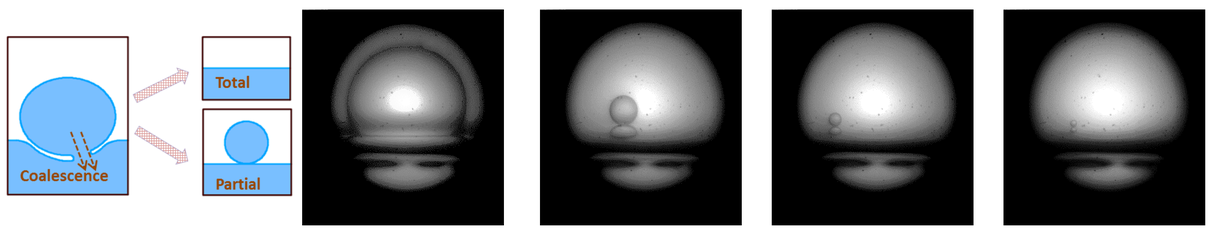

When a droplet coalesces with an underlying liquid, merging does not always proceed to completion, leaving a smaller droplet on the interface. The process can repeat itself for subsequent generations of daughter droplets, resulting in a cascade events.

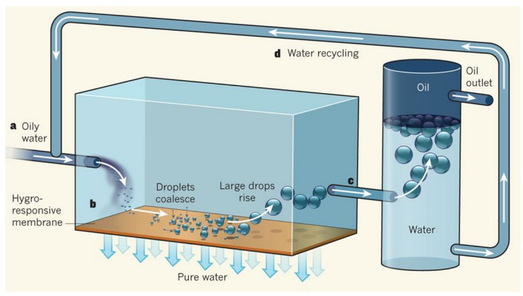

Separation of Water/oil mixture

Questions

- Under what conditions the partial coalescences are able to occur?
- How does surfactant affect the partial coalescence?

Methods

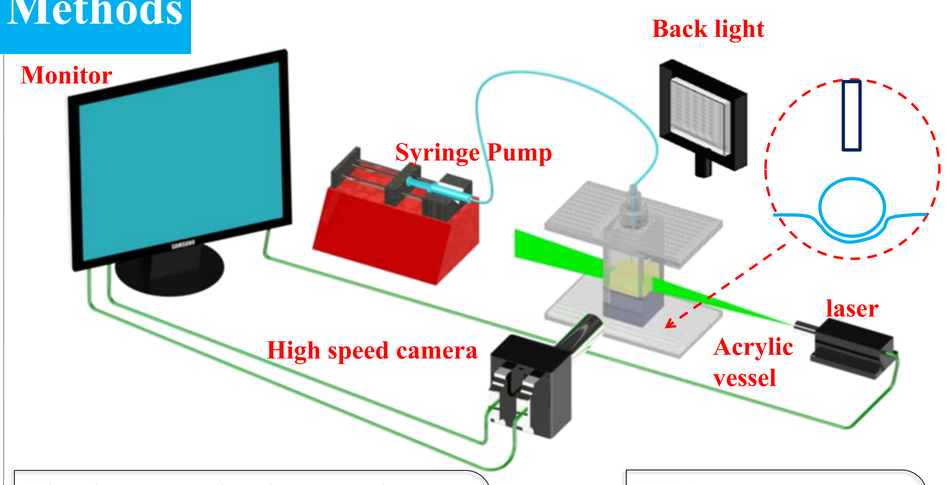

Shadowgraph observation

Working Fluids:

- Aqueous: water-glycerol
- Organic: 5cst silicone oil
- Surfactant: Span 80

Aim:

- Find the boundary of partial coalescence.
- Study the effect of surfactant on drop ratio.

PIV tests

Working Fluids:

- Aqueous: water-glycerol
- Organic: 0.65cst silicone oil
- Surfactant: Span80

Aim:

- Drop surface evolution.
- Fluid dynamics of partial coalescence

Region map

The Oh-Bo phase map indicating the coalescence region is plotted for surfactant and non-surfactant system.

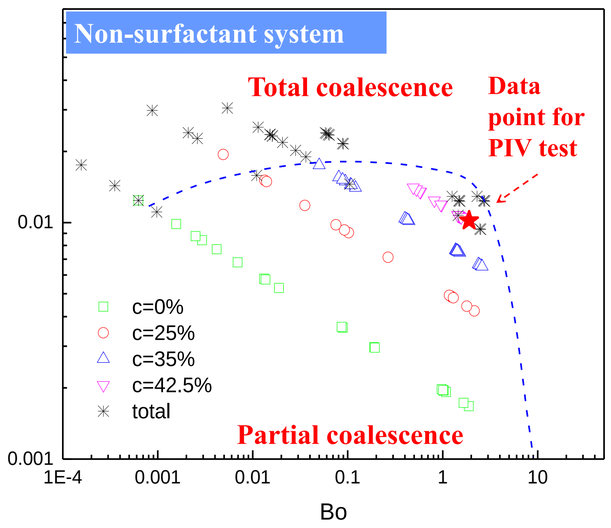

***c*– glycerol concentration.**

***φ*– surfactant concentration.**

$$Bo = \frac{(\rho_w - \rho_o) g D^2}{\sigma} \qquad Oh = \frac{\mu_w}{\sqrt{\rho_m \sigma D}}$$

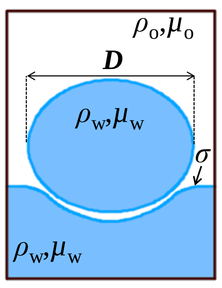

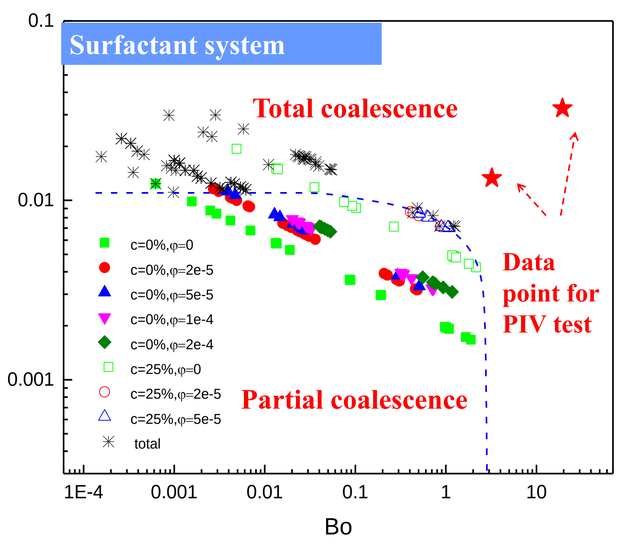

- The critical Oh_c exists when Bo <0.1.
- The Oh_c increases with the glycerol concentration.
- The partial coalescence region is reduced when surfactants are presented.
- The Oh_c decreases with the increase of surfactant concentration.

Drop ratio

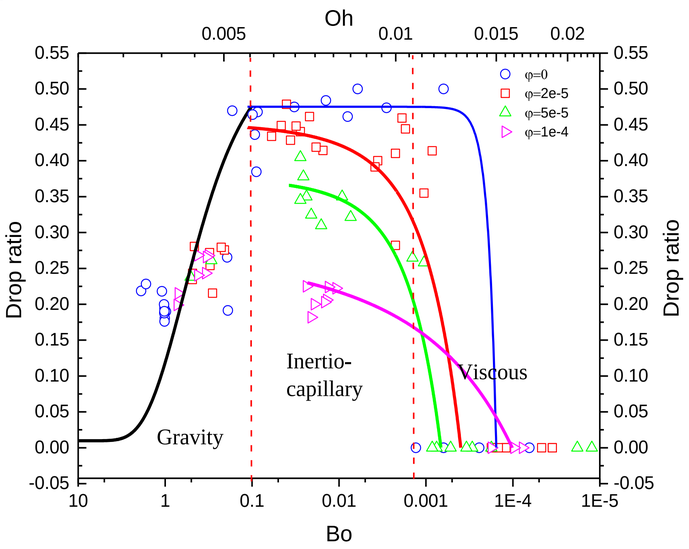

- The partial coalescence can be defined into three regimes: the gravity regime, the inertio-capillary regime and the viscous regime.
- In the inertio-capillary regime, the presence of surfactant reduces the value of drop ratio.

The ratio of the diameter of the daughter droplet to that of the mother droplet at each stage of the coalescence cascade is plotted in the figure.

Surface evolution

The data points shown with five-pointed star in both partial and total region are selected for the Particle Image Velocimetry test. The drop evolution for each case is extracted below.

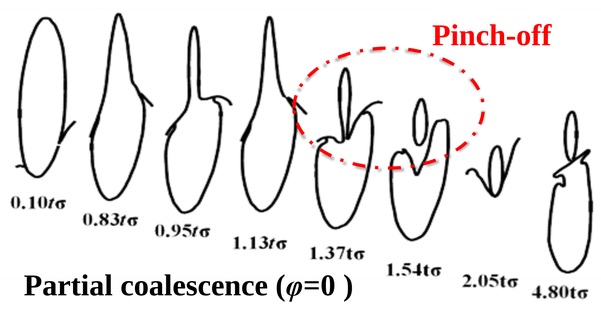

Partial coalescence (φ=0)

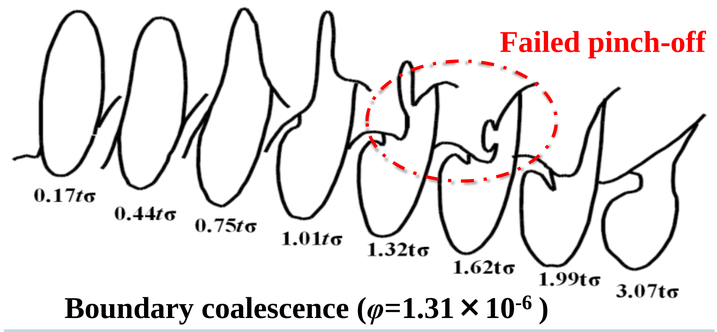

Boundary coalescence ($\varphi = 1.31 \times 10^{-6}$)

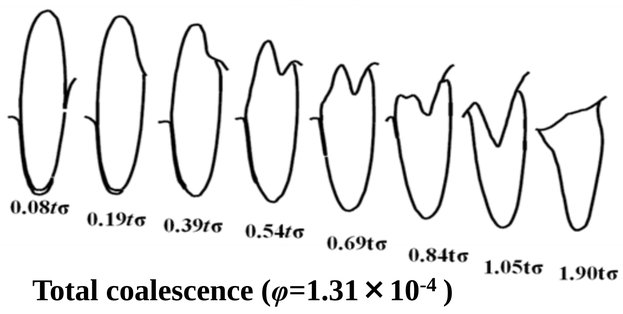

Total coalescence ($\varphi = 1.31 \times 10^{-4}$)

- Surfactant promotes the interface deformation;
- The liquid cylinder is observed for φ=0 and $\varphi = 1.31 \times 10^{-6}$, while no cylinder is created for $\varphi = 1.31 \times 10^{-4}$.
- The pinch-off of liquid cylinder is failed for boundary coalescence.

Velocity field

Horizontal velocity in opposite direction are created inside the liquid cylinder, which help the shrink of the cylinder.

The converge of the bulk liquid promote the pinch-off.

Horizontal velocity →

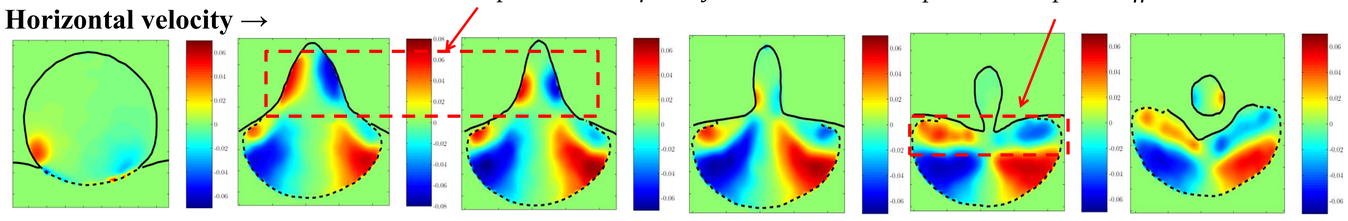

Prior to pinch off, the vertical velocity at the top part of cylinder is much lower than the bottom.

When pinch off is about to occur, the vertical velocity near the neck is much higher than other area.

Vertical velocity →

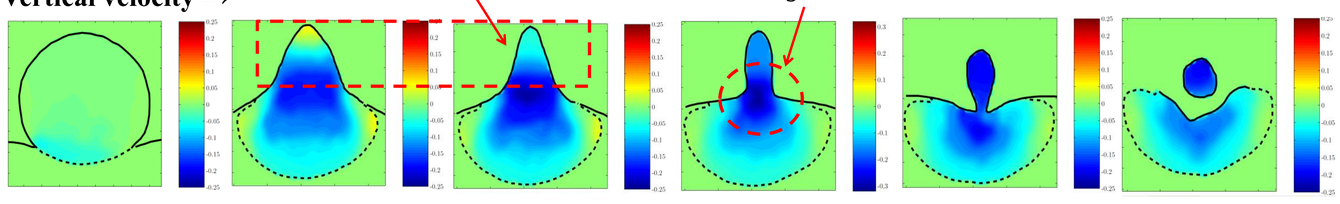

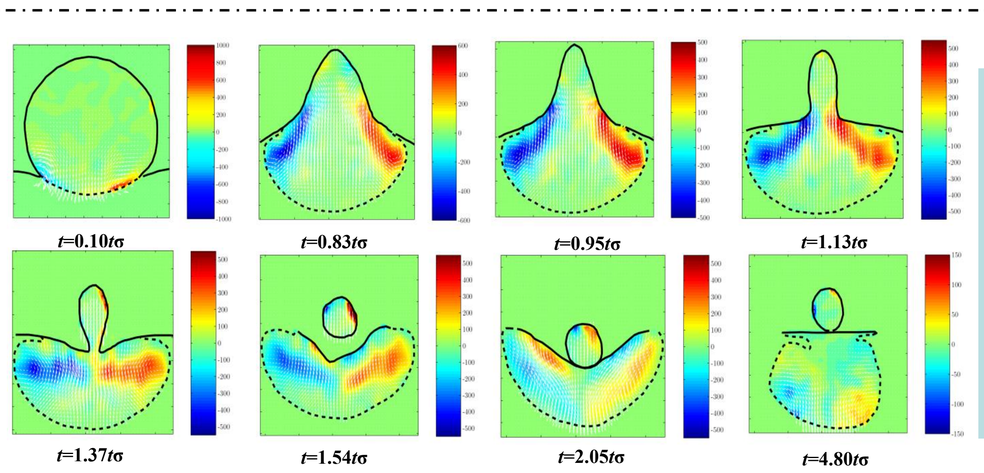

Vortices evolution during partial coalescence

- Vortices are observed at the bottom of droplet at the initial stage.
- The vortices keep moving upward but do not enter the liquid cylinder.
- Vortices in the secondary droplet are still observed.

Conclusions

- Bo-Oh diagram is plotted to show partial coalescence region.
- In the inertial-capillary regime, surfactant reduces the drop ratio.
- The pinch-off phenomenon is largely determined by the competition between horizontal and vertical flux of droplet liquid.

EPSRC Engineering and Physical Sciences Research Council
memphis multiphase
CHINA SCHOLARSHIP COUNCIL

Pattern Formation in Pulsed Gas-Solid Fluidised Beds: Insights from Experiments and Computations

Kaiqiao Wu, Victor Francia, Lilian de Martín, Marc-Olivier Coppens

University College London, Department of Chemical Engineering, Torrington Place, WC1E 7JE, London, UK

Introduction

Periodic perturbation is able to impose order onto chaotic systems. Inspired by ripples in the sand, produced by periodic gusts of wind and waves, gas-solid fluidized beds can display a dynamically structured, granular pattern when exposed to periodically oscillating air flows [1, 2].

In a quasi-2D geometry, bubbles rise and form a triangular tessellated structure, whereas, in a 3D geometry, the top surface oscillates and is covered by stripes or square configurations. This fascinating phenomenon holds the potential to structure the complex dynamics, facilitate scale-up, validate computational models and investigate the collective behaviour of solids [3].

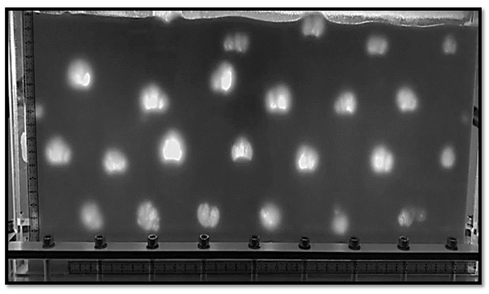

(a) Quasi-2D: hexagonal bubble array

(b) Shallow 3D: surface pattern

We present our recent experimental and computational insights on pattern formation in gas-solid fluidized systems, and discuss the bed dynamics during a patterned state.

[1] M.-O. Coppens *et al.*, *Proc. 4th WCPT*. Paper 355 (2002)
[2] M.-O. Coppens and J.R. van Ommen, *Chem. Eng. J.* **96**, 117-124 (2003)
[3] K. Wu *et al.*, *Powder Technol.* **295**, 35-42 (2016)

Experiments and Simulations

Experiments were undertaken in a 45cm wide ×1cm thick quasi-2D rectangular bed with a 4.5cm deep static loading. Glass beads with an average size of 238μm were fluidized with air at ambient conditions. The same configurations are simulated using a classical CFD-DEM approach in a small 3D domain.

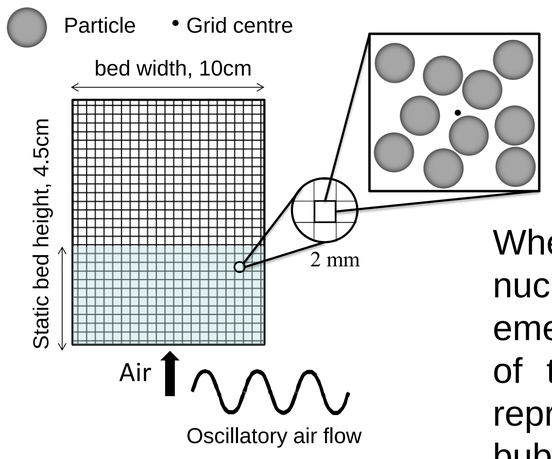

$$U_0 / U_{mf} = A + B\sin(2\pi f \cdot t)$$

Property	Value
Particle size	238 μm
Particle density	2500 kg/m^3
Simulated bed	10cm x 4.5cm x 0.2cm
Experimental bed	45cm x 4.5cm x 1cm

When bubble patterns form, the bubble nucleation sites in the subsequent cycle emerge in between the bubble locations of the previous row. The simulations reproduce these dynamic subharmonic bubble patterns in excellent agreement with the experiments.

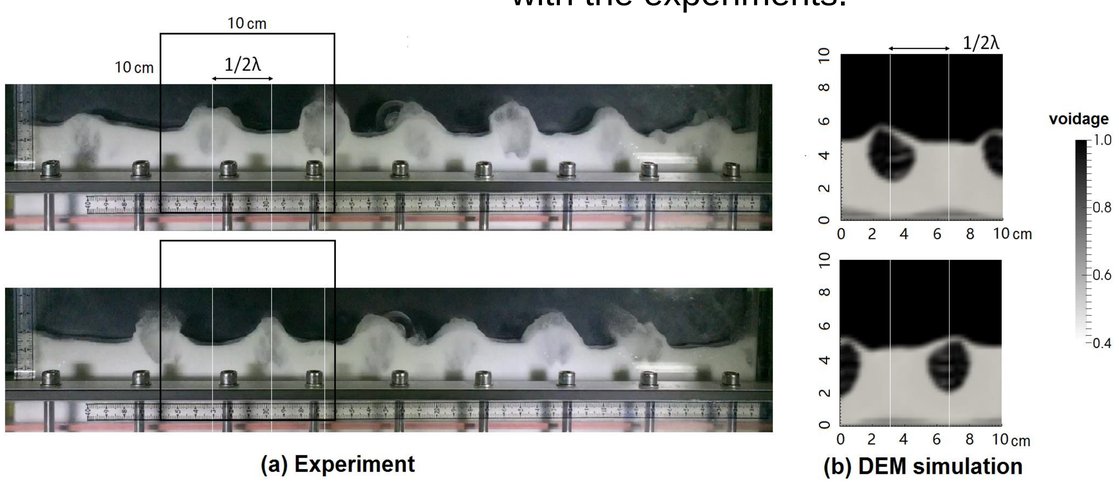

(a) Experiment **(b) DEM simulation**

The computational patterns agree with experimental observations. The bubble nucleation sites alternate every cycle, shifting half of the wavelength λ. A=2.64, B=2.14, f=5Hz.

Discussion

Structured patterns emerge within a certain range of pulse frequencies, and the regularity can be quantified by comparing to exact hexagonal arrays. When bubble patterns form, the size of the bubbles can be manipulated, with narrower distributions over continuous fluidization.

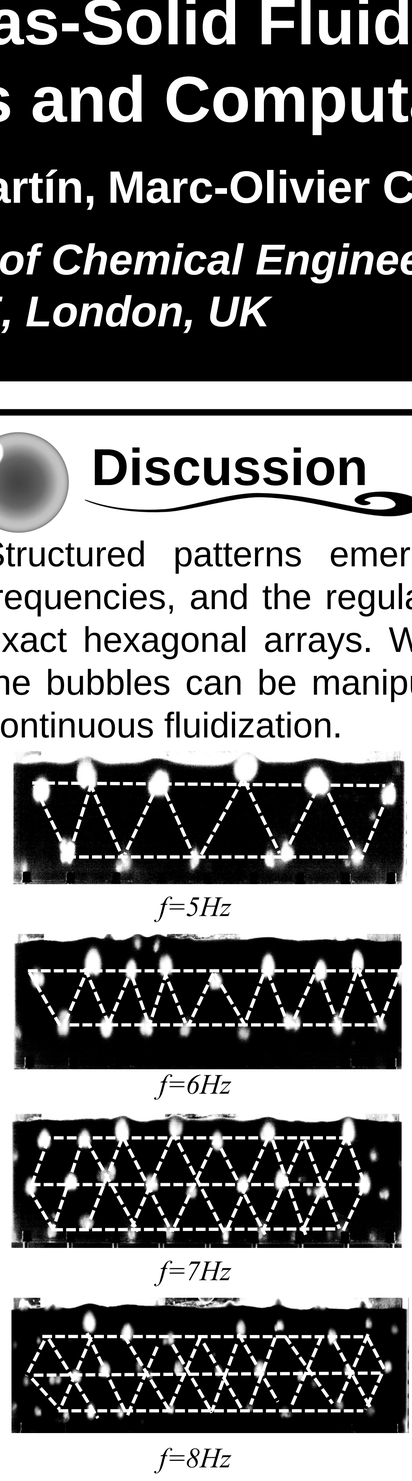

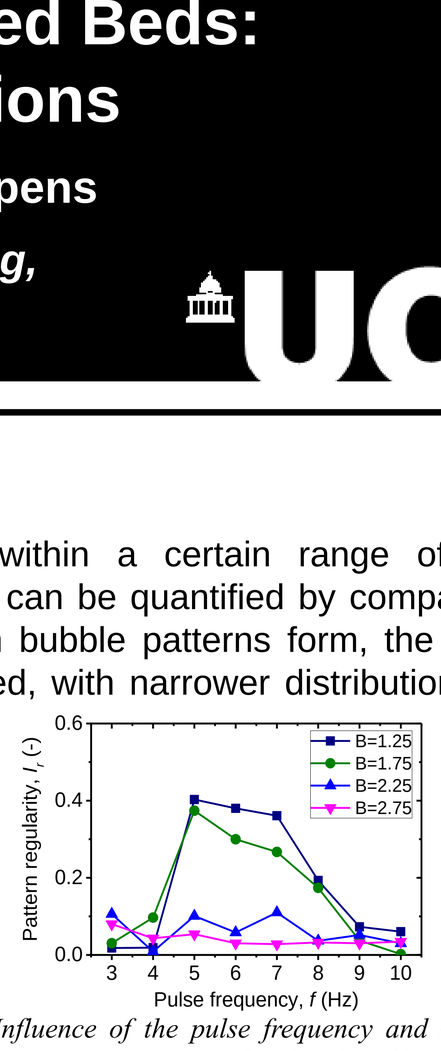

Influence of the pulse frequency and amplitude on pattern regularity. Bed height =10cm, A=0.5.

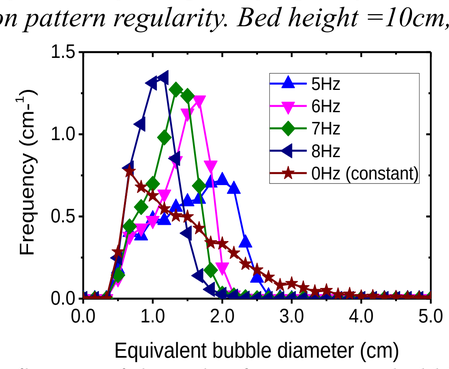

Influence of the pulse frequency on bubble size distribution. Bed height =10cm, B=1.25, A=0.5.

The bubble motion drives the displacement of the solids on either side, which then converge and come into contact vigorously within the wake of each bubble.

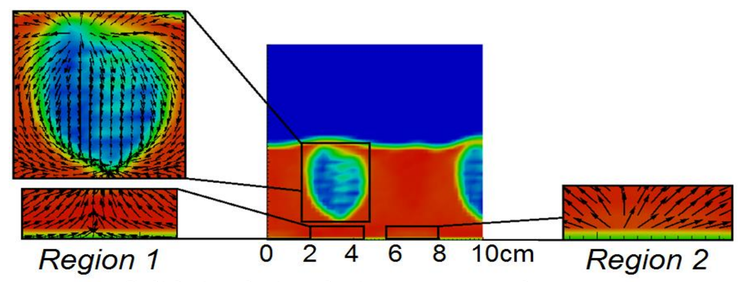

Solid circulation during a patterned state.

The sustained local multi-particle contacts in the bubble wake lead to long-range, large solids stresses near the distributor surface, which restricts the mobility of the particles beneath the bubbles, and suppresses the bubble formation [4].

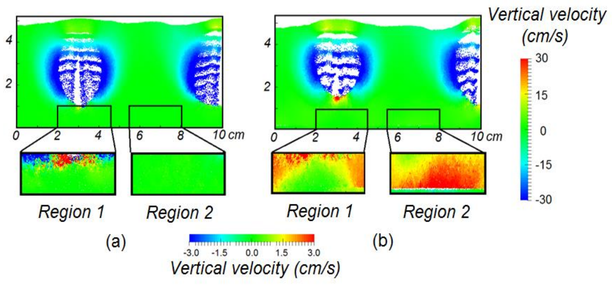

Solid vertical velocity profile at the beginning of each pulse period.

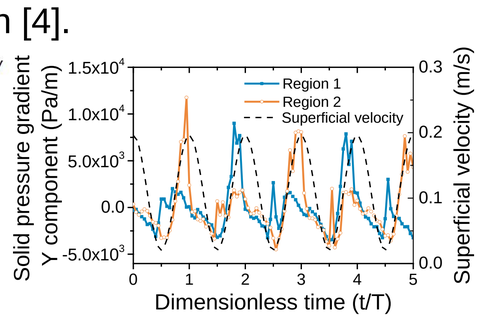

Time series of the vertical component of the average solid pressure gradient.

[4] K. Wu *et al.*, *Chem. Eng. J.* **329**, 4-14 (2017)

Conclusions

- ❖ Discrete treatment of the solid phase is able to correctly reproduce the experimentally witnessed structured bubble patterns in gas-pulsed fluidized beds.
- ❖ Computational results show that the solid friction is of paramount importance to induce the formation of regular bubble patterns in a quasi-2D geometry.
- ❖ For patterned states, adjusting the pulsed flow allows us to control and manipulate effectively the bubble size and spatial distribution in quasi-2D fluidized beds.

Further work

- ✓ Investigate the influence of the particle surface condition on quasi-2D bubble patterns.
- ✓ Extend the quasi-2D bubble pattern control to 3D systems.

Acknowledgements

The research leading to these results has received funding from an EPSRC Frontier Engineering Award (EP/K038656/1)

UCL ENGINEERING Change the world

CfNIE Centre for Nature Inspired Engineering

EPSRC Engineering and Physical Sciences Research Council

A Holistic Modelling Approach for Production of Crystalline Powder of Pharmaceutical Materials in Spray Drying Towers

ADDoPT — ADVANCED DIGITAL DESIGN OF PHARMACEUTICAL THERAPEUTICS

UNIVERSITY OF LEEDS

Muzammil Ali, Andrew Bayly, Caiyun Ma, Kevin Roberts, Peter Heggs and Tariq Mahmud

School of Chemical and Process Engineering, University of Leeds, Leeds LS2 9JT, UK

1. Introduction

- Spray drying is used for the manufacture of a variety of products, such as amorphous solid dispersions, crystalline APIs and inhalation powders, in the pharmaceutical industry.
- Modelling of spray drying processes is challenging due to difficulty associated with integrated transport processes between the droplets and particles with complex turbulent gas flow.
- A framework for spray drying modelling of pharmaceutical products is proposed.

2. Modelling Approach

Single droplet drying modelling

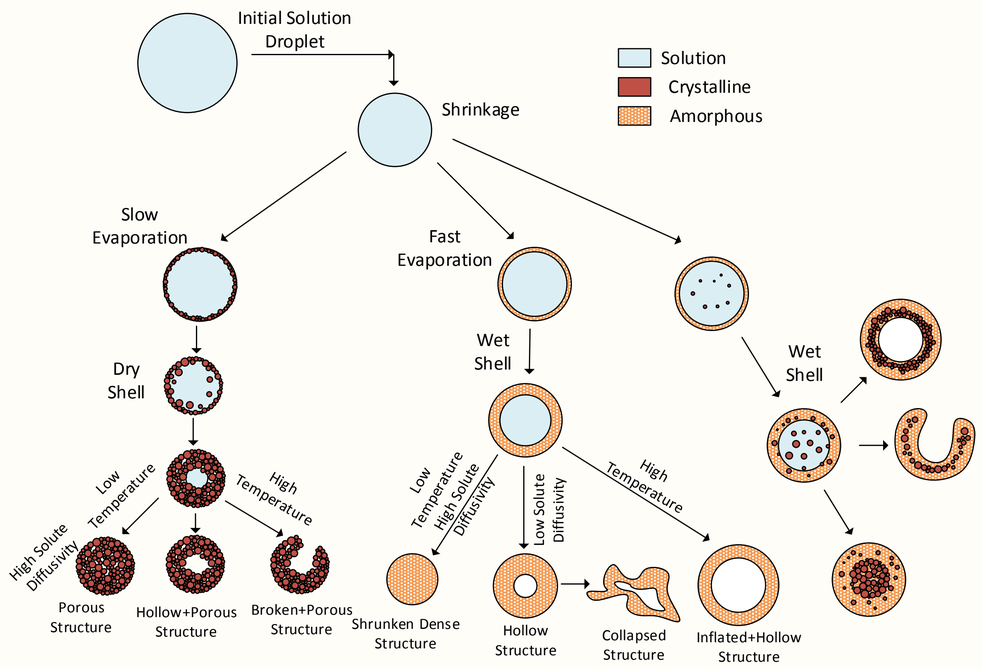

Multi-phase CFD modelling

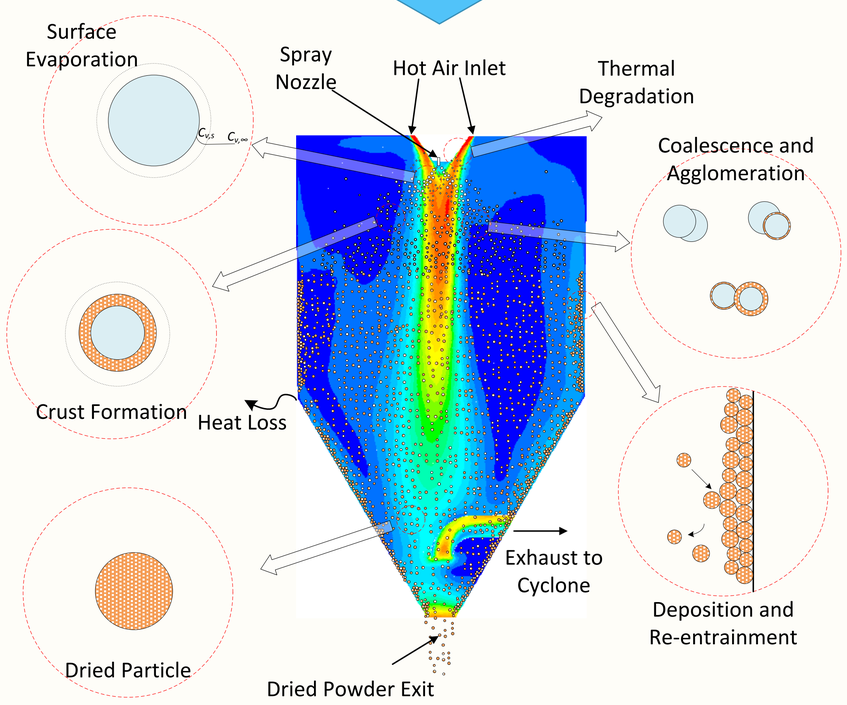

Zonal modelling

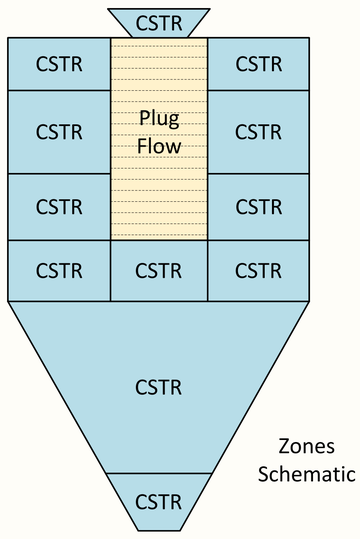

- A multi-zonal modelling approach enables estimation of spray dried powder characteristics in a computationally efficient manner.
- Zones can be identified based on a detailed analysis of gas flow fields and particle trajectories from CFD model results.
- Spray drier is divided into a series of interconnected well-mixed and plug-flow zones.
- Fluxes across the zone boundaries can be obtained from CFD results.

3. Formation of Crystalline Particles

Modelling Approach

- Diffusive transport (DT) model to capture concentration profile along the radius of the drying droplet/particle.
- Population balance (PB) model to track the size distribution of microcrystals within the drying droplet/particle.
- A zonal modelling approach to be used for faster solution of the coupled DT/PB models.
- The drying models will be integrated with the CFD model to predict dried powder characteristics in spray towers.

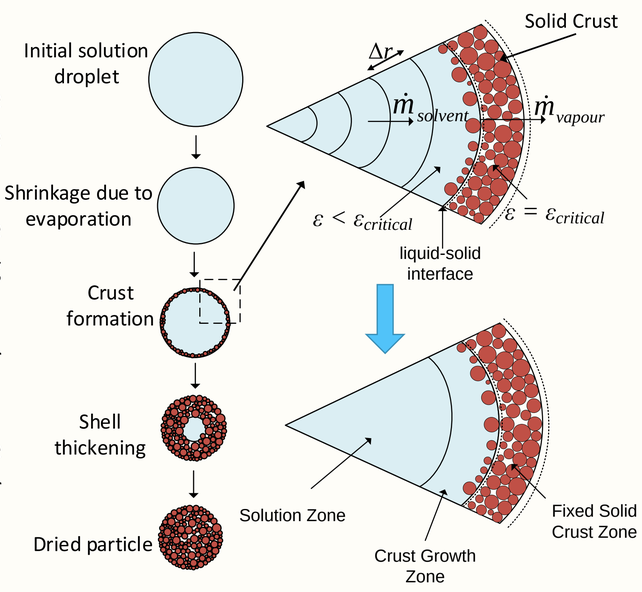

4. Formation of Amorphous Particles

Modelling of Single Droplet Drying

- A single droplet drying model based on diffusive transport of solvent is integrated with a qualitative crystallisation model for the prediction of formation of lactose particles.
- Variations of solute and solvent concentrations along the droplet radius is predicted.

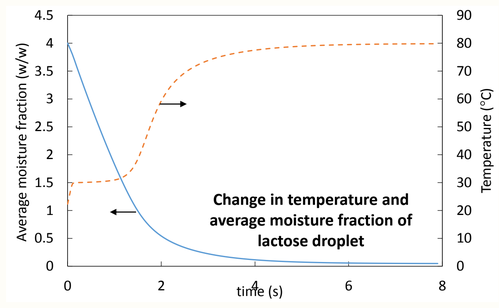

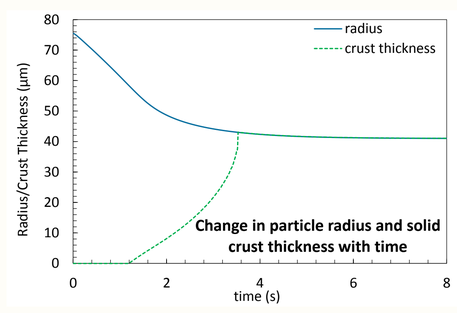

Droplet Drying Stages

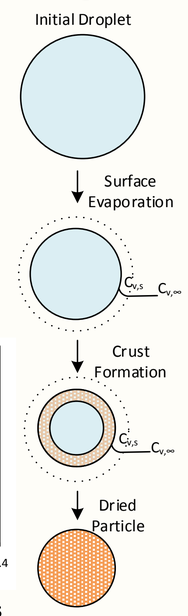

- Transformation from amorphous to crystalline form in the solid phase is predicted using Williams-Landel-Ferry[1] (WLF) model.

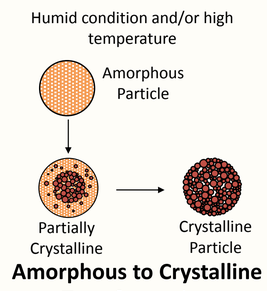

Amorphous to Crystalline Transformation

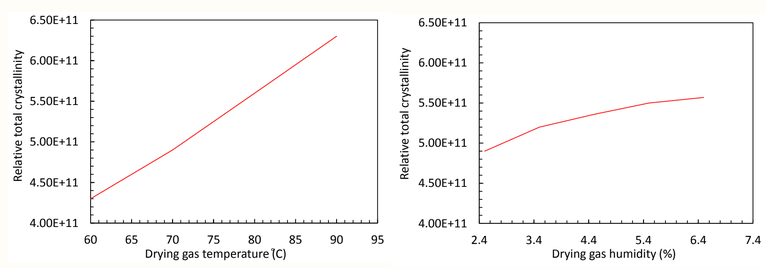

Predicted relative total crystallinity of spray dried particles (higher values indicate more crystalline material)

Multi-phase CFD Modelling of a Lab-Scale Spray Dryer

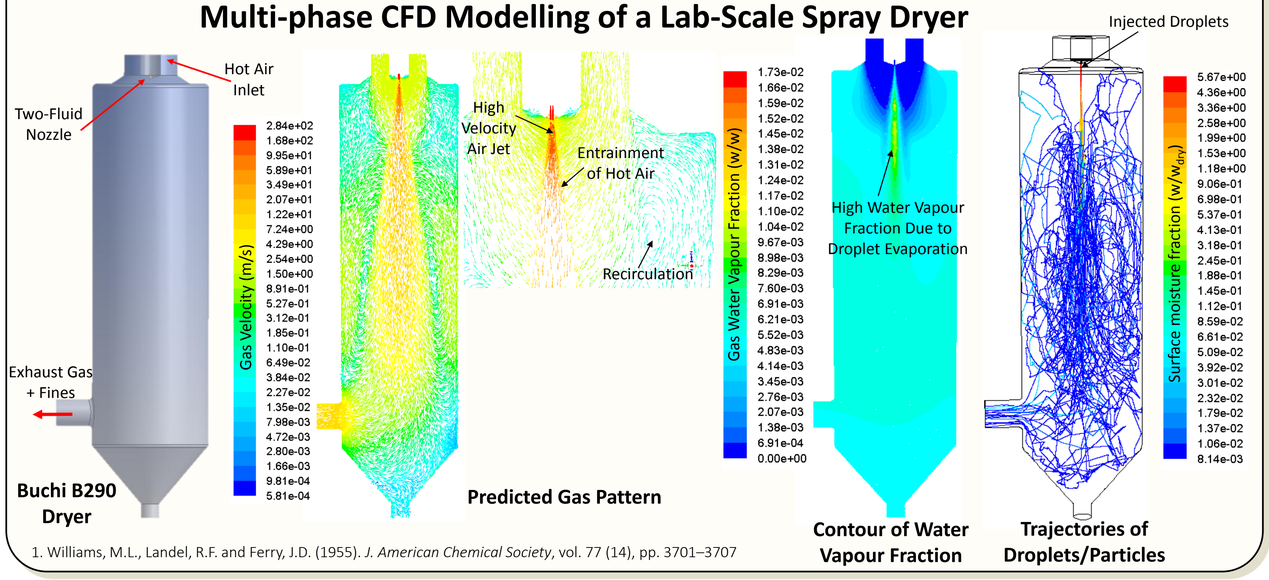

1. Williams, M.L., Landel, R.F. and Ferry, J.D. (1955). *J. American Chemical Society*, vol. 77 (14), pp. 3701–3707

5. Conclusions

- Modelling of pharmaceutical material is carried out to predict moisture and crystallinity.
- The proposed framework can be applied to predict spray dried powder characteristics in a computationally efficient manner.

ADDoPT is a collaboration instigated by the Medicines Manufacturing Industry Partnership, and part funded under the Advanced Manufacturing Supply Chain Initiative, a BEIS initiative delivered by Finance Birmingham and Birmingham City Council.

Analysis of industrial reactive powders flow properties at high temperature

Domenico Macri' [1], Massimo Poletto [2], Diego Barletta [2], Stephen Sutcliffe [3], Paola Lettieri [1]

[1] Department of Chemical Engineering, University College London, Torrington Place, London WC1E 7JE, UK
[2] Dipartimento di Ingegneria Industriale, Università degli Studi di Salerno, Via Ponte Don Melillo, 84084 Fisciano (SA), Italy
[3] Huntsman Pigments and Additives, Wynyard Park, Stockton-on-Tees TS22 5FD, UK

PROJECT OVERVIEW

PROBLEM

In fluidized bed operations at high temperatures the particles tend to stick and agglomerate, causing defluidization.

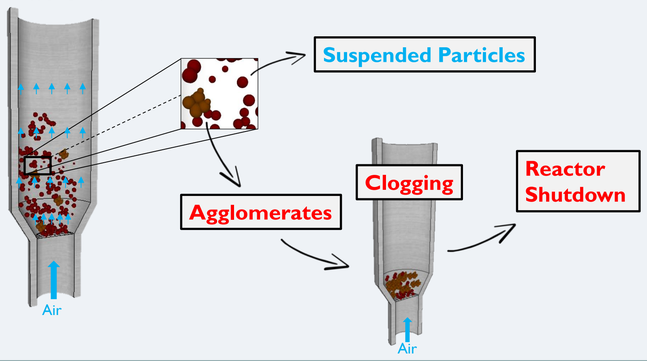

CAUSES

Temperature affects particles adhesion and flow behaviour, due to the enhanced role of the *interparticle forces* (IPFs)

OBJECTIVES & METHODS

Carry out a systematic study on the effect of temperature on the fluidization quality of industrial reactive powders (in particular TiO_2) by linking:

- Fundamental fluidization tests
- Rheological tests

MATERIALS & METHODS – RHEOLOGICAL MEASUREMENTS

Synthetic Rutile (SR)

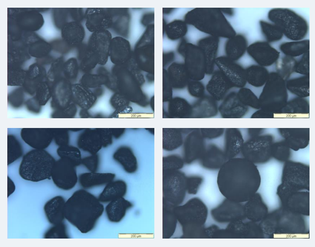

ρ_p = 3200 kg/m^3
ρ_b = 1500 kg/m^3
d_{50} = 162 µm
d_{sv} = 145 µm
RDS = 0.28

Natural Rutile (NR)

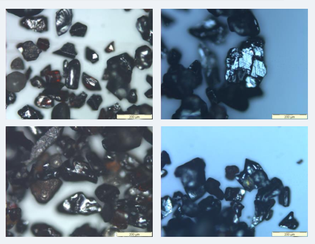

ρ_p = 4200 kg/m^3
ρ_b = 2320 kg/m^3
d_{50} = 202 µm
d_{sv} = 155 µm
RDS = 0.65

Yield Locus

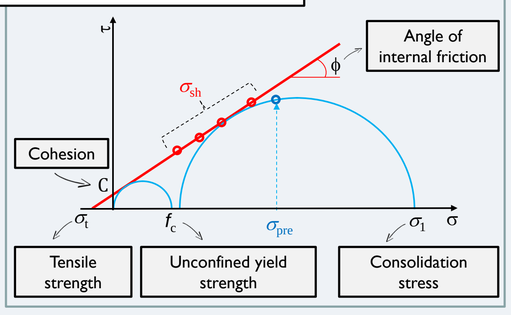

Annular Shear Cell

A modified Schulze Shear Cell[1] was used to characterize the bulk flow properties of the materials at ambient and high (500 °C) temperature.

HOW IT WORKS

- While the bottom ring is rotating, the torque necessary to keep the lid in place is measured.
- The normal stress and the corresponding yield shear stress are determined and plotted on the σ-τ plane.
- The best fitting line through the (σ-τ) experimental yield points gives the yield locus.
- Key bulk flow properties are evaluated from Yield Locus.

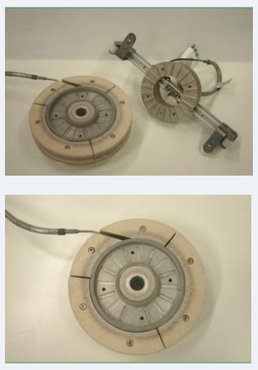

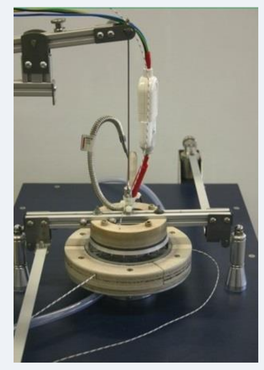

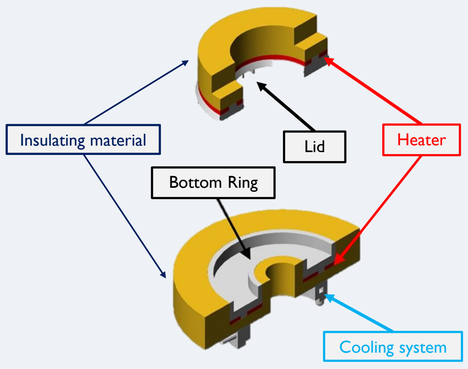

RESULTS

Experimental

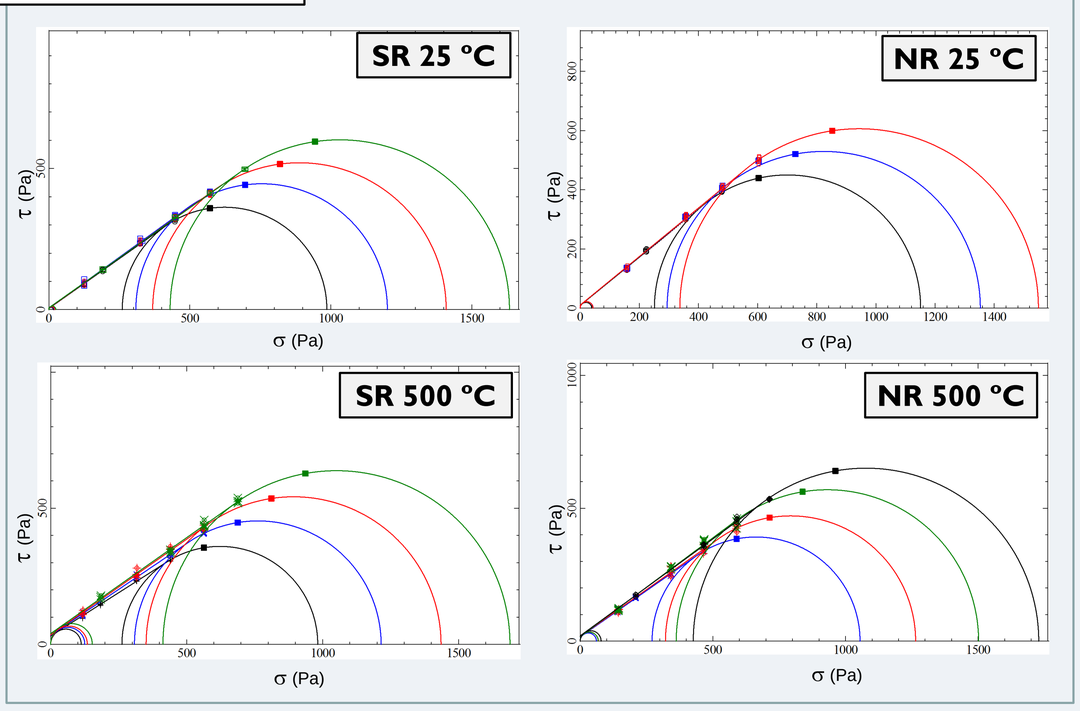

Theoretical

Macroscopic properties of bulk solids (from Shear Cell)

⇕

Microscopic interparticle interactions

⇩

Tomas modelling approach[2]

$$\sigma_t^* = \frac{F_H}{d_{sv}^2}\frac{1-\varepsilon}{\varepsilon}$$

⇩

IPFs estimation:

$$IPFs = (1+\kappa)F_{H0} + \kappa F_N$$

⇩

$$\kappa^* = \frac{\tan\phi_{st}}{\tan\phi_i} - 1 \qquad \kappa^{**} = \frac{\kappa_p}{\kappa_A - \kappa_p}$$

κ^*

- Evaluated from Stationary Yield Locus
- Independence from physical and mechanical parameters (e.g. compressive yield strength p_f and Hamaker constant C_H)

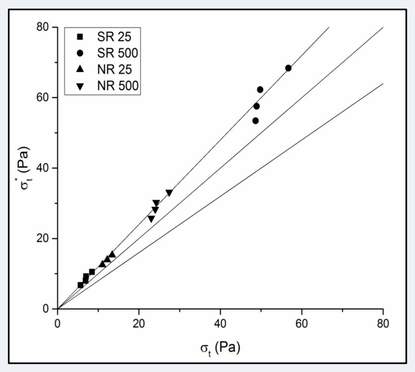

κ^{**}

- Evaluated from Tomas' particles contact constitutive model
- Strong dependence from physical and mechanical parameters (in particular p_f)

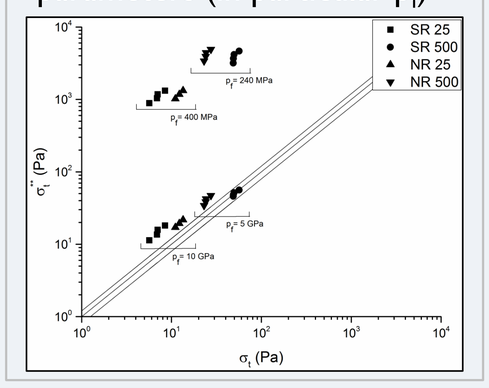

SENSITIVITY ANALISYS OF p_f ON κ^*

$p_{f,25}$

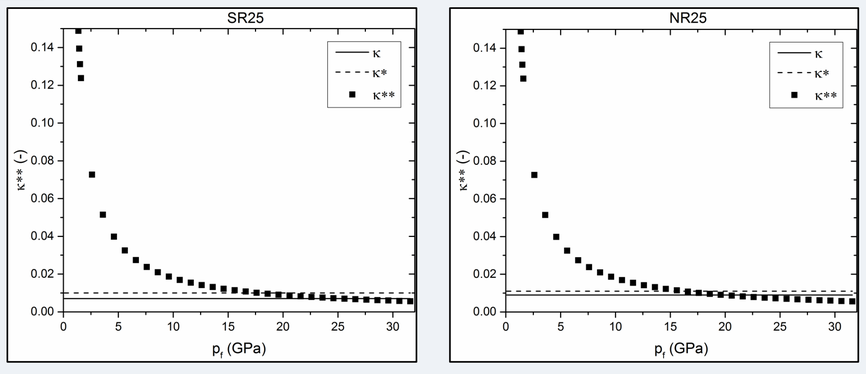

$p_{f,500} = \alpha\, p_{f,25}$

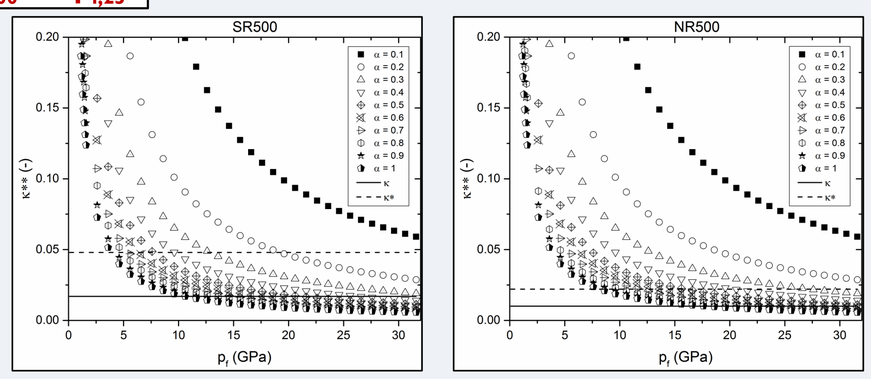

DISCUSSION & FUTURE WORKS

- Shear experiments highlighted interesting **changes of bulk flow properties with temperature** (e.g. unconfined yield strength, fc). This means that the materials show **lower flowability** with increasing temperature.
- Modelling predictions: the approach showed some problems related to the **difficulty in identifying** the accurate **physical and mechanical properties** of the materials at the different conditions investigated.
- The **fitting** of the model data with the experimental ones **improves** if proper values for the materials properties, in particular for the compressive yield strength at both ambient and high temperature, are taken into account.
- Fundamental **fluidization tests** will be conducted in order to **link** the rheological evidences to the corresponding fluidization behaviour.

REFERENCES

[1] Tomasetta I., Barletta D., Poletto M. The High Temperature Annular Shear Cell: A modified ring shear tester to measure the flow properties of powders at high temperature. *Advanced Powder Technology* 24 (2013) pp. 609-617.

[2] Tomas J. Mechanics of nanoparticle adhesion - A continuum approach, *Particles on Surfaces 8: Detection, Adhesion and Removal* (2003) pp. 1–47.

CONTACTS

domenico.macri.14@ucl.ac.uk

HUNTSMAN
Enriching lives through innovation

UCL ENGINEERING
Change the world

Imperial College London

Direct Numerical Simulation of Vertical Surfactant-laden Two-Phase Flow

A. Batchvarov,[1] L.Y.K. Ang,[1] J.S. Yong,[1] O.K. Matar[1] and R. V. Craster.[2]

[1]Departament of Chemical Engineering, Imperial College [2]Department of Mathematics, Imperial College

Abstract

Vertical air-water flows are investigated, and different flow regimes identified using Direct Numerical Simulations. The computations are carried out using a front-tracking-based CFD solver. Equations for the interfacial and bulk surfactant concentrations are coupled to the hydrodynamics. We present preliminary results that demonstrate good qualitative agreement with experimental observations in terms of interfacial phenomena; these include 3D large-amplitude wave formation, the development of long ligaments, and droplet entrainment.

Code BLUE and Simulation Set-up

- Massively parralel, high performance, DNS solver that can be used to describe wide variety of 3D multiphase systems (Chergui et al., 2016).
- Control volume dimensions (0.033m x 0.033m x 0.132m). Vertical solid cylinder (Radius=0.162m) represents pipe through which we observe the gas-liquid flow.
- Simulations ran on 54 cores (control volume split 3 x 3 x 6) with resolution of each sub control volume of 32 x 32 x 64.

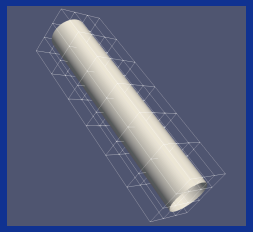

FIGURE 1 Control Volume In BLUE

Flow Regimes and Comparison with Experimental Visualisations

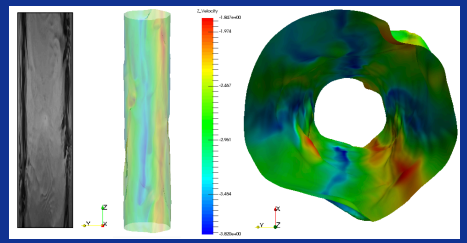

(A) Downward Annular Flow

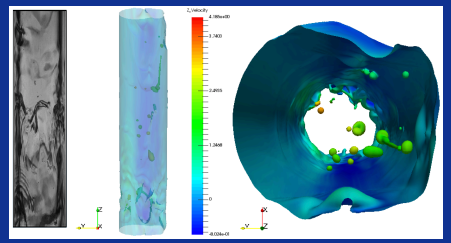

(B) Flow reversal

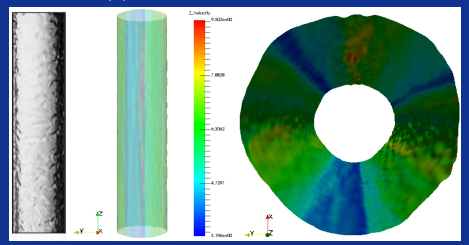

(C) Upward Annular Flow

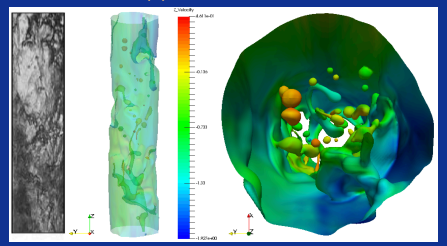

(D) Churn Flow

FIGURE 2 Flow Regime Comparison in Absence of Surfactants

(A, B) Comparison with Experimental Visualisation from Technical Report (2016)

(C, D) Comparison with Experimental Visualisation from van Nimwegen (2014)

The Marangoni Effect and its Effect on Waves

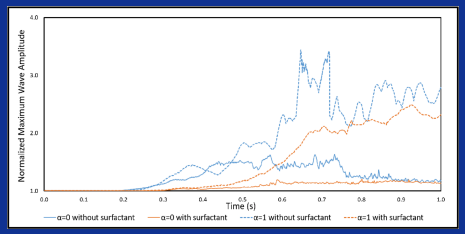

(A) Normalised Maximum Wave Amplitudes

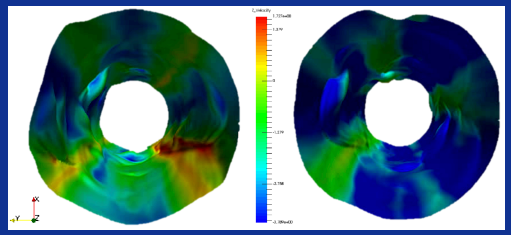

(B) Runs Without (Left) and With (Right) Surfactant

FIGURE 3 Surfactant Effect on Wave Amplitudes and Wave Perturbations

Surfactant Effect on Droplet Entrainment

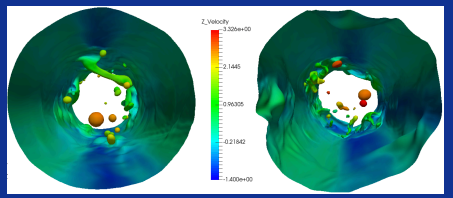

FIGURE 4 Droplet Entrainment in Annular Flow Without (Left) and With (Right) Surfactant

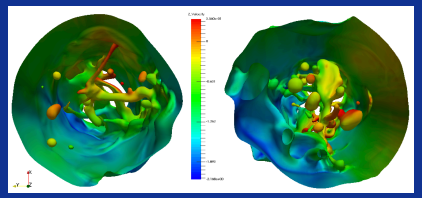

FIGURE 5 Churn Flow Without (Left) and With (Right) Surfactant

Acknowledgements

The authors would like to extend a special thank you to the team behind code BLUE: Dr. Damir Juric, Dr. Jalel Juric and Dr Seungwon Shin. A special acknowledgement should also be sent to Dr. Lyes Kahouadji for his tireless support. Funding from EPSRC through the MEMPHIS Programme Grant (OKM, PI) is acknowledged.

References

Chergui, J., Farhaoui, A., Juric, D., Kahouadji, L., Matar, O. K. and Shin, S. (2016), 'The code blue: Massively parallel direct numerical simulation of three-dimensional multi-phase flows'.

Technical Report (2016), The effect of surfactant on flooding phenomena, Technical report, Transient Multiphase Flow Consortium.

van Nimwegen, A. T., Portela, L. M. and Henkes, R. (2014), 'The effect of surfactants on air–water annular and churn flow in vertical pipes. part 1: Morphology of the air–water interface', International Journal of Multiphase Flow 74, 133–145.

Multiphase Three-Dimensional Direct Numerical Simulation of Rotating Impeller with BLUE

L. Kahouadji, *J. Chergui*, *D. Juric*, *S. Shin*, *R. Craster* & *O. Matar*

[a] Department of Chemical Engineering, Imperial College London, SW7 2AZ London, United Kingdom
[b] LIMSI, CNRS, Université Paris-Saclay, Bât 508, rue John von Neumann, Campus Universitaire, F-91405 Orsay, France
[c] Department of Mechanical and System Design Engineering, Hongik University, Seoul 121-791, Korea
[d] Department of Mathematics, Imperial College London, SW7 2AZ London, United Kingdom

The flow driven by a rotating impeller inside an open fixed cylindrical cavity is studied numerically using the code BLUE. The impeller is composed of four blades at a 45 degree inclination all attached to a central hub and tube stem. Solid forms are constructed by means of a module for the definition of immersed objects via a distance function that takes into account the object's interaction with the flow for both single and two-phase flows.

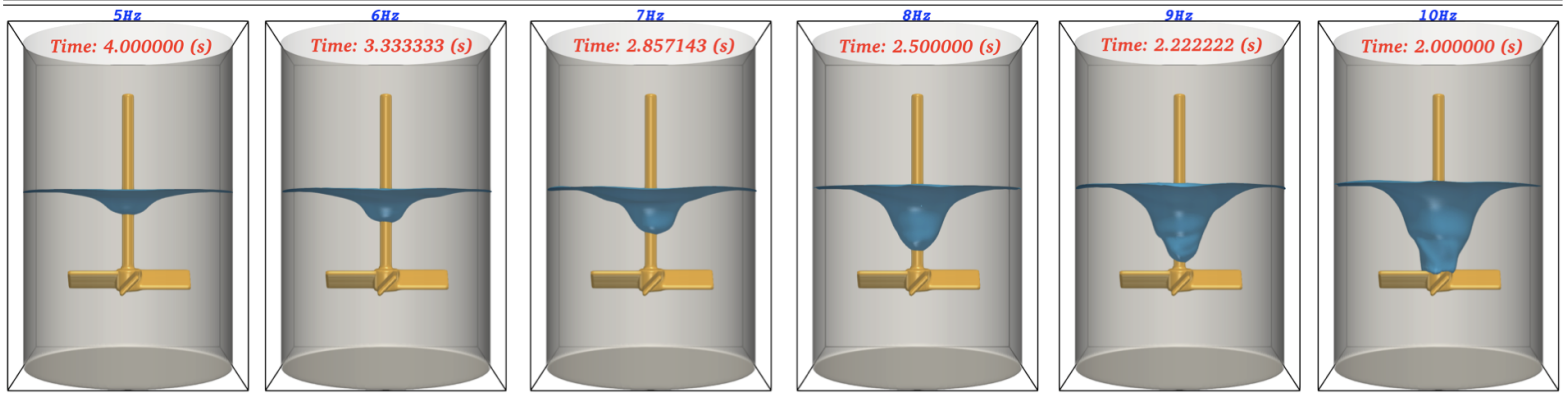

$$f = 11\mathbf{Hz} \quad \left(T = \frac{1}{11}(s)\right)$$

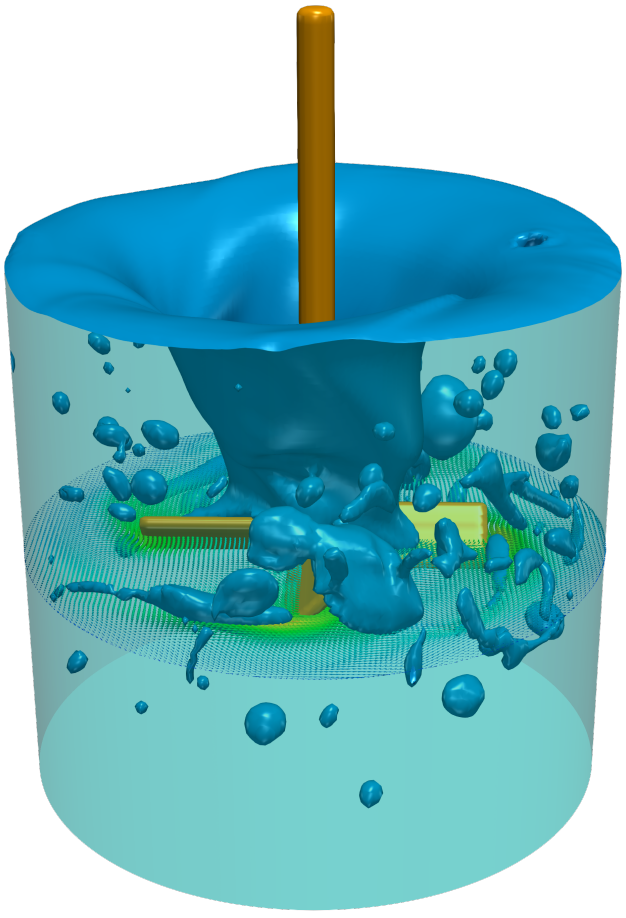

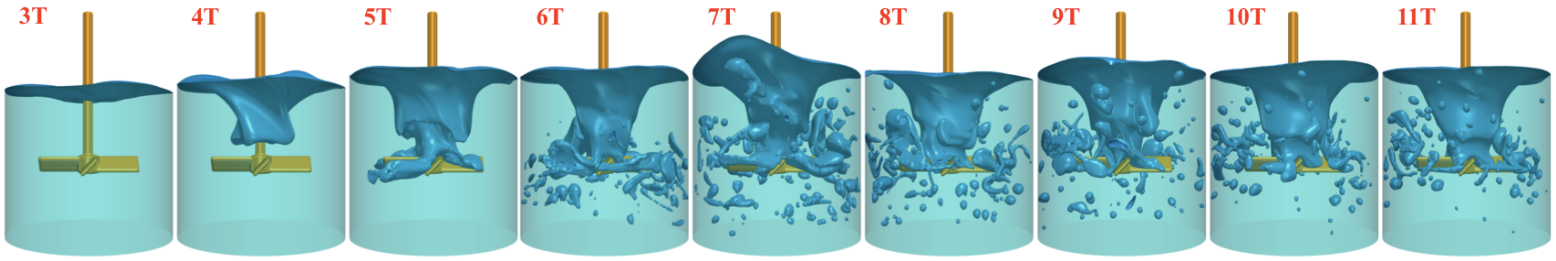

Combining microfluidic devices with coarse capillaries to reduce the size of monodisperse microbubbles

Miss Xinyue Jiang, Dr. Maryam Parhizkar, Prof. Mohan Edirisinghe

Introduction

Microbubbles, widely defined as bubbles with diameters in the range of 1-1000µm, are highly used in scientific and biomedical fields such as food, chemical industries1, contrast agents and gene delivery2. However, due to the restriction of conventional microbubble manufacturing methods, these microbubbles generation is lacking of monodispersity. The aim of this work is to use a novel microfluidic device made of two T-shaped PDMS (Polydimethylsiloxane) junctions combined in series with coarse capillaries (200µm) to produce monodispersed stable smaller diameter Bovine serum albumin (BSA) microbubbles, compared to single T-junction set up at given gas/liquid flow rate condition. In this work a scaling model which incorporated the number of T shape microfluidic devices to predict the diameter of microbubbles at different liquid-gas flow ratio was provided.

Methods

Single and double T-junction microfluidic devices (schematics shown in fig1.) were used to generate microbubbles with a BSA coating and nitrogen centre. Solution was prepared by dissolving 15 wt% BSA in distilled water. Microbubbles produced by single and double T-junction were both collected on a glass slides under ambient conditions (21° C).

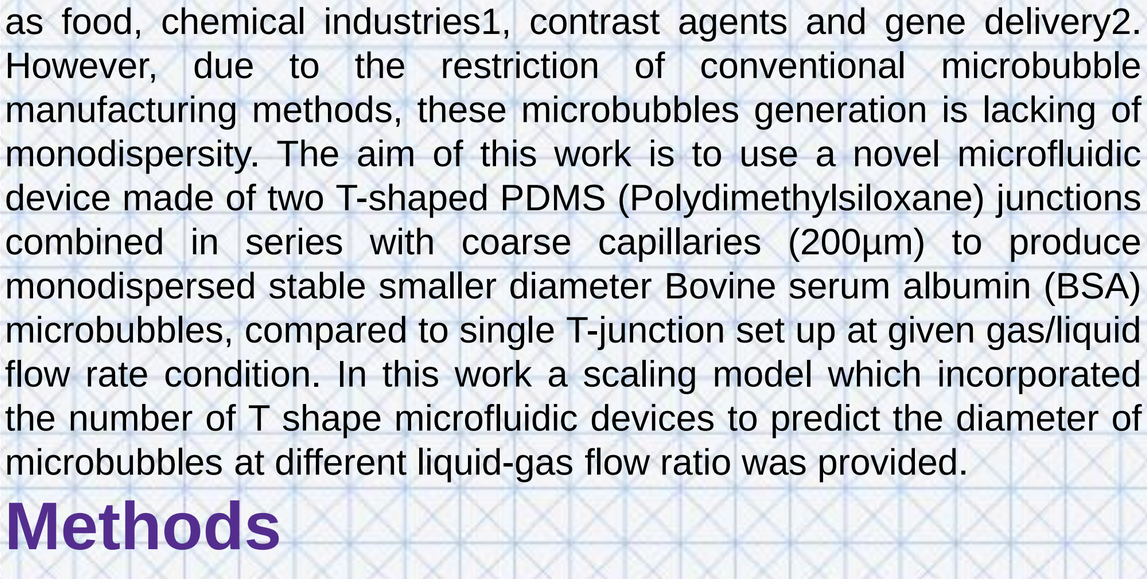

Figure 1: a) single and b) double T-junction experimental set ups. High speed camera images of microbubble formation from ai) single and bi) double T-junction. Optical microscopy from aii) single and bii) double T-junctions.

Microbubbles collected from the outlet of the device on microscope slides were immediately observed under an optical microscope (Nikon Eclipse ME 600) fitted with a camera (JVC KY-F55B). Microbubbles were studied at 5X, 10X and 20X magnifications. A phantom 7.3 high speed camera with a maximum resolution of 800 x 600 pixels were also used to exam microbubble formation.

Results

In order to investigate the effect of inserting the second T-junction on microbubble formation, comparative experiments were conducted between single and double T-junction.

For a fixed flow rate ratio, double T-junction geometry produced microbubbles with smaller diameters and better stability, due to increase in the total flow rate. It was also noted that microbubble diameter was decreased by inserting second T-junction (Figure 3).

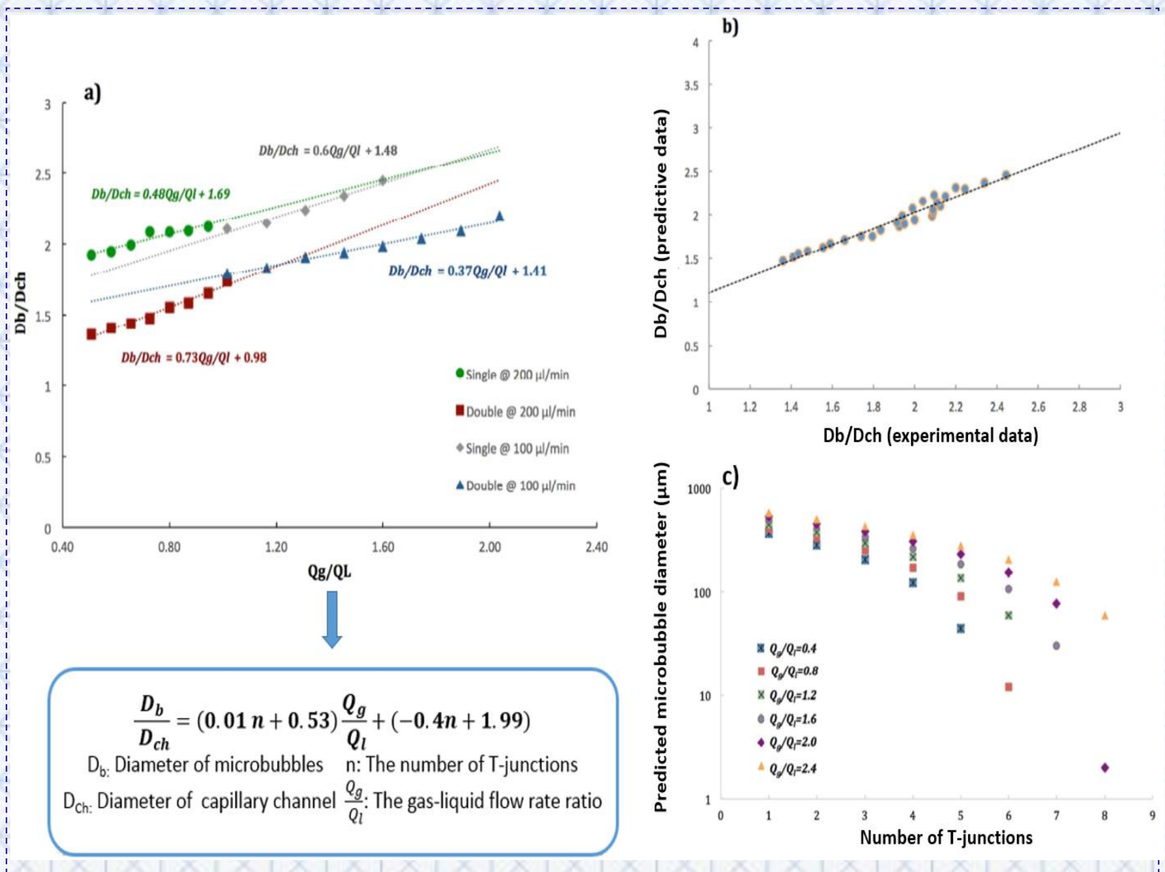

$$\frac{D_b}{D_{ch}} = (0.01\,n + 0.53)\frac{Q_g}{Q_l} + (-0.4n + 1.99)$$

D_b: Diameter of microbubbles n: The number of T-junctions

D_{Ch}: Diameter of capillary channel $\frac{Q_g}{Q_l}$: The gas-liquid flow rate ratio

Figure 2: a) Plot of dimensionless microbubble diameter produced by single and double T-junctions at various gas-liquid flow rate ratio from 0.4 to 2.40. b) scatter graph illustrates that experimental data and predicted data were in good agreement. C) predicted microbubble diameter based on scaling model .

Figure 3: Micrographs showing the lifetime of microbubbles for both single and double T-junctions at both flow rates studied (100 and 200 µl/min) and various gas pressures.

Conclusions & Future Work

In this work, it was shown that size, and stability can be manipulated by the introduction of a second T-junction into the commonly used single T-junction device. The predicted scaling model showed that the microbubble diameter can be reduced to 10 µm suitable for biomedical application, by using multiple T-junctions combined in series.

For future work, double T-junction device will be used to produce double layered microbubbles.

References

1. Campbell, G. M., & Mougeot, E. (1999). Creation and characterisation of aerated food products. Trends in Food Science & Technology, 10(9), 283-296.
2. Unger, E. C., Matsunaga, T. O., McCreery, T., Schumann, P., Sweitzer, R., & Quigley, R. (2002). Therapeutic applications of microbubbles. European journal of radiology, 42(2), 160-168.

Plug flow studies of non-Newtonian liquids in microchannels

Evangelia Roumpea[a], Maxime Chinaud[a], Lyes Kahouadji[b], Omar Matar[b], Panagiota Angeli[a]

[a]*ThAMeS Multiphase, Department of Chemical Engineering, University College London, Torrington Place, London WC1E 7JE, UK*

[b]*Department of Chemical Engineering, Imperial College London, South Kensington Campus, London , SW7 2AZ, UK*

Motivation

Demand for intensified and continuous processing makes **microfluidic devices** attractive alternatives to large-scale units.

Few studies have focused on **non-Newtonian** liquid–liquid flows in small channels. Fluids with complex rheology are very common industrially, including catalytic polymerization reactions, food processing and enhanced oil recovery .

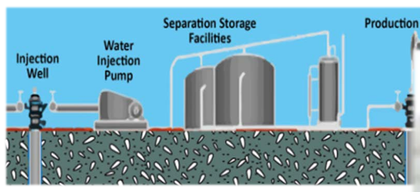

Enhanced oil recovery

Care products

Food industry

Objectives of the project

Detailed investigation of two-phase flow hydrodynamics using:

- different non-Newtonian fluid mixtures
- advanced laser system (two-colour μ-PIV system)
- different channel inlets for flow pattern formation studies.

Experimental set-up & conditions

Two-colour micro-PIV

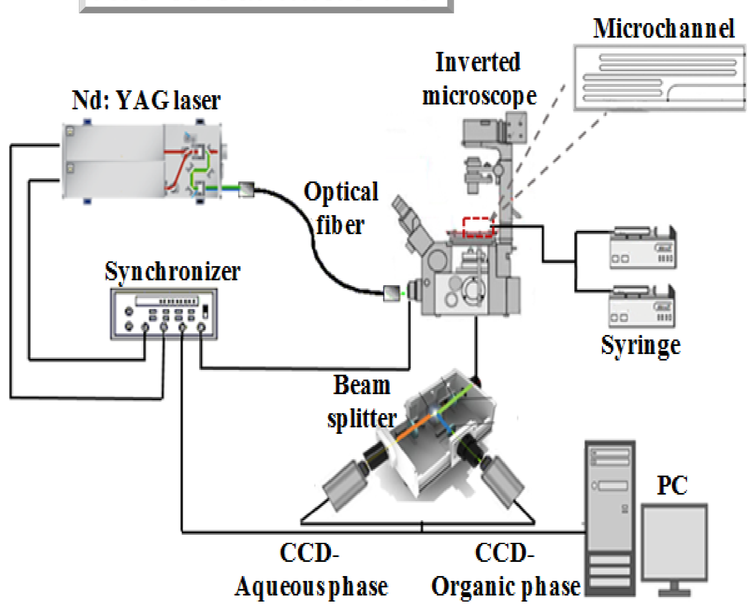

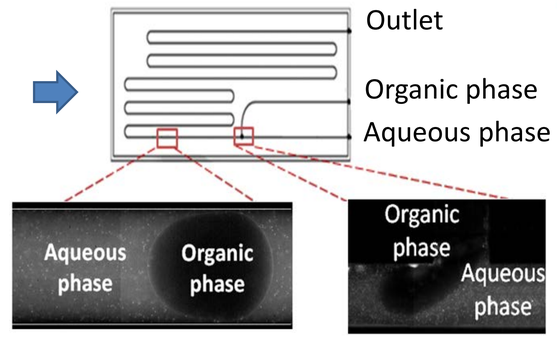

Simultaneous velocity fields in both phases

- **Organic phase**: Two silicone oils with viscosity 5 and 155 cSt
- **Aqueous phase**: Aqueous glycerol solutions + xanthan gum (1000 & 2000 ppm)
- Both phases seeded with different **fluorescent particles**

Flow pattern map

Xanthan gum → increases area of plug flow

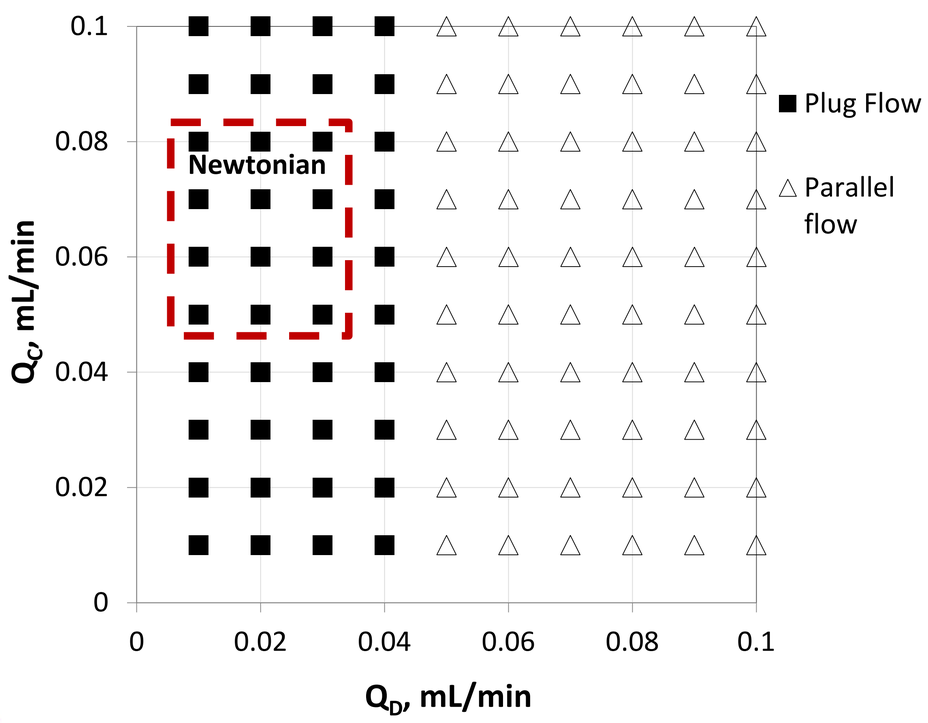

Flow pattern map for silicon oil (5 cSt) and water/glycerol mixture with (symbols) and without (line) xanthan gum

Plug formation study

Channel ID: 200 μm

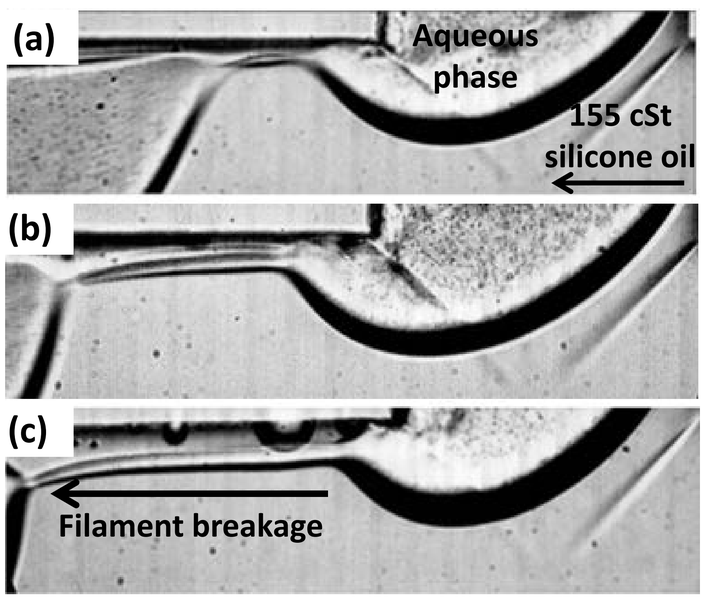

Dynamics of filament breakage for (a) Newtonian aqueous phase (b) non-Newtonian aqueous phase, 1000 ppm (c) non-Newtonian aqueous phase, 2000 ppm ($Q_A = Q_O = 0.01$ mL/min)

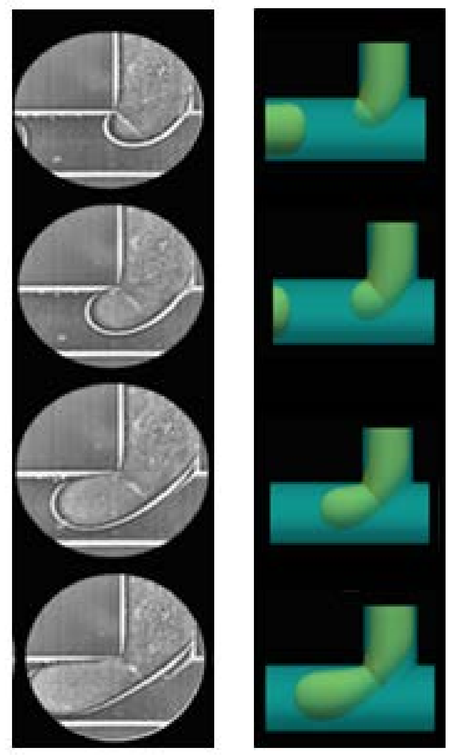

Comparison between experimental results and simulation. Collaboration with **Imperial College** (l.kahouadji@imperial.ac.uk)

Main channel study

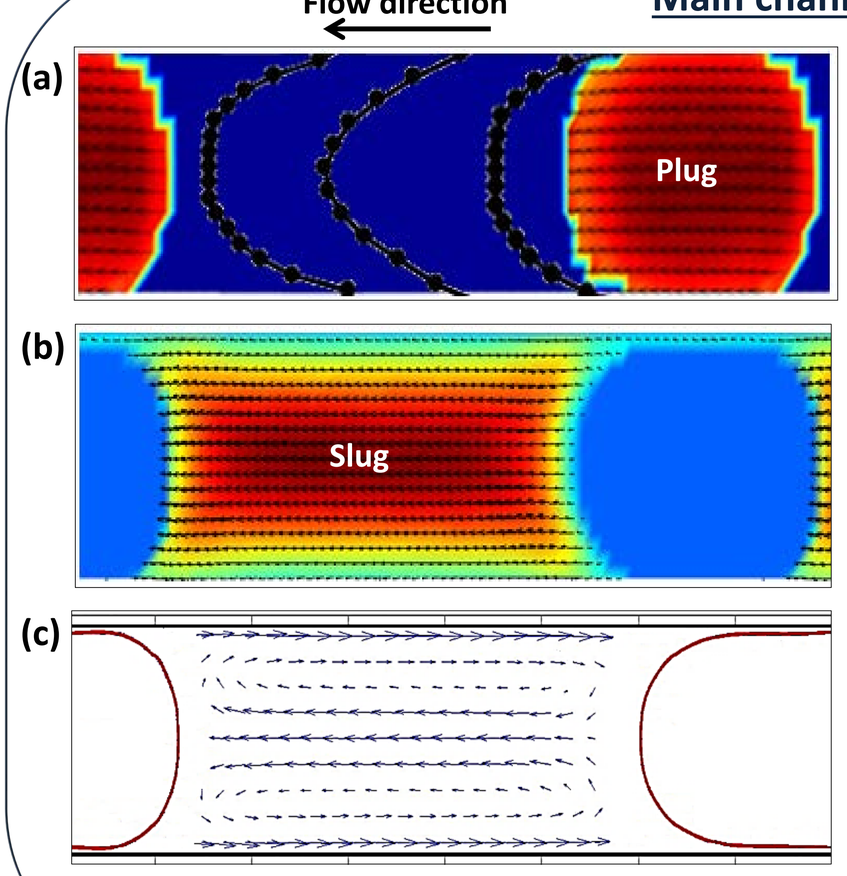

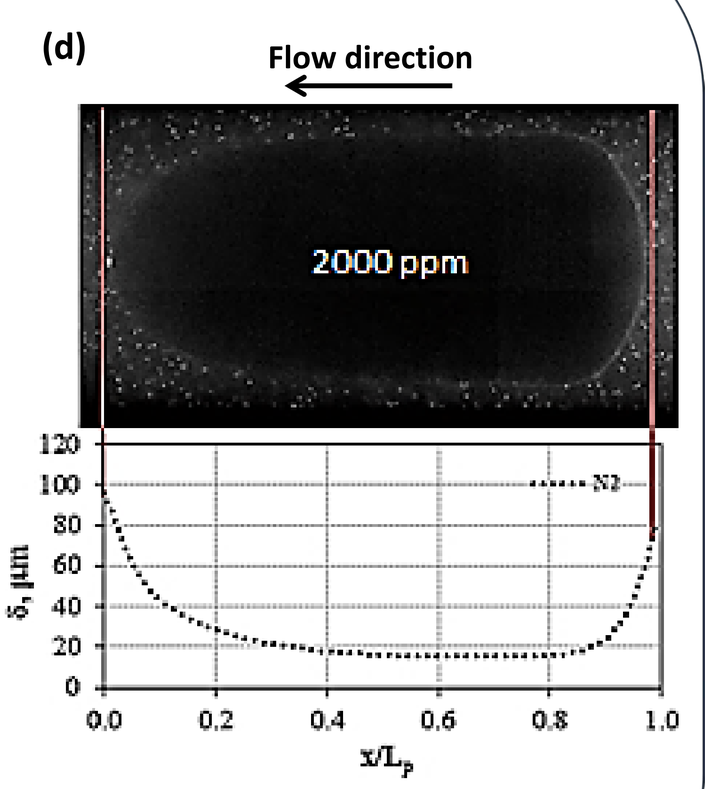

Velocity field obtained from micro-PIV into (a) plug (b) slug (c) recirculation pattern for Newtonian system (d) plug shape for non-Newtonian 2000 ppm ($Q_C = 0.07$ mL/min and $Q_D = 0.03$ mL/min)

Conclusions & future work

The use of xanthan gum **results in**:

- **increased** film thickness
- **bullet-shaped** plugs
- **different** flow pattern boundaries
- **different** dynamics of filament breakage

Future studies :

- Investigate different non-Newtonian solutions
- Understand mechanism of plug formation in non-Newtonian fluids

Corresponding papers

Roumpea E., Chinaud M., Angeli P. Experimental investigations of non-Newtonian/Newtonian liquid-liquid flows in microchannels. AIChE J, 2017; 63: 3599–3609.

Chinaud M, Roumpea E, Angeli P. Studies of plug formation in microchannel liquid–liquid flows using advanced particle image velocimetry techniques. Experimental Thermal and Fluid Science, 2015;69:99–110.

EPSRC MEMPHIS Programme Grant

EPSRC Engineering Instrument Pool